Fermilab FERMILAB-Pub-02-114-T

FERMILAB-Pub-02/114-T
SCIPP 02/07
hep–ph/0208209

arXiv:hep-ph/0208209 v3 13 Dec 2002

Higgs Boson Theory and Phenomenology

Marcela Carena* and Howard E. Haber†

* *Fermi National Accelerator Laboratory*
P.O. Box 500, Batavia, IL 60510, USA

† *Santa Cruz Institute for Particle Physics*
University of California, Santa Cruz, CA 95064, USA

Abstract

Precision electroweak data presently favors a weakly-coupled Higgs sector as the mechanism responsible for electroweak symmetry breaking. Low-energy supersymmetry provides a natural framework for weakly-coupled elementary scalars. In this review, we summarize the theoretical properties of the Standard Model (SM) Higgs boson and the Higgs sector of the minimal supersymmetric extension of the Standard Model (MSSM). We then survey the phenomenology of the SM and MSSM Higgs bosons at the Tevatron, LHC and a future e^+e^- linear collider. We focus on the Higgs discovery potential of present and future colliders and stress the importance of precision measurements of Higgs boson properties.

1 Introduction—Origin of Electroweak Symmetry Breaking

Deciphering the mechanism that breaks the electroweak symmetry and generates the masses of the known fundamental particles is one of the central challenges of particle physics. The Higgs mechanism [1] in its most general form can be used to explain the observed masses of the $W^\pm$ and Z bosons as a consequence of three Goldstone bosons ($G^\pm$ and G^0) that end up as the longitudinal components of the gauge bosons. These Goldstone bosons are generated by the underlying dynamics responsible for electroweak symmetry breaking. However, the fundamental nature of this dynamics is still unknown. Two broad classes of electroweak symmetry breaking mechanisms have been pursued theoretically. In one class of theories, electroweak symmetry breaking dynamics is weakly-coupled, while in the second class of theories the dynamics is strongly-coupled.

The electroweak symmetry breaking dynamics that is employed by the Standard Model posits a self-interacting complex doublet of scalar fields, which consists of four real degrees of freedom [2].

Renormalizable interactions are arranged in such a way that the neutral component of the scalar doublet acquires a vacuum expectation value, $v = 246$ GeV, which sets the scale of electroweak symmetry breaking. Consequently, three massless Goldstone bosons are generated, while the fourth scalar degree of freedom that remains in the physical spectrum is the CP-even neutral Higgs boson ($h_{\rm SM}$) of the Standard Model. It is further assumed in the Standard Model that the scalar doublet also couples to fermions through Yukawa interactions. After electroweak symmetry breaking, these interactions are responsible for the generation of quark and charged lepton masses. This approach is an example of weak electroweak symmetry breaking. Assuming that $m_{h_{\rm SM}} \lesssim 200$ GeV, all fields remain weakly interacting at energies up to the Planck scale. In the weakly-coupled approach to electroweak symmetry breaking, the Standard Model is very likely embedded in a supersymmetric theory [3] in order to stabilize the large gap between the electroweak and the Planck scales in a natural way [4,5]. These theories predict a spectrum of Higgs scalars [6], with the properties of the lightest Higgs scalar often resembling that of the Standard Model (SM) Higgs boson.

Alternatively, strong breaking of electroweak symmetry is accomplished by new strong interactions near the TeV scale [7]. More recently, so-called "little Higgs models" have been proposed in which the scale of the new strong interactions is pushed up above 10 TeV [8], and the lightest Higgs scalar resembles the weakly-coupled SM Higgs boson. In a more speculative direction, a new approach to electroweak symmetry breaking has been explored in which extra space dimensions beyond the usual $3 + 1$ dimensional spacetime are introduced [9] with characteristic sizes of order $(\text{TeV})^{-1}$. In such scenarios, the mechanisms for electroweak symmetry breaking are inherently extra-dimensional, and the resulting phenomenology may be significantly different from the usual approaches mentioned above. All these alternative approaches lie outside the scope of this review.

Although there is as yet no direct evidence for the nature of electroweak symmetry breaking dynamics, present data can be used to discriminate among the different approaches. For example, precision electroweak data, accumulated in the past decade at LEP, SLC, the Tevatron and elsewhere, strongly support the Standard Model with a weakly-coupled Higgs boson [10]. Moreover, the contribution of new physics, which can enter through $W^\pm$ and Z boson vacuum polarization corrections, is severely constrained. This fact has already served to rule out several models of strongly-coupled electroweak symmetry breaking dynamics. The Higgs boson contributes to the $W^\pm$ and Z boson vacuum polarization through loop effects, and so a global Standard Model fit to the electroweak data yields information about the Higgs mass. The results of the LEP Electroweak Working Group analysis shown in fig. 1(a) yield [10]: $m_{h_{\rm SM}} = 81^{+52}_{-33}$ GeV, and provides a 95% CL upper limit of $m_{h_{\rm SM}} < 193$ GeV. These results reflect the logarithmic sensitivity to the Higgs mass via the virtual Higgs loop contributions to the various electroweak observables. The 95% CL upper limit is consistent with the direct searches at LEP [11] that show no conclusive evidence for the Higgs boson, and imply that $m_{h_{\rm SM}} > 114.4$ GeV at 95% CL. Fig. 1(b) exhibits the most probable range of values for the SM Higgs mass [12]. This mass range is consistent with a weakly-coupled Higgs scalar that is expected to emerge from the Standard Model scalar dynamics.

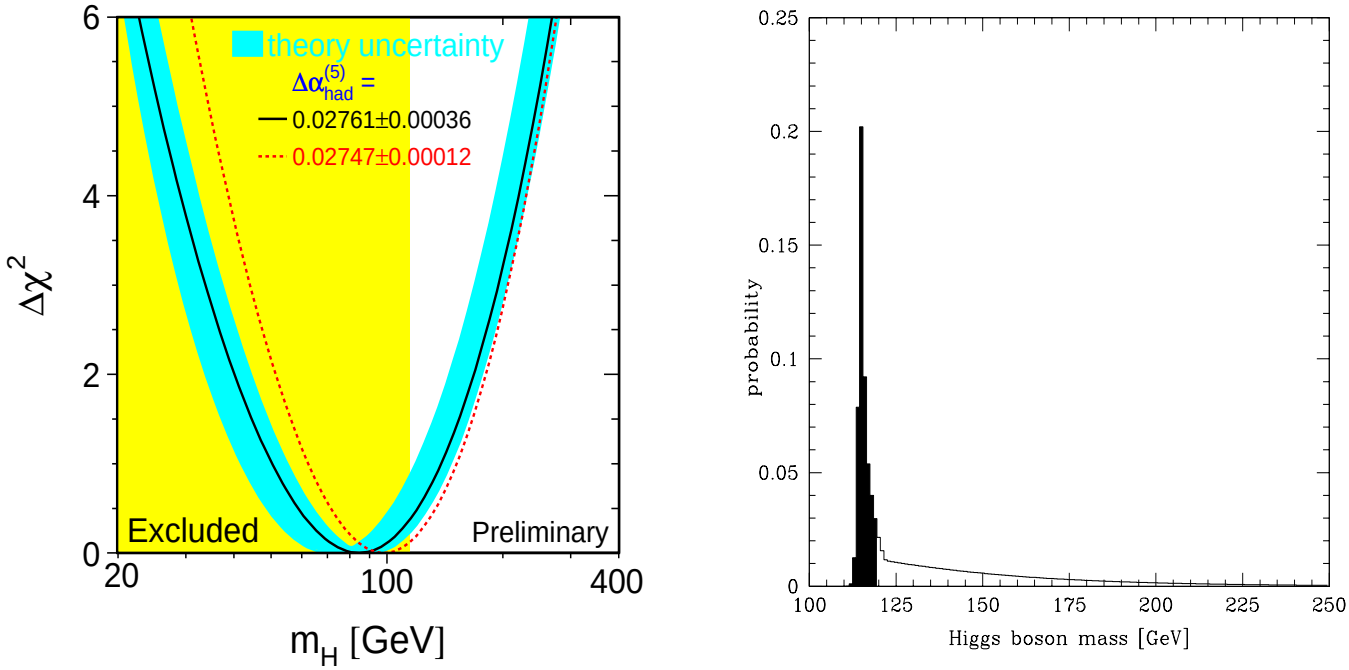

Figure 1: (a) The "blueband plot" shows $\Delta\chi^2 \equiv \chi^2 - \chi^2_{\rm min}$ as a function of the Standard Model Higgs mass [10]. The solid line is a result of a global fit using all data; the band represents the theoretical error due to missing higher order corrections. The rectangular shaded region shows the 95% CL exclusion limit on the Higgs mass from direct searches at LEP [11]. (b) Probability distribution function for the Higgs boson mass, including all available direct and indirect data [12]. The probability is shown for 1 GeV bins. The shaded and unshaded regions each correspond to an integrated probability of 50%

There are some loopholes that can be exploited to circumvent this conclusion. It is possible to construct models of new physics where the goodness of the global Standard Model fit to precision electroweak data is not compromised while the strong upper limit on the Higgs mass is relaxed. In particular, one can construct effective operators [13,14] or specific models [15] of new physics where the Higgs mass is significantly larger, but the new physics contributions to the $W^\pm$ and Z vacuum polarizations, parameterized by the Peskin-Takeuchi [16] parameters S and T, are still consistent with the experimental data. In addition, some have argued that the global Standard Model fit exhibits possible internal inconsistencies [17], which would suggest that systematic uncertainties have been underestimated and/or new physics beyond the Standard Model is required. Thus, although weakly-coupled electroweak symmetry breaking seems to be favored by the strong upper limit on the Higgs mass, one cannot definitively rule out all other approaches.

Nevertheless, one additional piece of data is very suggestive. Within the supersymmetric extension of the Standard Model, grand unification of the electromagnetic, the weak and the strong gauge interac-

tions can be achieved in a consistent way, strongly supported by the prediction of the electroweak mixing angle at low energy scales with an accuracy at the percent level [18,19]. The significance of this prediction is not easily matched by other approaches. For example, in strongly-coupled electroweak symmetry breaking models, unification of couplings is not addressed *per se*, whereas in extra-dimensional models it is often achieved by introducing new structures at intermediate energy scales. Unless one is willing to regard the apparent gauge coupling unification as a coincidence, it is tempting to conclude that weak electroweak symmetry breaking with low-energy supersymmetry is the preferred mechanism, leading to an expected mass of the lightest Higgs boson below 200 GeV (less than 135 GeV in the simplest supersymmetric models), and a possible spectrum of additional neutral and charged Higgs bosons with masses up to of order 1 TeV.

Henceforth, we shall assume that the dynamics of electroweak symmetry breaking is a result of a weakly-coupled scalar sector. The Standard Model is an effective field theory and provides a very good description of the physics of elementary particles and their interactions at an energy scale of $\mathcal{O}(100)$ GeV and below. However, there must exist some energy scale, Λ, at which the Standard Model breaks down. That is, the Standard Model is no longer adequate for describing the theory above Λ, and degrees of freedom associated with new physics become relevant. In particular, we know that $\Lambda \leq M_{\rm PL}$, since at an energy scale above the Planck scale, $M_{\rm PL} \simeq 10^{19}$ GeV, quantum gravitational effects become significant and the Standard Model must be replaced by a more fundamental theory that incorporates gravity. (Similar conclusions also apply to recently proposed extra-dimensional theories in which quantum gravitational effects can become significant at energies scales as low as $\mathcal{O}(1\ \text{TeV})$ [9].) Of course, it is possible that new physics beyond the Standard Model exists at an energy scale between the electroweak and Planck scale, in which case the value of Λ might lie significantly below $M_{\rm PL}$.[1]

The value of the Higgs mass itself can provide an important constraint on the value of Λ. If $m_{h_{\rm SM}}$ is too large, then the Higgs self-coupling blows up at some scale Λ below the Planck scale [20]. If $m_{h_{\rm SM}}$ is too small, then the Higgs potential develops a second (global) minimum at a large value of the scalar field of order Λ [21]. Thus new physics must enter at a scale Λ or below in order that the global minimum of the theory correspond to the observed SU(2)$\times$U(1) broken vacuum with $v = 246$ GeV. Thus, given a value of Λ, one can compute the minimum and maximum Higgs mass allowed. The results of this computation (with shaded bands indicating the theoretical uncertainty of the result) are illustrated in fig. 2(a) [22]. Consequently, a Higgs mass range 130 GeV $\lesssim m_{h_{\rm SM}} \lesssim$ 180 GeV is consistent with an effective Standard Model that survives all the way to the Planck scale.[2]

However, the survival of the Standard Model as an effective theory all the way up to the Planck

[1]For example, the recent experimental evidence for neutrino masses of order 10^{-2} eV or below cannot be strictly explained in the Standard Model. Yet, one can easily write down a dimension-5 operator responsible for neutrino masses that is suppressed by v/Λ. If $m_\nu \sim 10^{-2}$ eV, then one obtains as a rough estimate $\Lambda \lesssim 10^{15}$ GeV.

[2]The constraint on Λ due to vacuum stability in fig. 2 is less stringent if one allows for the electroweak vacuum to be metastable, with a lifetime greater than the age of the universe. An analysis of ref. [23] finds that for a sufficiently long-lived electroweak vacuum, the Higgs mass lower limit of 130 GeV just quoted is reduced to about 115 GeV.

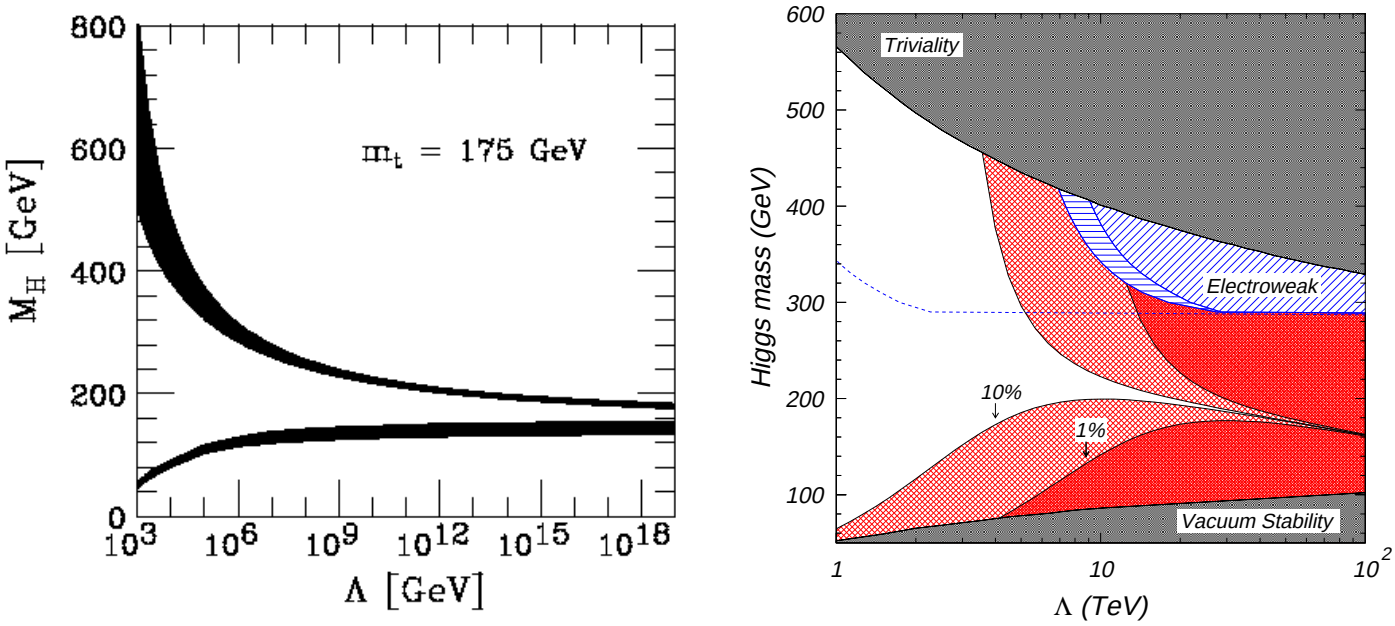

Figure 2: (a) The upper [20] and the lower [21] Higgs mass bounds as a function of the energy scale Λ at which the Standard Model breaks down, assuming $M_t = 175$ GeV and $\alpha_s(m_Z) = 0.118$, taken from ref. [22]. The shaded areas above reflect the theoretical uncertainties in the calculations of the Higgs mass bounds. (b) Following ref. [14], a reconsideration of the Λ *vs.* Higgs mass plot with a focus on $\Lambda < 100$ TeV. Precision electroweak measurements restrict the parameter space to lie below the dashed line, based on a 95% CL fit that allows for nonzero values of S and T and the existence of higher dimensional operators suppressed by v^2/Λ^2. The unshaded area has less than one part in ten fine-tuning.

scale is unlikely based on the following "naturalness" [4] argument. In an effective field theory, particle masses and dimensionless couplings of the low-energy theory are calculable in terms of parameters of a more fundamental theory that describes physics at the energy scale Λ. All low-energy couplings and fermion masses are logarithmically sensitive to Λ. In contrast, scalar squared-masses are *quadratically* sensitive to Λ. Thus, in this framework, the observed Higgs mass (at one-loop) has the following form:

$$m^2_{h_{\rm SM}} = (m^2_h)_0 + \frac{kg^2\Lambda^2}{16\pi^2}\,, \tag{1}$$

where $(m_h)_0$ is a parameter of the fundamental theory, g is an electroweak coupling and k is a constant, presumably of $\mathcal{O}(1)$, that is calculable within the low-energy effective theory. Because these two contributions arise from independent sources, it is very unlikely that the magnitude of $m^2_{h_{\rm SM}}$ is significantly smaller than either of the two terms. That is, the "natural" value for the physical scalar squared-mass is at least of order $g^2\Lambda^2/16\pi^2$. In order for this value to be consistent with the requirement

that the Higgs mass is of order the electroweak symmetry breaking scale (as required from unitarity constraints [24,25]), the value of Λ must satisfy

$$\Lambda \simeq \frac{4\pi m_{h_{\rm SM}}}{g} \sim \mathcal{O}(1 \text{ TeV}) . \tag{2}$$

If Λ is significantly larger than 1 TeV (often called the hierarchy problem in the literature), then the only way to generate a Higgs mass of $\mathcal{O}(m_Z)$ is to have an "unnatural" cancellation between the two terms of eq. (1). This seems highly unlikely given that the two terms of eq. (1) have completely different origins. The requirement of $\Lambda \sim \mathcal{O}(1 \text{ TeV})$ as a condition for the absence of fine-tuning of the Higgs mass parameter is nicely illustrated in fig. 2(b), taken from ref. [14].

A viable theoretical framework that incorporates weakly-coupled Higgs bosons and satisfies the constraint of eq. (2) is that of "low-energy" or "weak-scale" supersymmetry [3]. If supersymmetry (which relates fermion and boson masses and interactions) is exact, then boson masses must exhibit the same logarithmically sensitivity to Λ as do the fermion masses. Since no supersymmetric partners of the Standard Model particles have been found, it follows that supersymmetry is not an exact symmetry of the fundamental particle interactions. Hence, in the framework of low-energy supersymmetry, Λ should be identified with the energy scale of supersymmetry-breaking. The naturalness constraint of eq. (2) is still relevant, which implies that the scale of supersymmetry breaking should not be much larger than a few TeV in order that the naturalness of scalar masses be preserved. Moreover, low-energy supersymmetry with a supersymmetry-breaking scale of $\mathcal{O}(1 \text{ TeV})$ is precisely what is needed to explain the observed gauge coupling unification as previously noted. We conclude that a suitable replacement for the Standard Model is a supersymmetric extension of the Standard Model as the effective field theory of the TeV scale. One good feature of the supersymmetric approach is that the effective low-energy supersymmetric theory *can* be valid all the way up to the Planck scale, while still being natural!

The physics of the Higgs bosons will be explored by experiments now underway at the upgraded proton-antiproton Tevatron collider at Fermilab and in the near future at the Large Hadron Collider (LHC) at CERN. Once evidence for electroweak symmetry breaking dynamics is obtained, a more complete understanding of the mechanism involved will require experimentation at a future e^+e^- linear collider (LC) now under development. In this review we focus primarily on the theory and phenomenology of the Standard Model Higgs boson and the Higgs bosons of low-energy supersymmetry. In Section 2, we review the theoretical properties of the Standard Model Higgs boson, and exhibit its main branching ratio and production rates at hadron colliders and at the LC. The main Higgs boson search techniques at the Tevatron, LHC and the LC are described. In Section 3, we examine the Higgs bosons of the minimal supersymmetric Standard Model (MSSM). We summarize the tree-level properties of the MSSM Higgs sector and describe the most significant effects of the radiative corrections to the computation of the Higgs masses and couplings. We then exhibit the main branching ratios and production rates of the MSSM Higgs bosons and survey the phenomenology of the MSSM Higgs sector at the Tevatron, LHC and LC. A brief summary concludes this review in Section 4.

2 The Standard Model Higgs Boson

In the Standard Model, the Higgs mass is given by: $m^2_{h_{\rm SM}} = \frac{1}{2}\lambda v^2$, where λ is the Higgs self-coupling parameter. Since λ is unknown at present, the value of the Standard Model Higgs mass is not predicted. However, other theoretical considerations, discussed in Section 1, place constraints on the Higgs mass as exhibited in fig. 2. In contrast, the Higgs couplings to fermions [bosons] are predicted by the theory to be proportional to the corresponding particle masses [squared-masses]. In particular, the SM Higgs boson is a CP-even scalar, and its couplings to gauge bosons, Higgs bosons and fermions are given by:[3]

$$g_{hf\bar{f}} = \frac{m_f}{v}\,, \qquad g_{hVV} = \frac{2m_V^2}{v}\,, \qquad g_{hhVV} = \frac{2m_V^2}{v^2}\,, \tag{3}$$

$$g_{hhh} = \tfrac{3}{2}\lambda v = \frac{3m^2_{h_{\rm SM}}}{v}\,, \qquad g_{hhhh} = \tfrac{3}{2}\lambda = \frac{3m^2_{h_{\rm SM}}}{v^2}\,, \tag{4}$$

where $h \equiv h_{\rm SM}$, $V = W$ or Z and $v = 2m_W/g = 246$ GeV. In Higgs production and decay processes, the dominant mechanisms involve the coupling of the Higgs boson to the $W^\pm$, Z and/or the third generation quarks and leptons. Note that a $h_{\rm SM}gg$ coupling (g=gluon) is induced by virtue of a one-loop graph in which the Higgs boson couples to a virtual $t\bar{t}$ pair. Likewise, a $h_{\rm SM}\gamma\gamma$ coupling is generated, although in this case the one-loop graph in which the Higgs boson couples to a virtual W^+W^- pair is the dominant contribution. Further details of the SM Higgs boson properties are given in ref. [2]. A review of the SM Higgs properties and its phenomenology, with an emphasis on the impact of loop corrections to the Higgs decay rates and cross-sections can be found in ref. [26].

2.1 Standard Model Higgs Boson Decay Modes

The branching ratios for the main decay modes of a SM Higgs boson are shown as a function of Higgs boson mass in fig. 3 and 4(a), based on the results obtained using the `HDECAY` program [27]. For Higgs boson masses below 135 GeV, the decay $h_{\rm SM} \to b\bar{b}$ dominates, whereas above 135 GeV, the dominant decay mode is $h_{\rm SM} \to WW^{(*)}$ (below W^+W^- threshold, one of the W bosons is virtual as indicated by the star). Above $t\bar{t}$ threshold, the branching ratio into top-quark pairs increases rapidly as a function of Higgs mass, reaching a maximum of about 20% at $m_{h_{\rm SM}} \sim 450$ GeV. The total Higgs width is obtained by summing all the Higgs partial widths and is displayed as a function of Higgs mass in fig. 4(b).

The leading effects of the QCD corrections to the Higgs decay to quark pairs [28][4] can be taken into account by using the tree-level formula for the Higgs partial width (which depends on the quark

[3]The corresponding Feynman rules are obtained by multiplying the Higgs boson-VV couplings by $ig^{\mu\nu}$ and the other Higgs couplings of eqs. (3) and (4) by a factor of $-i$. The appropriate combinatorial factors have been included.

[4]The formulae for the leading order QCD-corrections to $\Gamma(h_{\rm SM} \to q\bar{q})$ are nicely summarized in ref. [29]. The leading electroweak radiative corrections have been obtained in ref. [30]. A useful summary of results, which includes new two-loop contributions to the radiatively corrected $h_{\rm SM} \to b\bar{b}$ partial width, can be found in ref. [31].

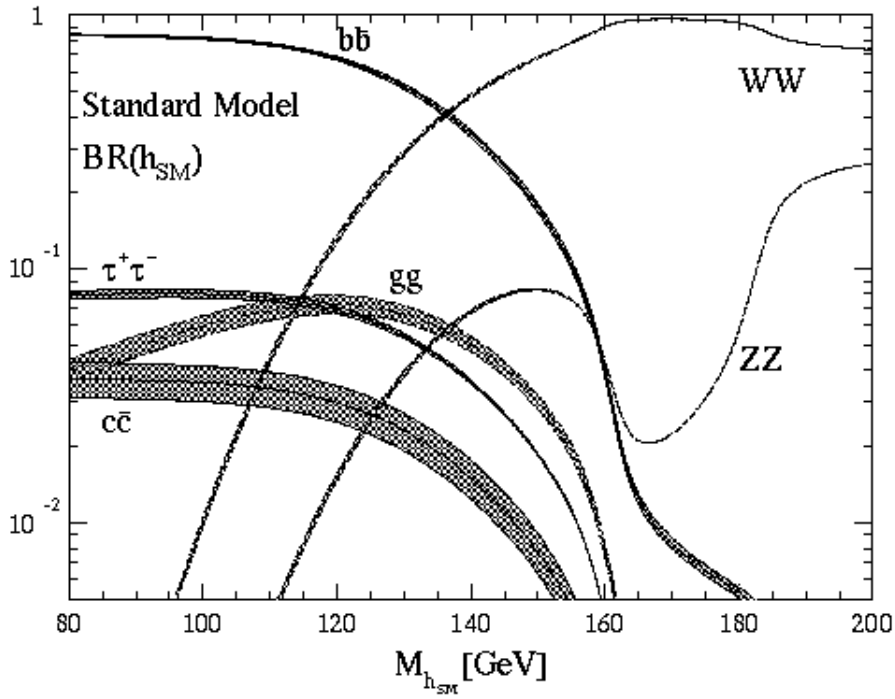

Figure 3: Branching ratios of the dominant decay modes of the Standard Model Higgs boson as a function of Higgs mass for $m_{h_{\rm SM}} \leq 200$ GeV, taken from ref. [32]. These results have been obtained with the program `HDECAY` [27], and include QCD corrections beyond the leading order [29]. The shaded bands represent the variations due to the uncertainties in the input parameters: $\alpha_s(M_Z^2) = 0.120 \pm 0.003$, $\overline{m}_b(M_b) = 4.22 \pm 0.05\,\mathrm{GeV}$, $\overline{m}_c(M_c) = 1.22 \pm 0.06\,\mathrm{GeV}$, and $M_t = 174 \pm 5\,\mathrm{GeV}$.

mass), and identifying the quark mass with the *running* quark mass evaluated at the Higgs mass, $\overline{m}_Q(m_{h_{\rm SM}})$. The running quark mass, $\overline{m}_Q(m_{h_{\rm SM}})$ is obtained from the $\overline{\rm MS}$ mass, $\overline{m}_Q(M_Q)$ [where M_Q is the corresponding quark pole mass], by renormalization group evolution. The $\overline{\rm MS}$ quark masses are obtained from fits to experimental data [33]. Note that the large decrease in the charm quark mass due to QCD running is responsible for suppressing BR($c\bar{c}$) relative to BR($\tau^+\tau^-$), in spite of the color enhancement of the former, thereby reversing the naively expected hierarchy. Below the corresponding two-body thresholds, the $WW^{(*)}$, $ZZ^{(*)}$ and $t^{(*)}\bar{t}$ decay modes (where the asterisk indicates an off-shell particle) are still relevant as shown in fig. 4.

The $h_{\rm SM}gg$, $h_{\rm SM}\gamma\gamma$ and $h_{\rm SM}Z\gamma$ vertices are generated at one-loop. The partial width for $h_{\rm SM} \to gg$ is primarily of interest because it determines the $gg \to h_{\rm SM}$ production cross-section. The $h_{\rm SM}\gamma\gamma$ vertex is especially relevant both for the $h_{\rm SM} \to \gamma\gamma$ discovery mode at the LHC and for the $\gamma\gamma \to h_{\rm SM}$ production mode at the LC operating as a $\gamma\gamma$ collider.

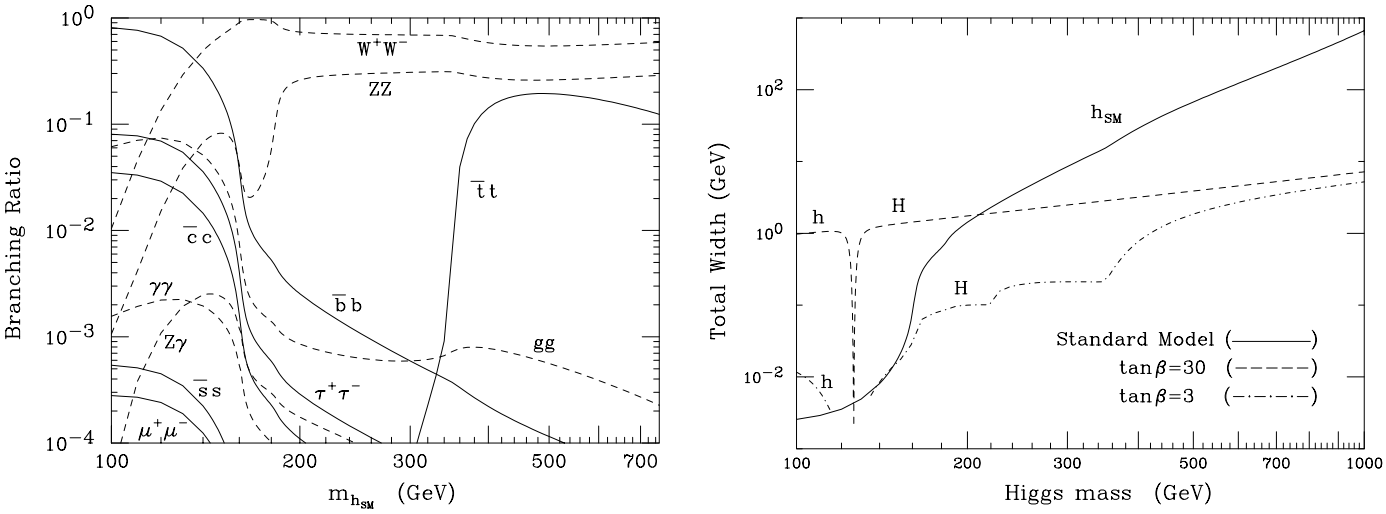

Figure 4: (a) Branching ratios of the Standard Model Higgs boson as a function of Higgs mass. Two-boson [fermion-antifermion] final states are exhibited by solid [dashed] lines. As compared with fig. 3, a larger range of Higgs masses and branching ratios are shown. (b) The total width of the Standard Model Higgs boson is shown as a function of its mass. For comparison, we exhibit the widths of the two CP-even scalars, h and H of the MSSM for two different choices of MSSM parameters ($\tan\beta = 3$ and 30 in the maximal mixing scenario; the onset of the $H \to hh$ and $H \to t\bar{t}$ thresholds in the $\tan\beta = 3$ curve are clearly evident). The central values of α_s, $\overline{m}_b(M_b)$ and $\overline{m}_c(M_c)$ quoted in the caption of fig. 3 are employed in both (a) and (b).

2.2 Standard Model Higgs Boson Production at Hadron Colliders

2.2.1 Cross-sections at hadron colliders

This section describes the most important Higgs production processes at the Tevatron ($\sqrt{s} = 2$ TeV) and the LHC ($\sqrt{s} = 14$ TeV). The relevant cross-sections are exhibited in figs. 5 and 6 [32,34,35,36]. Combining these Higgs production mechanisms with the decays discussed in Section 2.1, one obtains the most promising signatures.

Due to the large luminosity of gluons at high energy hadron colliders, $gg \to h_{\rm SM}$ is the Higgs production mechanism with the largest cross-section at the Tevatron and the LHC [37,38]. The two-loop, next-to-leading order (NLO) QCD corrections enhance the gluon fusion cross-section by about a factor of two [38,39]. The corresponding NLO differential cross-section (as a function of the Higgs boson p_T and rapidity) has also been obtained [40]. Recently, the next-to-NLO (NNLO) QCD corrections have been evaluated [41], and show a further enhancement of about 10% to 30% depending on the Higgs mass and center-of-mass energy of the collider. The remaining scale dependence and the effects of higher order terms not yet computed are estimated to give a theoretical uncertainty of 10–20%. The

dependence of the gluon fusion cross-section on different parton densities yields roughly an additional uncertainty of order 10%.

The cross-section for $q\bar{q} \to W^{\pm}h_{\rm SM}$ (summed over both W charge states) is the second largest Higgs cross-section at the Tevatron for $m_{h_{\rm SM}} \lesssim 175$ GeV. At the LHC, the $W^{\pm}h_{\rm SM}$ cross-section is not as prominent over the Higgs mass range of interest. The corresponding $q\bar{q} \to Zh_{\rm SM}$ cross-section is roughly a factor of two lower than the corresponding $W^{\pm}h_{\rm SM}$ cross-section. The QCD corrections to $\sigma(q\bar{q} \to Vh_{\rm SM})$ [$V = W$ or Z] coincide with those of the Drell-Yan process and increase the cross-sections by about 30% [42,43,44]. The theoretical uncertainty is estimated to be about 15% from the remaining scale dependence. The dependence on different sets of parton densities is rather weak and also leads to a variation of the production cross-sections by about 15%.

Vector boson fusion is a shorthand notation for the full $q\bar{q} \to q\bar{q}h_{\rm SM}$ process, where the quark and anti-quark both radiate virtual vector bosons (V^*) which then annihilate to produce the Higgs boson. Vector boson fusion via $ud \to duh_{\rm SM}$ (and its charge-conjugate process) is also possible. In figs. 5 and 6, all contributing processes are included, and the sum of all such contributions is labeled $qq \to qqh_{\rm SM}$ for simplicity. The QCD corrections enhance the cross-section by about 10% [44,45]. The vector boson fusion process is the second largest Higgs cross-section at the LHC; its cross-section approaches the $gg \to h_{\rm SM}$ cross-section for $m_{h_{\rm SM}} \sim 1$ TeV.

The cross-sections for gg, $q\bar{q} \to t\bar{t}h_{\rm SM}$ at the Tevatron and the LHC are displayed in figs. 5 and 6. The NLO QCD corrections to $q\bar{q} \to t\bar{t}h_{\rm SM}$ have recently been computed in refs. [46] and [47], and the corrections to $gg \to t\bar{t}h_{\rm SM}$ have been obtained in ref. [47]. Fig. 5 includes the complete NLO QCD corrections from ref. [47] (at Tevatron energies, $t\bar{t}h_{\rm SM}$ production is dominated by the $q\bar{q} \to t\bar{t}h_{\rm SM}$ subprocess). The size of the QCD corrections depends sensitively on the choice of scale, μ, employed in the running coupling constant and parton distribution functions. Changes in μ can significantly modify the tree-level cross-sections, whereas the NLO-corrected cross-sections are rather insensitive to reasonable changes in μ. In fig. 6, the tree-level $t\bar{t}h_{\rm SM}$ cross-section is shown for $\mu^2 = \hat{s}$ (the square of the partonic center-of-mass energy), and is roughly a factor of two smaller than the corresponding cross-section with $\mu = m_t$. With respect to the latter choice, the NLO-corrections of ref. [47] are rather small, typically of order 10–20% depending on the precise choice of μ.

The tree-level gg, $q\bar{q} \to b\bar{b}h_{\rm SM}$ cross-section (as a function of $m_{h_{\rm SM}}$) shown in fig. 5 has been computed by fixing the scales of the parton distribution functions, the running coupling α_s and the running Higgs–bottom-quark Yukawa coupling (or equivalently, the running b-quark mass) at the value of the corresponding $h_{\rm SM}$ mass. In fig. 6, the b-quark pole mass is employed,[5] while the scales for α_s and the parton distribution functions were set equal to the partonic center-of-mass energy.

By using the running b quark mass, one implicitly resums large logarithms associated with the QCD-corrected Yukawa coupling. Thus, the tree-level $b\bar{b}h_{\rm SM}$ cross-section displayed in fig. 5 implicitly includes

[5] The effect of using the b-quark pole mass [$M_b \simeq 5$ GeV] as opposed to the running b-quark mass [$\overline{m}_b(m_{h_{\rm SM}})$] is to *increase* the cross-section by roughly a factor of two.

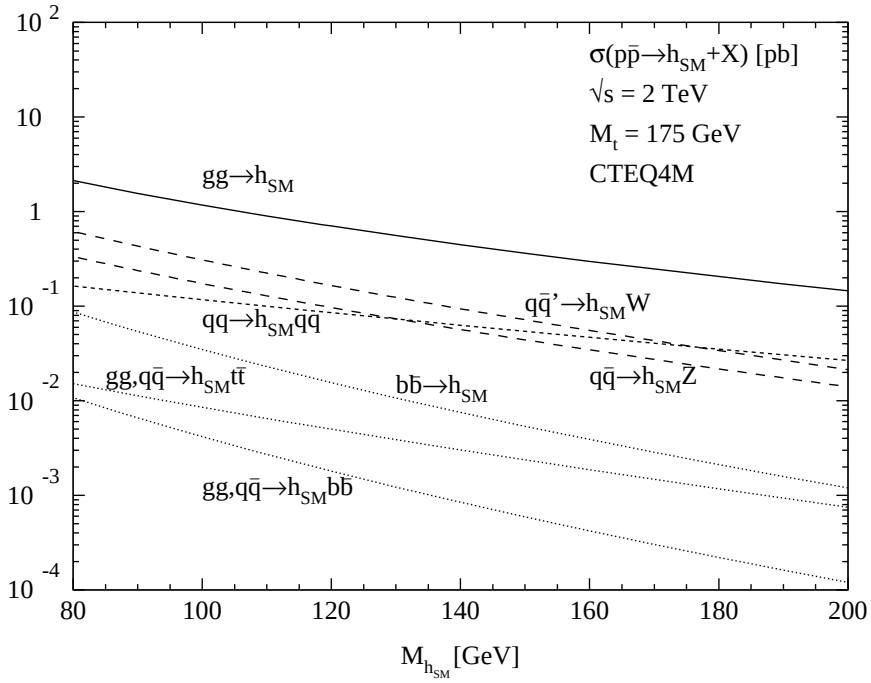

Figure 5: Higgs production cross-sections (in units of pb) at the Tevatron [$\sqrt{s} = 2$ TeV], for the various production mechanisms as a function of the Higgs mass, taken primarily from refs. [32] and [35]. The full NLO QCD-corrected results are employed for the gluon fusion $gg \to h_{\rm SM}$, vector boson fusion $qq \to V^*V^*qq \to h_{\rm SM}qq$ (here, qq refers to both ud and $q\bar{q}$ scattering), Higgs-strahlung processes $q\bar{q} \to V^* \to Vh_{\rm SM}$ (where $V = W^\pm, Z$), $b\bar{b} \to h_{\rm SM}$ (taken from ref. [36]), and $gg, q\bar{q} \to h_{\rm SM}t\bar{t}$. Tree-level cross-sections are exhibited for $gg, q\bar{q} \to h_{\rm SM}b\bar{b}$. In the latter case, the cross-section has been computed with a running b-quark mass, α_s and the parton distribution functions all evaluated at the corresponding Higgs mass.

a part of the QCD corrections to the full inclusive cross-section. However, the most significant effect of the QCD corrections to $b\bar{b}h_{\rm SM}$ production arises from the kinematical region where the b quarks are emitted near the forward direction. In fact, large logarithms arising in this region spoil the convergence of the QCD perturbation series since $\alpha_s \ln(m^2_{h_{\rm SM}}/m^2_b) \sim \mathcal{O}(1)$. These large logarithms (already present at lowest order) must be resummed to all orders, and this resummation is accomplished by the generation of the b-quark distribution function [48,49]. Thus, the QCD-corrected *fully* inclusive $b\bar{b}h_{\rm SM}$ cross-section can be approximated by $b\bar{b} \to h_{\rm SM}$ and its QCD corrections.[6] The latter is also exhibited in fig. 5 and is

[6] This result, although correct in the far asymptotic regime (where $\sqrt{s} \gg m_{h_{\rm SM}} \gg m_b$), may still not be reliable for Higgs production at the Tevatron and LHC. In ref. [50], it is argued that even at the LHC for $m_{h_{\rm SM}} = 500$ GeV, sizable m_b-effects still remain and $\sigma(b\bar{b} \to h_{\rm SM})$ is an overestimate of the true QCD-corrected $b\bar{b}h_{\rm SM}$ cross-section.

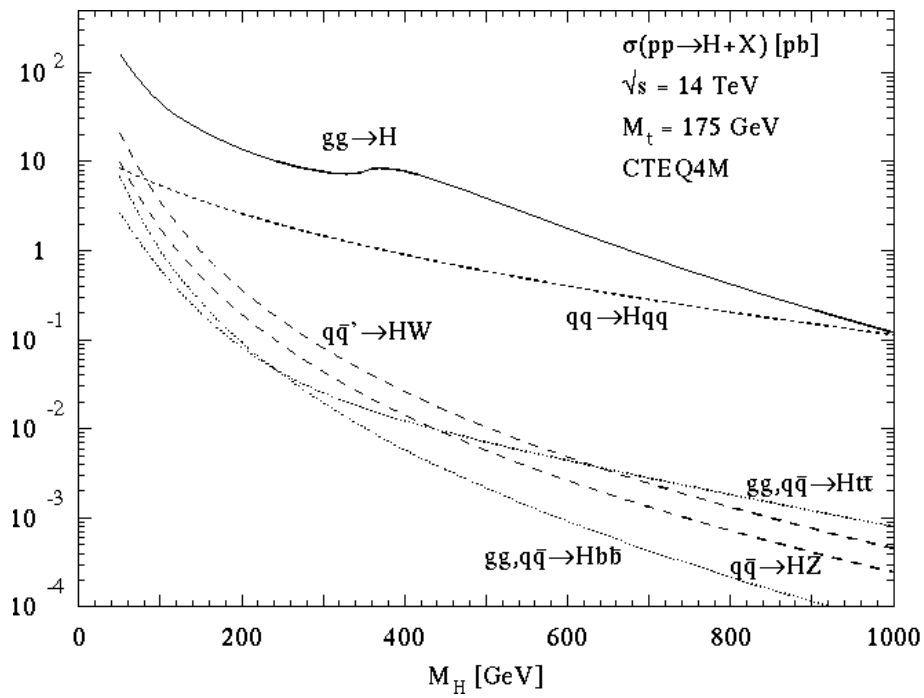

Figure 6: Higgs production cross-sections (in units of pb) at the LHC [$\sqrt{s}$ = 14 TeV], for the various production mechanisms as a function of the Higgs mass, taken from ref. [44]. The cross-section curves for gg, $q\bar{q} \to h_{\rm SM} t\bar{t}$ (which has not been updated to include the NLO calculation of ref. [47]) and gg, $q\bar{q} \to h_{\rm SM} b\bar{b}$ are based on a tree-level calculation with t-quark and b-quark pole masses and α_s and the parton distribution functions evaluated at the partonic center-of-mass energy.

seen to be roughly an order of magnitude larger than the tree-level $b\bar{b}h_{\rm SM}$ cross-section [36]. Of course, this result is not very relevant for the searches at hadron colliders in which transverse momentum cuts on the b-jets are employed. Ultimately, one needs the QCD-corrected *differential* cross-section for $b\bar{b}h_{\rm SM}$ (as a function of the final state b-quark transverse momentum) in order to do realistic simulations of the Higgs signal in this channel. However, if only one b-quark jet is tagged, it may be sufficient to consider the process $bg \to bh_{\rm SM}$. The cross-section for $bg \to bh_{\rm SM}$ at lowest order can be found in ref. [51]; the NLO QCD-corrected cross-section has been recently obtained in ref. [52]. For example, assuming that $p_T > 15$ GeV, and the pseudorapidity $|\eta| < 2$ for the observed b-quark jet, the NLO cross-section at the Tevatron ranges from about 6 fb to 0.25 fb for 100 GeV $\leq m_{h_{\rm SM}} \leq$ 200 GeV. Increasing the cuts to $p_T > 30$ GeV and $|\eta| < 2.5$ at the LHC yields a range of cross-sections from about 200 fb to 1.2 fb for 100 GeV $\leq m_{h_{\rm SM}} \leq$ 500 GeV.

Not shown in figs. 5 and 6 is the cross-section for inclusive double Higgs production ($h_{\rm SM}h_{\rm SM} + X$).

Double Higgs production is not observable at the Tevatron, but may be possible to detect at the LHC given sufficient luminosity. The main contributions to double Higgs production in order of importance are: (i) $gg \to h_{\rm SM}h_{\rm SM}$; (ii) $VV \to h_{\rm SM}h_{\rm SM}$; and (iii) $q\bar{q} \to Vh_{\rm SM}h_{\rm SM}$, where $V = W$ or Z. The gluon-gluon fusion cross-section dominates by at least an order of magnitude, so we focus on this subprocess [53,54,55,56]. Including NLO QCD corrections, typical cross-sections for $pp \to h_{\rm SM}h_{\rm SM} + X$ at $\sqrt{s} = 14$ TeV range from about 40 fb to 10 fb for $100 < m_{h_{\rm SM}} < 200$ GeV [55,56]. There are two classes of diagrams that contribute to $h_{\rm SM}h_{\rm SM}$ production via gluon fusion: $gg \to h^*_{\rm SM} \to h_{\rm SM}h_{\rm SM}$ (via the top-quark triangle diagram) which is sensitive to the triple-Higgs vertex, and $gg \to t^*t^* \to h_{\rm SM}h_{\rm SM}$ (via the top-quark box diagram) which is independent of the triple-Higgs vertex. Due to the relatively low cross-sections, it will be very challenging to extract information on the Higgs self-coupling parameter from LHC data.

Finally, assuming that very forward protons can be tagged, diffractive production of Higgs bosons may provide a viable signal at the LHC (the corresponding cross-sections at the Tevatron are probably too small) [57,58].[7] Such events are characterized by rapidity gaps, *i.e.*, the absence of particle production between the forward protons and the centrally produced Higgs boson. In particular, for $m_{h_{\rm SM}} \sim 130$ GeV, the exclusive process $pp \to pph_{\rm SM}$ (with $h_{\rm SM} \to b\bar{b}$) can be used at the LHC to obtain the Higgs mass with an accuracy of about 1% by measuring the invariant mass recoiling against the final state protons [59].

2.2.2 Standard Model Higgs Boson Searches at the Tevatron

In the mass region of interest to the Tevatron Higgs search (100 GeV$\lesssim m_{h_{\rm SM}} \lesssim$ 200 GeV), the SM Higgs boson is produced most copiously via gg fusion, with a cross-section from about 1.0—0.1 pb. For $m_{h_{\rm SM}} \lesssim 135$ GeV, the Higgs boson decays dominantly to $b\bar{b}$. Since the cross-section for the QCD production of $b\bar{b}$ dijet events is orders of magnitude larger than the Higgs production cross-section, the $gg \to h_{SM} \to b\bar{b}$ channel is not a promising channel. For $m_{h_{\rm SM}} \gtrsim 135$ GeV, the Higgs boson decays dominantly to $WW^{(*)}$ (where W^* is a virtual W), and the channel $gg \to h_{\rm SM} \to WW^{(*)}$ is accessible to the Tevatron Higgs search [60].

Given sufficient luminosity, the most promising SM Higgs discovery mechanism at the Tevatron for $m_{h_{\rm SM}} \lesssim 135$ GeV consists of $q\bar{q}$ annihilation into a virtual V^* ($V = W$ or Z), where $V^* \to Vh_{\rm SM}$ followed by a leptonic decay of the V and $h_{\rm SM} \to b\bar{b}$ [61]. The sum of the $Wh_{\rm SM}$ and $Zh_{\rm SM}$ cross-sections is about 0.2—0.5 pb in the mass region of interest ($100 \lesssim m_{h_{\rm SM}} \lesssim 135$ GeV), in which the dominant Higgs decay is $h_{\rm SM} \to b\bar{b}$. These processes lead to three main final states, $\ell\nu b\bar{b}$, $\nu\bar{\nu}b\bar{b}$ and $\ell^+\ell^- b\bar{b}$, that exhibit distinctive signatures on which the experiments can trigger (high p_T leptons and/or missing E_T). The backgrounds are manageable and are typically dominated by vector-boson pair production, $t\bar{t}$ production and QCD dijet production. The signal efficiencies and backgrounds have all been estimated

[7] A critical comparison of various theoretical approaches to diffractive Higgs production can be found in ref. [58].

with both the CDF Run 1 detector simulation and with the simple SHW simulation [62]. Monte Carlo estimates have been used for the backgrounds everywhere except in the $\nu\bar{\nu}b\bar{b}$ channel, where there is a significant contribution from QCD $b\bar{b}$ dijet production. To be conservative, in ref. [62] the unknown QCD $b\bar{b}$ dijet background to the $\nu\bar{\nu}b\bar{b}$ channel has been taken to be equal in size to the sum of all other contributing background processes. In addition, the separation of signal from background was optimized using neural network techniques [63], resulting in a demonstrable gain in the significance of the Higgs signal for the $\ell\nu b\bar{b}$ and $\nu\bar{\nu}b\bar{b}$ channels [62]. The b-tagging efficiencies and the $b\bar{b}$ mass resolution play a key role in determining the ultimate efficiency and background rejection. Much work remains, using real data studies, to optimize the performance in both these areas.

For larger Higgs masses ($m_{h_{\rm SM}} \gtrsim 135$ GeV) it is possible to exploit the distinct signatures present when the Higgs boson decay branching ratio to $WW^{(*)}$ becomes appreciable. In this case, there are final states with WW (from the gluon-fusion production of a single Higgs boson), and WWW and ZWW arising from associated vector boson–Higgs boson production. Three search channels were identified in ref. [62] as potentially sensitive at these high Higgs masses: like-sign dilepton plus jets ($\ell^\pm\ell^\pm jj$) events, high-p_T lepton pairs plus missing E_T ($\ell^+\ell^-\nu\bar{\nu}$), and trilepton ($\ell^\pm\ell'^\pm\ell^\mp$) events. Of these, the first two were found to be most sensitive. The strong angular correlations of the final state leptons resulting from WW^* is one of the crucial ingredients for these discovery channels [64,65,60].

The integrated luminosity required per Tevatron experiment as a function of Higgs mass to either exclude the SM Higgs boson at 95% CL or discover it at the 3σ or 5σ level of significance, for the SHW analyses with neural net selection (see ref. [62] for details), is shown in Fig. 7(a). These results are based on the combined statistical power of *both* the CDF and DØ experiments. The bands extend from the neural net result on the low side upward in required integrated luminosity by 30% to the high side, as an indication of the range of uncertainty in the b-tagging efficiency, $b\bar{b}$ mass resolution and background uncertainties. As the plots show, the required integrated luminosity increases rapidly with Higgs mass to 140 GeV, beyond which the high-mass channels play the dominant role. If $m_{h_{\rm SM}} = 115$ GeV, which lies just above the 95% CL exclusion limit achieved by LEP [11], then 5 fb^{-1} of integrated luminosity per experiment would provide sufficient data to see a 3σ excess above background. With 15 fb^{-1} of integrated luminosity per experiment, a 5σ discovery of the Higgs boson would be possible.

The final result shows that for an integrated luminosity of 10 fb^{-1}, if the SM Higgs boson mass lies beyond the discovery reach of the Tevatron, then one can attain a 95% CL exclusion for masses up to about 180 GeV. Moreover, if the SM Higgs happens to be sufficiently light ($m_{h_{\rm SM}} \lesssim 125$ GeV), then a tantalizing 3σ effect will be visible with the same integrated luminosity. With about 25 fb^{-1} of data, 3σ evidence for the Higgs boson can be obtained for the entire Higgs mass range up to 180 GeV. However, the discovery reach is considerably more limited for a 5σ Higgs boson signal. With 30 fb^{-1} integrated luminosity delivered per detector, a 5σ Higgs boson discovery may be possible for Higgs masses up to about 130 GeV, a significant extension of the LEP Standard Model Higgs search. The latter figure of merit is particularly significant when applied to the search for the lightest Higgs bosons of the MSSM. We address this case in Section 3.5.3.

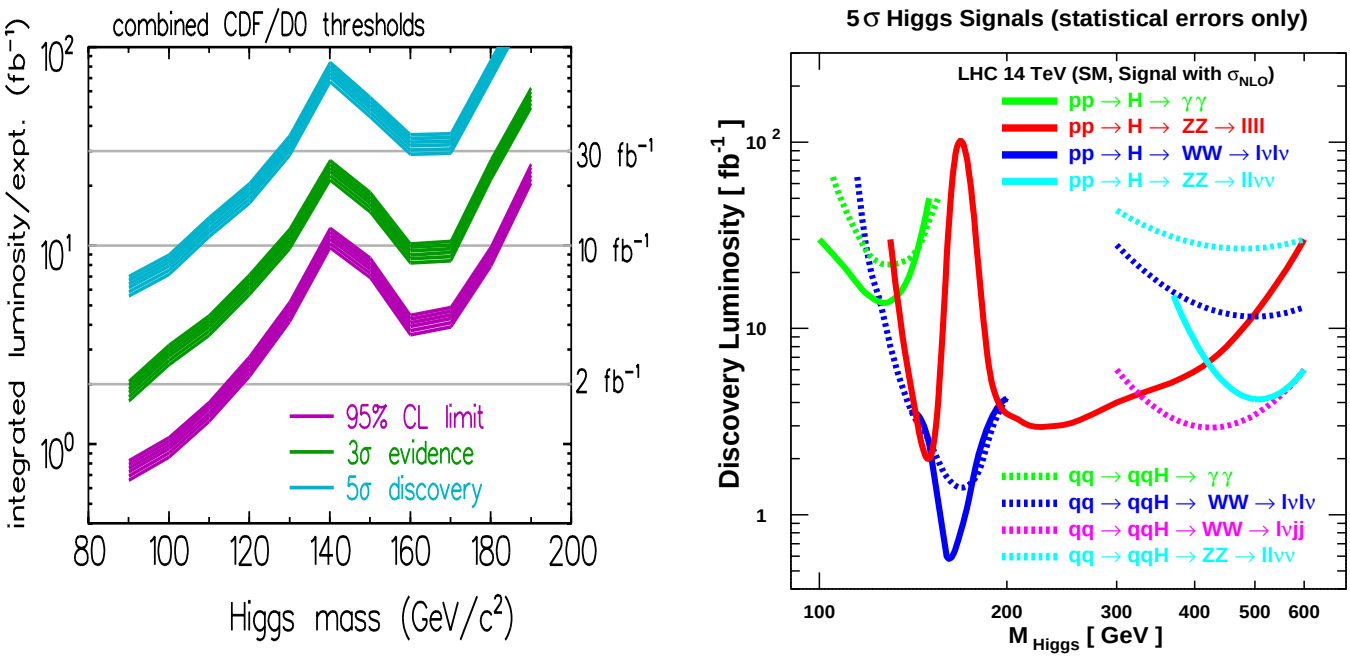

Figure 7: (a) The integrated luminosity required per Tevatron experiment, to either exclude a SM Higgs boson at 95% CL or observe it at the 3σ or 5σ level, as a function of the Higgs mass [62]. (b) Expected 5σ discovery luminosity requirements for the SM Higgs boson at the LHC for one experiment, based on a study performed with CMS fast detector simulation, assuming statistical errors only [72]. The gg and W^+W^- fusion processes are indicated respectively by the solid and dotted lines.

Other Higgs signatures could help improve the sensitivity of the Higgs search at the Tevatron. In ref. [62], channels containing the $h_{\rm SM} \to \tau^+\tau^-$ decay mode have not been studied, as the small branching ratio (less than 8%) makes the corresponding signal rates small. Still, a significant improvement of τ-lepton identification could lead to a viable Higgs signal in the Higgs mass region 120 GeV$\lesssim m_{h_{\rm SM}} \lesssim$ 140 GeV [66]. Another possibility which has been explored is the detection of the Higgs boson via $t\bar{t}h_{\rm SM}$ production (the Higgs boson is radiated off the top-quark), followed by $h_{\rm SM} \to b\bar{b}$. Initial studies [67] suggested that this channel could be observable at the upgraded Tevatron for $m_{h_{\rm SM}} \lesssim 140$ GeV, with a statistical significance comparable to the Higgs signals in the $Wh_{\rm SM}$ and $Zh_{\rm SM}$ channels.

If a Higgs boson is discovered at the Tevatron, one can begin to measure some of its properties. The Higgs mass can be measured with an accuracy of about 2 GeV [68]. However, the determination of the Higgs couplings to W and Z bosons and to $b\bar{b}$ will be model-dependent and rather crude. To improve and expand the possible Higgs measurements and determine its phenomenological profile will require Higgs studies at the LHC.

2.2.3 Standard Model Higgs Boson Searches at the LHC

Production rates for the Higgs boson in the Standard Model are significantly larger at the LHC [44,69]. The dominant Higgs production process, gluon fusion, can be exploited in conjunction with a variety of other channels, *e.g.*, WW/ZZ fusion of the Higgs boson and Higgs radiation off top quarks [70,71,72,73,74,75]. Integrated luminosities between 30 and 100 fb^{-1}, achievable within the first few years of LHC operation, will be sufficient to cover the entire canonical Higgs mass range of the Standard Model up to values close to 1 TeV with a significance greater than 5σ. The required LHC luminosities for a Higgs discovery in various channels are shown in fig. 7(b) [72]. Thus, there is no escape route for the SM Higgs boson at the LHC.

The properties of the SM Higgs boson can be determined with some precision at the LHC. The $h_{\rm SM} \to ZZ^{(*)} \to \ell^+\ell^-\ell^+\ell^-$ channel allows for an accurate Higgs mass determination of about 0.1% for 120 GeV $\lesssim m_{h_{\rm SM}} \lesssim$ 400 GeV, assuming an integrated luminosity of 300 fb^{-1} [76]. For larger Higgs masses, the precision in the Higgs mass measurement deteriorates due to the effect of the increasing Higgs width; nevertheless a 1% Higgs mass measurement is possible for $m_{h_{\rm SM}} \simeq 700$ GeV. The Higgs width can be extracted with a precision of 5 to 6% over the mass range 300—700 GeV from the Breit-Wigner shape of the Higgs resonance [76]. Below 300 GeV, the instrumental resolution becomes larger than the Higgs width, and the accuracy of the Higgs width measurement degrades. For example, the four-lepton invariant mass spectrum from $h_{\rm SM} \to ZZ$ yields a precision of about 25% at $m_{h_{\rm SM}} = 240$ GeV [68]. For lower Higgs masses, indirect methods must be employed to measure the Higgs width.

For Higgs masses below 200 GeV, a number of different Higgs decay channels can be studied at the LHC. The most relevant processes are

$$
\begin{aligned}
&gg \to h_{\rm SM} \to \gamma\gamma\,, \\
&gg \to h_{\rm SM} \to VV^{(*)}\,, \\
&qq \to qqV^{(*)}V^{(*)} \to qqh_{\rm SM}, \quad h_{\rm SM} \to \gamma\gamma,\ \tau^+\tau^-,\ VV^{(*)}\,, \\
&gg, q\bar{q} \to t\bar{t}h_{\rm SM}, \quad h_{\rm SM} \to b\bar{b},\ \gamma\gamma,\ WW^{(*)}\,,
\end{aligned}
$$

where $V = W$ or Z. The gluon-gluon fusion mechanism is the dominant Higgs production mechanism at the LHC, yielding a total cross-section of about 30 pb [15 pb] for $m_{h_{\rm SM}} = 120$ GeV [$m_{h_{\rm SM}} = 200$ GeV]. One also has appreciable Higgs production via VV electroweak gauge boson fusion, with a total cross-section of about 6 pb [3 pb] for the Higgs masses quoted above. The electroweak gauge boson fusion mechanism can be separated from the gluon fusion process by employing a forward jet tag and central jet vetoing techniques. Note that for $2m_W \lesssim m_{h_{\rm SM}} \lesssim 2m_Z$, the Higgs branching ratio to ZZ^* is quite suppressed with respect to WW (since one of the Z bosons is off-shell). Hence, in this mass window, $h_{\rm SM} \to W^+W^- \to \ell^+\nu\ell^-\bar{\nu}$ is the main Higgs discovery channel [65], as exhibited in fig. 7(b).

The cross-section for $t\bar{t}h_{\rm SM}$ production can be significant for Higgs masses in the intermediate mass range [47], 0.8 pb [0.2 pb] at $m_{h_{\rm SM}} = 120$ GeV [$m_{h_{\rm SM}} = 200$ GeV], although this cross-section falls faster

with Higgs mass as compared to the gluon and gauge boson fusion mechanisms. Finally, we note that the preferred channel at the Tevatron, $q\bar{q} \to W h_{\rm SM} \to \ell\nu b\bar{b}$, is not a discovery mode at the LHC due in part to the larger background cross-sections at $\sqrt{s} = 14$ TeV. Nevertheless, with 300 fb^{-1} of data, it may be possible to observe a SM Higgs signal (with $S/\sqrt{B} \geq 5$) if $m_{h_{\rm SM}} \lesssim 125$ GeV [77].

The measurements of Higgs decay branching ratios can be used to infer the ratios of the Higgs couplings, and provide an important first step in clarifying the nature of the Higgs boson [78,79,80]. These can be extracted from a variety of Higgs signals that are observable over a limited range of Higgs masses. In the mass range 110 GeV $\lesssim m_{h_{\rm SM}} \lesssim$ 150 GeV, the Higgs boson can be detected [with 100 fb^{-1} of data] in the $\gamma\gamma$ and the $\tau^+\tau^-$ channels indicated above. (The $\mu^+\mu^-$ channel was considered in ref. [80]. With 300 fb^{-1} of data, a 3σ excess above background may be possible for 110 GeV $\lesssim m_{h_{\rm SM}} \lesssim$ 140 GeV.) For $m_{h_{\rm SM}} \gtrsim 130$ GeV, the Higgs boson can also be detected in gluon-gluon fusion through its decay to $WW^{(*)}$, with both final gauge bosons decaying leptonically [81], and to $ZZ^{(*)}$ in the four-lepton decay mode [70,74]. There is additional sensitivity to Higgs production via VV fusion followed by its decay to $WW^{(*)}$ for $m_{h_{\rm SM}} \gtrsim 120$ GeV. These data can be used to extract the ratios of the Higgs partial widths to gluon pairs, photon pairs, $\tau^+\tau^-$, and W^+W^- [78,79]. The expected accuracies in Higgs width ratios, partial widths, and the total Higgs width are exhibited in fig. 8. These results are obtained under the assumption that the partial Higgs widths to W^+W^- and ZZ are fixed by electroweak gauge invariance, and the ratio of the partial Higgs widths to $b\bar{b}$ and $\tau^+\tau^-$ are fixed by the universality of Higgs couplings to down-type fermions. One can then extract the total Higgs width under the assumption that all other unobserved modes, in the Standard Model and beyond, possess small branching ratios of order 1%. Finally, we note that the specific Lorentz structure predicted for the $h_{\rm SM}W^+W^-$ coupling by the Higgs mechanism can be tested in angular correlations between the spectator jets in WW fusion of the Higgs boson at the LHC [79].

With an integrated luminosity of 100 fb^{-1} per experiment, the relative accuracy expected at the LHC for various ratios of Higgs partial widths Γ_i (or equivalently, ratios of Higgs squared-couplings) range from 10% to 30%, as shown in fig. 8. The ratio Γ_τ/Γ_W measures the coupling of down-type fermions relative to the Higgs couplings to gauge bosons. To the extent that the one-loop $h_{\rm SM}\gamma\gamma$ amplitude is dominated by the W-loop, the partial width ratio $\Gamma_\tau/\Gamma_\gamma$ probes the same relationship. In contrast, under the usual assumption that the one-loop $h_{\rm SM}gg$ amplitude is dominated by the top-quark loop, the ratio Γ_g/Γ_W probes the coupling of up-type fermions relative to the $h_{\rm SM}WW$ coupling. In addition, one can measure the $h_{\rm SM}t\bar{t}$ coupling directly by making use of the $t\bar{t}h_{\rm SM}$ production mode at the LHC. Recent studies suggest that for an integrated luminosity of 100 fb^{-1}, this signal is viable for the $h_{\rm SM} \to b\bar{b}$ [82,83] and $h_{\rm SM} \to \tau^+\tau^-$ [84] decay modes if $m_{h_{\rm SM}} \lesssim$ 130–140 GeV, and for the $h_{\rm SM} \to WW^{(*)}$ decay mode for 130 $\lesssim m_{h_{\rm SM}} \lesssim$ 200 GeV [85]. In this way, one expects to be able to measure the Higgs-top quark Yukawa coupling with a relative accuracy in the range of 10–20%.

Finally, the measurement of the triple Higgs self-coupling with an accuracy of order 25% can be obtained, in a very limited Higgs mass window, with 3000 fb^{-1} of data [86] (which requires at least a factor-of-ten luminosity upgrade of the LHC [87]).

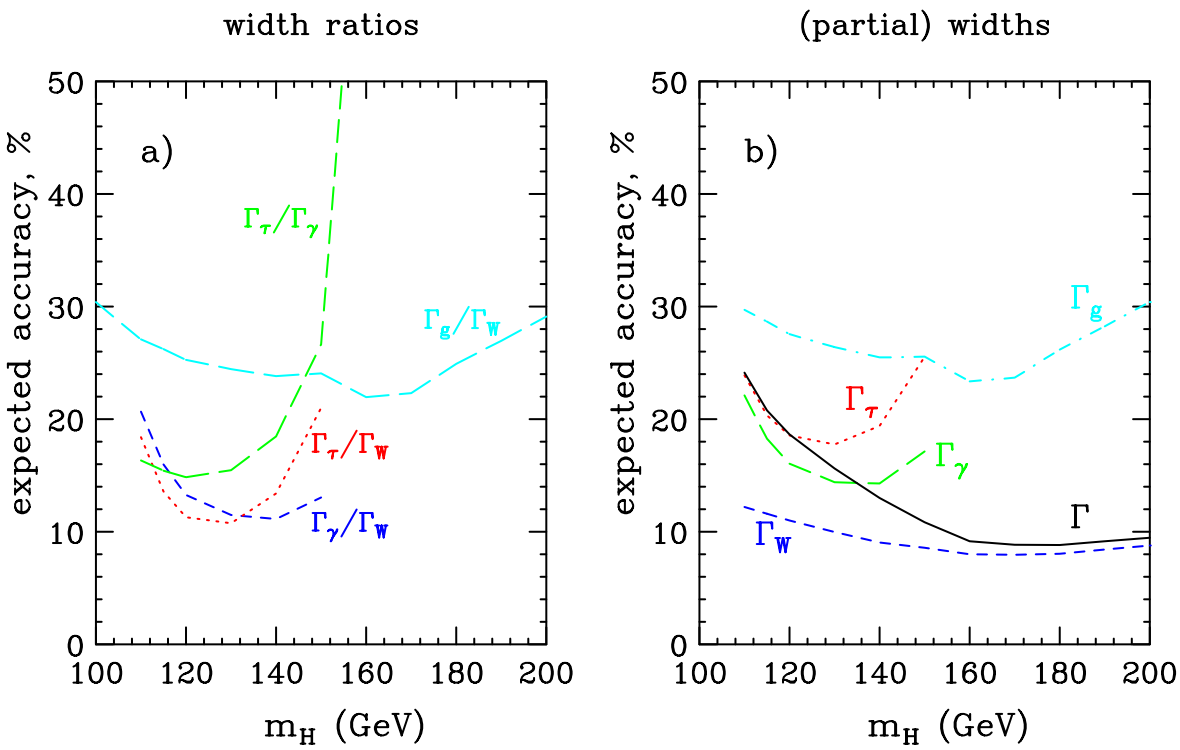

Figure 8: Relative accuracy expected at the LHC with 200 fb^{-1} of data for (a) various ratios of Higgs boson partial widths and (b) the indirect determination of partial and total widths. Expectations for width ratios assume W, Z universality; indirect width measurements also assume b, τ universality and a small branching ratio for unobserved modes. Taken from the parton-level analysis of ref. [78].

2.3 Standard Model Higgs Boson Searches at the LC

The next generation of high energy e^+e^- linear colliders is expected to operate at energies from 300 GeV up to about 1 TeV (JLC, NLC, TESLA), henceforth referred to as the LC [88,89,90]. The possibility of a multi-TeV linear collider operating in an energy range of 3–5 TeV (CLIC) is also under study [91]. With the expected high luminosities up to 1 ab^{-1}, accumulated within a few years in a clean experimental environment, these colliders are ideal instruments for reconstructing the mechanism of electroweak symmetry breaking in a comprehensive and conclusive form.

Weakly-coupled electroweak symmetry breaking dynamics involving an elementary scalar Higgs field can be established experimentally in three steps. First, the Higgs boson must be observed clearly and unambiguously, and its basic properties—mass, width, spin and C and P quantum numbers—must be determined. Second, the couplings of the Higgs boson to the $W^\pm$ and Z bosons and to leptons and

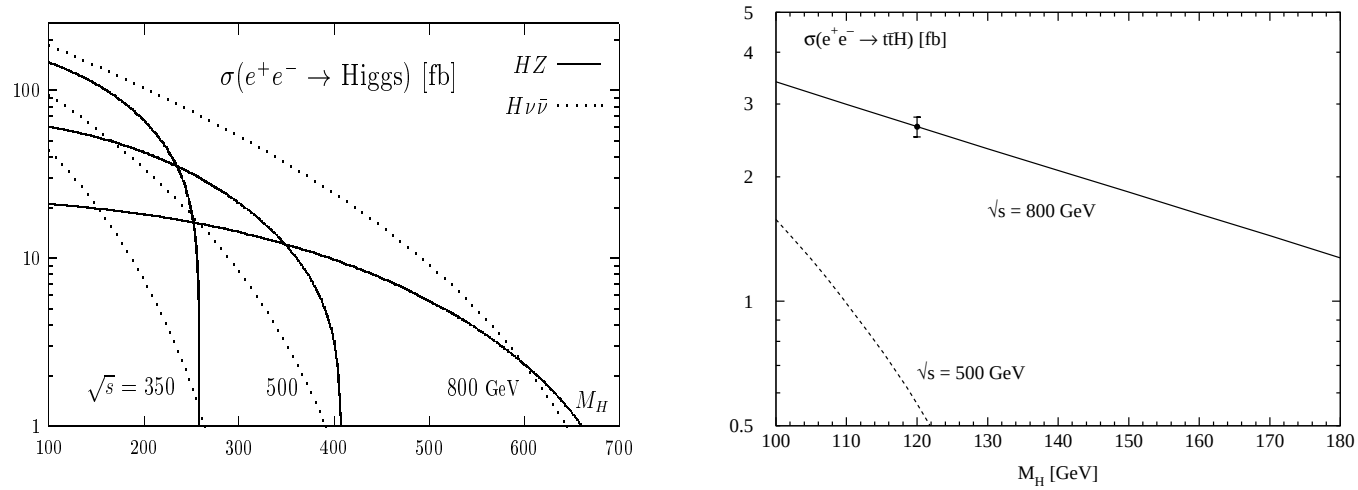

Figure 9: (a) The Higgs-strahlung and WW fusion production cross-sections as functions of $m_{h_{\rm SM}}$ for $\sqrt{s} = 350$ GeV, 500 GeV and 800 GeV. (b)The cross-section for $e^+e^- \to t\bar{t}h_{\rm SM}$, including NLO QCD corrections [102], as a function of $m_{h_{\rm SM}}$ for $\sqrt{s} = 500$ GeV and 800 GeV with the expected experimental accuracy for $m_{h_{\rm SM}} = 120$ GeV shown by the dot with error bar for an integrated luminosity of 1000 fb^{-1}. Taken from ref. [92].

quarks must be measured. Demonstrating that these couplings scale with the mass of the corresponding particle would provide critical support for the Higgs mechanism based on scalar dynamics as the agent responsible for generating the masses of the fundamental particles. Finally, the Higgs potential must be reconstructed by measuring the self-coupling of the Higgs field. The specific form of the potential shifts the ground state to a non-zero value, thereby providing the mechanism for electroweak symmetry breaking based on the self-interactions of scalar fields. Essential elements of this program can be realized at a high-luminosity e^+e^- linear collider, and high-precision analyses of the Higgs boson are possible in these machines [92,93,94].

The main production mechanisms of the SM Higgs boson at the LC are the Higgs-strahlung process [95,25], $e^+e^- \to Zh_{\rm SM}$, and the WW fusion process [96] $e^+e^- \to \bar{\nu}_e\nu_e W^*W^* \to \bar{\nu}_e\nu_e h_{\rm SM}$. With an accumulated luminosity of 500 fb^{-1}, about 10^5 Higgs bosons can be produced by Higgs-strahlung in the theoretically preferred intermediate mass range below 200 GeV. As $\sqrt{s}$ is increased, the cross-section for the Higgs-strahlung process decreases as s^{-1} and is dominant at low energies, while the cross-section for the WW fusion process grows as $\ln(s/m^2_{h_{\rm SM}})$ and dominates at high energies (see ref. [97] for a convenient form for the corresponding cross-sections), as shown in fig. 9(a).[8] The ZZ fusion mechanism,

[8]The cross-sections shown in fig. 9(a) are based on a tree-level computation. The complete one-loop electroweak corrections for $e^+e^- \to Zh_{\rm SM}$ have been computed [98,97], whereas only the leading one-loop corrections to the vector boson fusion process are known [99].

$e^+e^- \to e^+e^- Z^* Z^* \to e^+e^- h_{\rm SM}$, also contributes to Higgs production, with a cross-section suppressed with respect to that of WW fusion by a factor of $16\cos^4\theta_W/[1+(1-4\sin^2\theta_W)^2] \simeq 9.4$. The cross-sections for the Higgs-strahlung and the WW fusion processes are shown in fig. 9(a) for three values of $\sqrt{s}$. The Higgs-strahlung process, $e^+e^- \to Zh_{\rm SM}$, with $Z \to \ell^+\ell^-$, offers a very distinctive signature. For $\sqrt{s} = 350$ and 500 GeV and an integrated luminosity of 500 fb^{-1}, this ensures the observation of the SM Higgs boson up to the production kinematical limit independently of its decay [92]. At $\sqrt{s} = 500$ GeV, the Higgs-strahlung and the WW fusion processes have approximately the same cross-sections, $\mathcal{O}(50$ fb), for 100 GeV $\lesssim m_{h_{\rm SM}} \lesssim 200$ GeV. At $\sqrt{s} = 800$ GeV with 500 fb^{-1} of data, the analysis of ref. [100] suggests that a Higgs boson with mass up to about 650 GeV will be observable at the LC. Finally, the process $e^+e^- \to t\bar{t}h_{\rm SM}$ [101] yields a distinctive signature consisting of two W bosons and four b-quark jets, and can be observed at the LC given sufficient energy and luminosity if the Higgs mass is not too large. The QCD-corrected cross-sections for this process [102] for $\sqrt{s} = 500$ GeV and 800 GeV are shown in fig. 9(b).

The phenomenological profile of the Higgs boson can be determined by precision measurements. For example, consider the case of $m_{h_{\rm SM}} = 120$ GeV at the LC with $\sqrt{s} = 350$ GeV and 500 fb^{-1} of data [92]. The spin and parity of the Higgs boson can be determined unambiguously from the steep onset of the excitation curve in Higgs-strahlung near the threshold (see fig. 10(a) [103]) and the angular correlations in this process [104]. By measuring final state angular distributions and various angular and polarization asymmetries, one can check whether the Higgs boson is a state of definite CP, or whether it exhibits CP-violating behavior in its production and/or decays [105]. The Higgs mass can be measured to an accuracy of 40 MeV by reconstructing the Higgs boson in $Zh_{\rm SM}$ production and combining the results from the various final state channels. The Higgs width can be inferred in a model-independent way, with an accuracy of about 6%, by combining the partial width to W^+W^-, accessible in the vector boson fusion process, with the WW^* decay branching ratio. Similar results (with precisions within a factor of two of those quoted above) are obtained for larger Higgs masses in the intermediate mass regime. The $h_{\rm SM}ZZ$, $h_{\rm SM}Z\gamma$ and $h_{\rm SM}t\bar{t}$ couplings can be determined (with some sensitivity to possible anomalous couplings, if present) by the optimal-observable method [106], which makes optimal use of the polarized angular distributions and asymmetries for Higgs-strahlung and $h_{\rm SM}t\bar{t}$ production.

Higgs decay branching ratios can be measured very precisely for $m_{h_{\rm SM}} \lesssim 150$ GeV [107,108,109,110]. When such measurements are combined with measurements of Higgs production cross-sections, the absolute values of the Higgs couplings to the $W^\pm$ and Z gauge bosons and the Yukawa couplings to leptons and quarks can be determined to a few percent in a model-independent way. In addition, the Higgs-top quark Yukawa coupling can be inferred from the cross-section for Higgs emission off $t\bar{t}$ pairs [102,111]. As an example, Table 1 exhibits the anticipated fractional uncertainties in the measurements of Higgs branching ratios for $m_{h_{\rm SM}} = 120$ GeV at the LC.[9] Using this data, a program

[9]Here, BR($h_{\rm SM} \to gg$) is assumed to be roughly equal to the Higgs branching ratio into light hadrons (*i.e.*, excluding hadrons that contain c and b quarks).

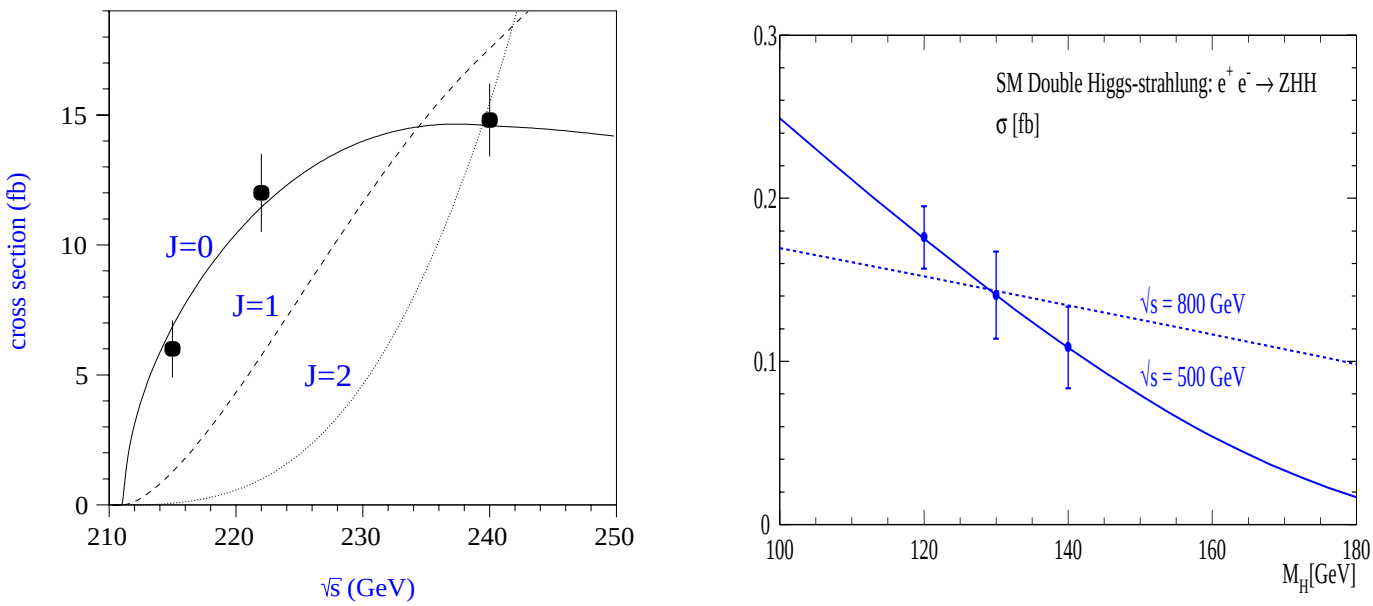

Figure 10: (a) Simulated measurement of the $e^+e^- \to Zh_{\rm SM}$ cross-section for $m_{h_{\rm SM}} = 120$ GeV with 20 fb^{-1} per point at three center of mass energies compared to the predictions for spin-0 (solid line) and typical examples of spin-1 (dashed line) and spin-2 (dotted line) [103]. (b) Cross-section for the double Higgs-strahlung process $e^+e^- \to Zh_{\rm SM}h_{\rm SM}$ at $\sqrt{s} = 500$ GeV (solid line) and 800 GeV (dashed line) [114]. The data points show the accuracy for 1 ab^{-1}.

Higgs coupling	δBR/BR	$\delta g/g$
hWW	5.1%	1.2%
hZZ	—	1.2%
htt	—	2.2%
hbb	2.4%	2.1%
hcc	8.3%	3.1%
$h\tau\tau$	5.0%	3.2%
$h\mu\mu$	$\sim$ 30%	$\sim$ 15%
hgg	5.5%	
$h\gamma\gamma$	16%	
hhh	—	$\sim$ 20%

Table 1: Expected fractional uncertainties for measurements of Higgs branching ratios [BR$(h \to X\overline{X})$] and couplings [g_{hXX}], for various choices of final state $X\overline{X}$, assuming $m_h = 120$ GeV at the LC. In all but four cases, the results shown are based on 500 fb^{-1} of data at $\sqrt{s} = 500$ GeV [107]. Results for $h\gamma\gamma$ [108], $ht\bar{t}$ [107], $h\mu\mu$ [109] and hhh [114,115] are based on 1 ab^{-1} of data at $\sqrt{s} = 500$ GeV (for $\gamma\gamma$ and hh) and $\sqrt{s} = 800$ GeV (for tt and $\mu\mu$), respectively.

HFITTER was developed in ref. [107] to perform a Standard Model global fit based on the measurements of the $Zh_{\rm SM}$, $\nu\bar{\nu}h_{\rm SM}$ and $t\bar{t}h_{\rm SM}$ cross-sections and the Higgs branching ratios listed in Table 1. The output of the program is a set of Higgs couplings along with their fractional uncertainties (which are also exhibited in Table 1). These results should be considered representative of what can eventually be achieved at the LC. For example, a comprehensive analysis of LC Higgs data will have to take into account the relevant electroweak loop corrections (which are not presently included in HFITTER). One should also note that theoretical uncertainties for the predicted Higgs couplings have not been taken into account in this analysis. The theoretical uncertainty in $g_{h_{\rm SM}c\bar{c}}$ is the most significant among the channels listed in Table 1, due to the uncertainties in c quark-mass and in α_s (which governs the running of the quark masses from the quark mass to the Higgs mass). Ref. [112] estimates a theoretical fractional uncertainty in $g_{hc\bar{c}}$ of about 12%, significantly greater than the experimental uncertainty listed in Table 1. In contrast, the theoretical fractional uncertainty in $g_{hb\bar{b}}$ is about 1.8% due to the uncertainty of the b-quark mass. Although this is less than the anticipated experimental uncertainty, it should not be neglected in the determination of the overall $g_{h_{\rm SM}b\bar{b}}$ uncertainty. The theoretical uncertainties in the other channels listed above are not significant compared to the quoted experimental uncertainties.

The measurement of the Higgs self-couplings is a very ambitious task that requires the highest luminosities possible at the LC, which possess unique capabilities for addressing this question. The trilinear Higgs self-coupling can be measured in double Higgs-strahlung, in which a virtual Higgs boson splits into two real Higgs particles in the final state [113]. A simulation based on 1 ab^{-1} of data is exhibited in fig. 10(b) [114]. In this way, for $m_{h_{\rm SM}} = 120$ GeV, the cubic term of the scalar potential can be established at the LC with a precision of about 20% [114,115]. Such a measurement is a prerequisite for determining the form of the Higgs potential that is responsible for spontaneous electroweak symmetry breaking generated by scalar sector dynamics. Finally, the total SM Higgs width can be obtained indirectly by using $\Gamma_{\rm tot} = \Gamma_{h_{\rm SM}WW}/{\rm BR}(h_{\rm SM} \to WW^*)$. The partial width is proportional to $g^2_{h_{\rm SM}WW}$, so the fractional uncertainty in $\Gamma_{\rm tot}$ can be obtained from the results of Table 1. For $m_{h_{\rm SM}} \lesssim 150$ GeV, an accuracy in the range of 5–10% can be achieved for the total Higgs width [116].

If the SM Higgs mass is above 150 GeV, then the precision determination of Higgs couplings will have to be reconsidered. The Higgs branching ratios into $c\bar{c}$, gg and $\tau^+\tau^-$ are now too small to be accurately measured. Due to the growing importance of the WW and ZZ modes, one can perform a precision measurement of the Higgs branching ratios to WW and ZZ, while the precision of the $b\bar{b}$ branching ratio is significantly reduced as $m_{h_{\rm SM}}$ increases to 200 GeV and beyond [117]. Moreover, due to the rapid decline of $t\bar{t}h_{\rm SM}$ production cross-section with increasing $m_{h_{\rm SM}}$, the Higgs-top quark Yukawa coupling cannot be extracted until $m_{h_{\rm SM}} \gtrsim 2m_t$, at which point the $t\bar{t}h_{\rm SM}$ coupling can be obtained by observing Higgs bosons produced by vector boson fusion which subsequently decay to $t\bar{t}$. The analysis of Ref. [118] finds that at the LC with $\sqrt{s} = 800$ GeV and 1 ab^{-1} of data, the $t\bar{t}h_{\rm SM}$ Yukawa coupling can be determined with an accuracy of about 10% for a Higgs mass in the range 350—500 GeV. The total Higgs width can be obtained directly from measuring the Higgs boson line-shape if $m_{h_{\rm SM}} \gtrsim 200$ GeV.

The e^+e^- linear collider with center-of-mass energy $\sqrt{s}$ can also be designed to operate in a $\gamma\gamma$ col-

lision mode. This is achieved by using Compton backscattered photons in the scattering of intense laser photons on the initial polarized $e^{\pm}$ beams [119,120]. The resulting $\gamma\gamma$ center of mass energy is peaked for proper choices of machine parameters at about $0.8\sqrt{s}$. The luminosity achievable as a function of the photon beam energy depends strongly on the machine parameters (in particular, the choice of laser polarizations). The $\gamma\gamma$ collider provides additional opportunities for Higgs physics [120,121,122,123,124]. The Higgs boson can be produced as an s-channel resonance in $\gamma\gamma$ collisions, and one can perform independent measurements of various Higgs couplings. For example, the product $\Gamma(h_{\rm SM} \to \gamma\gamma){\rm BR}(h_{\rm SM} \to b\bar{b})$ can be measured with a statistical accuracy of about 2—10% for 120 GeV$\lesssim m_{h_{\rm SM}} \lesssim$ 160 GeV with about 50 fb^{-1} of data [122,123,124]. In order to reach such a precision, it is critical to control the overwhelming two-jet background (with efficient b-tagging) and overcome the irreducible $\gamma\gamma \to b\bar{b}$ background by optimal use of the polarization of the photon beams and by judicious kinematic cuts. Knowledge of the QCD corrections to signal and background processes is essential for this task [122,125].

Using values for ${\rm BR}(h_{\rm SM} \to b\bar{b})$ and ${\rm BR}(h_{\rm SM} \to \gamma\gamma)$ measured at the e^+e^- linear collider, one can obtain a value for the total Higgs width with an error dominated by the expected error in ${\rm BR}(h_{\rm SM} \to \gamma\gamma)$. For heavier Higgs bosons, $m_{h_{\rm SM}} \gtrsim 200$ GeV, the total Higgs width can in principle be measured *directly* by tuning the collider to scan across the Higgs resonance. One can also use the polarization of the photon beams to measure various asymmetries in Higgs production and decay, which are sensitive to the CP quantum numbers of the Higgs boson [123].

3 The Higgs Bosons of Low-Energy Supersymmetry

Electroweak symmetry breaking dynamics driven by a weakly-coupled elementary scalar sector requires a mechanism for the stability of the electroweak symmetry breaking scale with respect to the Planck scale [5]. Supersymmetry-breaking effects, whose origins may lie at energy scales much larger than 1 TeV, can induce a radiative breaking of the electroweak symmetry due to the effects of the large Higgs-top quark Yukawa coupling [126]. In this way, the origin of the electroweak symmetry breaking scale is intimately tied to the mechanism of supersymmetry breaking. Thus, supersymmetry provides an explanation for the stability of the hierarchy of scales, provided that supersymmetry-breaking masses in the low-energy effective electroweak theory are of $\mathcal{O}(1\ {\rm TeV})$ or less [5].

A fundamental theory of supersymmetry-breaking is presently unknown. Nevertheless, one can parameterize the low-energy theory in terms of the most general set of soft-supersymmetry-breaking terms [127]. The simplest realistic model of low-energy supersymmetry is a minimal supersymmetric extension of the Standard Model (MSSM), which employs the minimal supersymmetric particle spectrum. However, even in this minimal model with the most general set of soft-supersymmetry-breaking terms, more than 100 new supersymmetric parameters are introduced [128]. Fortunately, most of these parameters have no impact on Higgs phenomenology. Thus, we will focus primarily on the Higgs sector of the MSSM and identify the parameters that govern the main properties of the Higgs bosons.

3.1 The Tree-Level Higgs Sector of the MSSM

Both hypercharge $Y = -1$ and $Y = +1$ complex Higgs doublets are required in any Higgs sector of an anomaly-free supersymmetric extension of the Standard Model. The supersymmetric structure of the theory also requires (at least) two Higgs doublets to generate mass for both "up"-type and "down"-type quarks (and charged leptons) [6]. Thus, the MSSM contains the particle spectrum of a two-Higgs-doublet extension of the Standard Model and the corresponding supersymmetric partners.

The two-doublet Higgs sector [129] contains eight scalar degrees of freedom: one complex $Y = -1$ doublet, $\boldsymbol{\Phi_d} = (\Phi_d^0, \Phi_d^-)$ and one complex $Y = +1$ doublet, $\boldsymbol{\Phi_u} = (\Phi_u^+, \Phi_u^0)$. The notation reflects the form of the MSSM Higgs sector coupling to fermions: Φ_d^0 [Φ_u^0] couples exclusively to down-type [up-type] fermion pairs. When the Higgs potential is minimized, the neutral components of the Higgs fields acquire vacuum expectation values:[10]

$$\langle \mathbf{\Phi_d} \rangle = \frac{1}{\sqrt{2}} \begin{pmatrix} v_d \\ 0 \end{pmatrix}, \qquad \langle \mathbf{\Phi_u} \rangle = \frac{1}{\sqrt{2}} \begin{pmatrix} 0 \\ v_u \end{pmatrix}, \tag{5}$$

where the normalization has been chosen such that $v^2 \equiv v_d^2 + v_u^2 = 4m_W^2/g^2 = (246\ \mathrm{GeV})^2$. Spontaneous electroweak symmetry breaking results in three Goldstone bosons, which are absorbed and become the longitudinal components of the $W^\pm$ and Z. The remaining five physical Higgs particles consist of a charged Higgs pair

$$H^\pm = \Phi_d^\pm \sin\beta + \Phi_u^\pm \cos\beta\,, \tag{6}$$

one CP-odd scalar

$$A = \sqrt{2}\left(\mathrm{Im}\,\Phi_d^0 \sin\beta + \mathrm{Im}\,\Phi_u^0 \cos\beta\right)\,, \tag{7}$$

and two CP-even scalars:

$$\begin{aligned} h &= -(\sqrt{2}\,\mathrm{Re}\,\Phi_d^0 - v_d)\sin\alpha + (\sqrt{2}\,\mathrm{Re}\,\Phi_u^0 - v_u)\cos\alpha\,, \\ H &= (\sqrt{2}\,\mathrm{Re}\,\Phi_d^0 - v_d)\cos\alpha + (\sqrt{2}\,\mathrm{Re}\,\Phi_u^0 - v_u)\sin\alpha\,, \end{aligned} \tag{8}$$

(with $m_h \leq m_H$). The angle α arises when the CP-even Higgs squared-mass matrix (in the Φ_d^0—Φ_u^0 basis) is diagonalized to obtain the physical CP-even Higgs states (explicit formulae will be given below).

The supersymmetric structure of the theory imposes constraints on the Higgs sector of the model. For example, the Higgs self-interactions are not independent parameters; they can be expressed in terms of the electroweak gauge coupling constants. As a result, all Higgs sector parameters at tree-level are determined by two free parameters: the ratio of the two neutral Higgs field vacuum expectation values,

$$\tan\beta \equiv \frac{v_u}{v_d}\,, \tag{9}$$

[10] The phases of the Higgs fields can be chosen such that the vacuum expectation values are real and positive. That is, the tree-level MSSM Higgs sector conserves CP, which implies that the neutral Higgs mass eigenstates possess definite CP quantum numbers.

and one Higgs mass, conveniently chosen to be m_A. In particular,

$$m_{H^\pm}^2 = m_A^2 + m_W^2 \,, \tag{10}$$

and the CP-even Higgs bosons h and H are eigenstates of the following squared-mass matrix

$$\mathcal{M}_0^2 = \begin{pmatrix} m_A^2 \sin^2\beta + m_Z^2 \cos^2\beta & -(m_A^2 + m_Z^2)\sin\beta\cos\beta \\ -(m_A^2 + m_Z^2)\sin\beta\cos\beta & m_A^2\cos^2\beta + m_Z^2 \sin^2\beta \end{pmatrix} \,. \tag{11}$$

The eigenvalues of $\mathcal{M}_0^2$ are the squared-masses of the two CP-even Higgs scalars

$$m_{H,h}^2 = \tfrac{1}{2}\left(m_A^2 + m_Z^2 \pm \sqrt{(m_A^2 + m_Z^2)^2 - 4m_Z^2 m_A^2 \cos^2 2\beta} \right) \,, \tag{12}$$

and α is the angle that diagonalizes the CP-even Higgs squared-mass matrix. From the above results, one obtains:

$$\cos^2(\beta - \alpha) = \frac{m_h^2(m_Z^2 - m_h^2)}{m_A^2(m_H^2 - m_h^2)} \,. \tag{13}$$

In the convention where $\tan\beta$ is positive (*i.e.*, $0 \leq \beta \leq \pi/2$), the angle α lies in the range $-\pi/2 \leq \alpha \leq 0$.

An important consequence of eq. (12) is that there is an upper bound to the mass of the light CP-even Higgs boson, h. One finds that:

$$m_h \leq m_Z |\cos 2\beta| \leq m_Z \,. \tag{14}$$

This is in marked contrast to the Standard Model, in which the theory does not constrain the value of $m_{h_{\rm SM}}$ at tree-level. The origin of this difference is easy to ascertain. In the Standard Model, $m_{h_{\rm SM}}^2 = \frac{1}{2}\lambda v^2$ is proportional to the Higgs self-coupling λ, which is a free parameter. On the other hand, all Higgs self-coupling parameters of the MSSM are related to the squares of the electroweak gauge couplings.

Note that the Higgs mass inequality [eq. (14)] is saturated in the limit of large m_A. In the limit of $m_A \gg m_Z$, the expressions for the Higgs masses and mixing angle simplify and one finds

$$m_h^2 \simeq m_Z^2 \cos^2 2\beta \,, \tag{15}$$

$$m_H^2 \simeq m_A^2 + m_Z^2 \sin^2 2\beta \,, \tag{16}$$

$$m_{H^\pm}^2 = m_A^2 + m_W^2 \,, \tag{17}$$

$$\cos^2(\beta - \alpha) \simeq \frac{m_Z^4 \sin^2 4\beta}{4m_A^4} \,. \tag{18}$$

Two consequences are immediately apparent. First, $m_A \simeq m_H \simeq m_{H^\pm}$, up to corrections of $\mathcal{O}(m_Z^2/m_A)$. Second, $\cos(\beta - \alpha) = 0$ up to corrections of $\mathcal{O}(m_Z^2/m_A^2)$. This limit is known as the *decoupling* limit [130]

because when m_A is large, there exists an effective low-energy theory below the scale of m_A in which the effective Higgs sector consists only of one CP-even Higgs boson, h. As we shall demonstrate below, the tree-level couplings of h are precisely those of the Standard Model Higgs boson when $\cos(\beta-\alpha)=0$. From eq. (18), one can also derive:

$$\cot\alpha = -\tan\beta - \frac{2m_Z^2}{m_A^2}\tan\beta\cos 2\beta + \mathcal{O}\left(\frac{m_Z^4}{m_A^4}\right) . \tag{19}$$

This result will prove useful in evaluating the CP-even Higgs boson couplings to fermion pairs in the decoupling limit.

The phenomenology of the Higgs sector depends in detail on the various couplings of the Higgs bosons to gauge bosons, Higgs bosons and fermions. The couplings of the two CP-even Higgs bosons to W and Z pairs are given in terms of the angles α and β by

$$g_{hVV} = g_V m_V \sin(\beta-\alpha)\,, \qquad\qquad g_{HVV} = g_V m_V \cos(\beta-\alpha)\,, \tag{20}$$

where $g_V \equiv 2m_V/v$ for $V = W$ or Z. There are no tree-level couplings of A or $H^\pm$ to VV. The couplings of V to two neutral Higgs bosons (which must have opposite CP-quantum numbers) are given by $g_{\phi AZ}(p_\phi - p_A)$, where $\phi = h$ or H and the momenta p_ϕ and p_A point into the vertex, and

$$g_{hAZ} = \frac{g\cos(\beta-\alpha)}{2\cos\theta_W}\,, \qquad\qquad g_{HAZ} = \frac{-g\sin(\beta-\alpha)}{2\cos\theta_W}\,. \tag{21}$$

From the expressions above, we see that the following sum rules must hold separately for $V = W$ and Z:

$$g_{HVV}^2 + g_{hVV}^2 = g_V^2 m_V^2\,, \tag{22}$$

$$g_{hAZ}^2 + g_{HAZ}^2 = \frac{g^2}{4\cos^2\theta_W}\,, \tag{23}$$

$$g_{\phi ZZ}^2 + 4m_Z^2 g_{\phi AZ}^2 = \frac{g^2 m_Z^2}{\cos^2\theta_W}\,, \qquad \phi = h, H\,. \tag{24}$$

Similar considerations also hold for the coupling of h and H to $W^\pm H^\mp$. Four-point couplings of vector bosons and Higgs bosons can be found in ref. [2]. The properties of the three-point and four-point Higgs boson-vector boson couplings are conveniently summarized by listing the couplings that are proportional

to either $\sin(\beta-\alpha)$ or $\cos(\beta-\alpha)$, and the couplings that are independent of α and β [2]:

$\cos(\beta-\alpha)$	$\sin(\beta-\alpha)$	angle-independent
HW^+W^-	hW^+W^-	—
HZZ	hZZ	—
ZAh	ZAH	ZH^+H^- , γH^+H^-
$W^\pm H^\mp h$	$W^\pm H^\mp H$	$W^\pm H^\mp A$
$ZW^\pm H^\mp h$	$ZW^\pm H^\mp H$	$ZW^\pm H^\mp A$
$\gamma W^\pm H^\mp h$	$\gamma W^\pm H^\mp H$	$\gamma W^\pm H^\mp A$
—	—	$VV\phi\phi$, $VVAA$, VVH^+H^-

(25)

where $\phi = h$ or H and $VV = W^+W^-$, ZZ, $Z\gamma$ or $\gamma\gamma$. Note in particular that *all* vertices in the theory that contain at least one vector boson and *exactly one* non-minimal Higgs boson state (H, A or $H^\pm$) are proportional to $\cos(\beta-\alpha)$. This can be understood as a consequence of unitarity sum rules which must be satisfied by the tree-level amplitudes of the theory [24,25,131,132].

In the MSSM, the tree-level Higgs couplings to fermions obey the following property: Φ_d^0 couples exclusively to down-type fermion pairs and Φ_u^0 couples exclusively to up-type fermion pairs. This pattern of Higgs-fermion couplings defines the Type-II two-Higgs-doublet model [133,2]. The gauge-invariant Type-II Yukawa interactions (using 3rd family notation) are given by:

$$-\mathcal{L}_{\rm Yukawa} = h_t\left[\bar{t}P_L t\Phi_u^0 - \bar{t}P_L b\Phi_u^+\right] + h_b\left[\bar{b}P_L b\Phi_d^0 - \bar{b}P_L t\Phi_d^-\right] + \text{h.c.}\,, \tag{26}$$

where $P_L \equiv \frac{1}{2}(1-\gamma_5)$ is the left-handed projection operator. [Note that $(\overline{\Psi}_1 P_L \Psi_2)^\dagger = \overline{\Psi}_2 P_R \Psi_1$, where $P_R \equiv \frac{1}{2}(1+\gamma_5)$.] Fermion masses are generated when the neutral Higgs components acquire vacuum expectation values. Inserting eq. (5) into eq. (26) yields a relation between the quark masses and the Yukawa couplings:

$$h_b = \frac{\sqrt{2}\,m_b}{v_d} = \frac{\sqrt{2}\,m_b}{v\cos\beta}\,, \qquad\qquad h_t = \frac{\sqrt{2}\,m_t}{v_u} = \frac{\sqrt{2}\,m_t}{v\sin\beta}\,. \tag{27}$$

Similarly, one can define the Yukawa coupling of the Higgs boson to τ-leptons (the latter is a down-type fermion). The couplings of the physical Higgs bosons to the third generation fermions is obtained from eq. (26) by using eqs. (6)–(8). In particular, the couplings of the neutral Higgs bosons to $f\bar{f}$ relative to the Standard Model value, $gm_f/2m_W$, are given by

$$hb\bar{b} \quad (\text{or } h\tau^+\tau^-): \quad -\frac{\sin\alpha}{\cos\beta} = \sin(\beta-\alpha) - \tan\beta\cos(\beta-\alpha)\,, \tag{28}$$

$$ht\bar{t}: \quad \frac{\cos\alpha}{\sin\beta} = \sin(\beta-\alpha) + \cot\beta\cos(\beta-\alpha)\,, \tag{29}$$

$$Hb\bar{b} \quad (\text{or } H\tau^+\tau^-): \qquad \frac{\cos\alpha}{\cos\beta} = \cos(\beta-\alpha) + \tan\beta\sin(\beta-\alpha)\,, \tag{30}$$

$$Ht\bar{t}: \qquad \frac{\sin\alpha}{\sin\beta} = \cos(\beta-\alpha) - \cot\beta\sin(\beta-\alpha)\,, \tag{31}$$

$$Ab\bar{b} \quad (\text{or } A\tau^+\tau^-): \qquad \gamma_5\tan\beta\,, \tag{32}$$

$$At\bar{t}: \qquad \gamma_5\cot\beta\,, \tag{33}$$

(the γ_5 indicates a pseudoscalar coupling), and the charged Higgs boson couplings to fermion pairs, with all particles pointing into the vertex, are given by

$$g_{H^-t\bar{b}} = \frac{g}{\sqrt{2}m_W}\left[m_t\cot\beta\,P_R + m_b\tan\beta\,P_L\right], \tag{34}$$

$$g_{H^-\tau^+\nu} = \frac{g}{\sqrt{2}m_W}\left[m_\tau\tan\beta\,P_L\right]. \tag{35}$$

We next examine the behavior of the Higgs couplings at large $\tan\beta$. This limit is of particular interest since at large $\tan\beta$, some of the Higgs couplings to down-type fermions can be significantly enhanced.[11] Consider two large $\tan\beta$ regions of interest: *(i)* If $m_A \gg m_Z$, then the decoupling limit is reached, in which $|\cos(\beta-\alpha)| \ll 1$ and $m_H \simeq m_A$. From eqs. (18)–(33), it follows that the $b\bar{b}H$ and $b\bar{b}A$ couplings have equal strength and are significantly enhanced (by a factor of $\tan\beta$) relative to the $b\bar{b}h_{\rm SM}$ coupling, whereas the VVH coupling is negligibly small. In contrast, the values of the VVh and $b\bar{b}h$ couplings are equal to the corresponding couplings of the Standard Model Higgs boson. To show that the value of the $b\bar{b}h$ coupling [eq. (28)] reduces to that of $b\bar{b}h_{\rm SM}$ in the decoupling limit, note that eq. (18) implies that $|\tan\beta\cos(\beta-\alpha)| \ll 1$ when $m_A \gg m_Z$ even when $\tan\beta \gg 1$. Indeed, h is a SM-like Higgs boson. *(ii)* If $m_A \lesssim m_Z$ and $\tan\beta \gg 1$, then $|\cos(\beta-\alpha)| \sim 1$ [see fig. 11] and $m_h \simeq m_A$. In this case, the $b\bar{b}h$ and $b\bar{b}A$ couplings have equal strength and are significantly enhanced (by a factor of $\tan\beta$) relative to the $b\bar{b}h_{\rm SM}$ coupling, while the VVh coupling is negligibly small. Using eq. (22) it follows that the VVH coupling is equal in strength to the $VVh_{\rm SM}$ coupling. In this case, it is conventional to refer to H as a SM-like Higgs boson. However, this nomenclature is somewhat inaccurate, since the value of the $b\bar{b}H$ coupling can differ from the corresponding $b\bar{b}h_{\rm SM}$ coupling when $\tan\beta \gg 1$ [since in case *(ii)*, where $|\sin(\beta-\alpha)| \ll 1$, the product $\tan\beta\sin(\beta-\alpha)$ need not be particularly small]. Note that in both cases *(i)* and *ii)* above, only two of the three neutral Higgs bosons have enhanced couplings to $b\bar{b}$.

The decoupling limit of $m_A \gg m_Z$ is effective for all values of $\tan\beta$. It is easy to check that the pattern of all Higgs couplings displayed in eqs. (20)–(33) respect the decoupling limit. That is, in the

[11] In models of low-energy supersymmetry, there is some theoretical prejudice that suggests that $1 < \tan\beta \lesssim m_t/m_b$, with the fermion running masses evaluated at the electroweak scale. For example, $\tan\beta \lesssim 1$ [$\tan\beta > m_t/m_b$] is disfavored since in this case, the Higgs–top-quark [Higgs–bottom-quark] Yukawa coupling blows up at an energy scale significantly below the Planck scale.

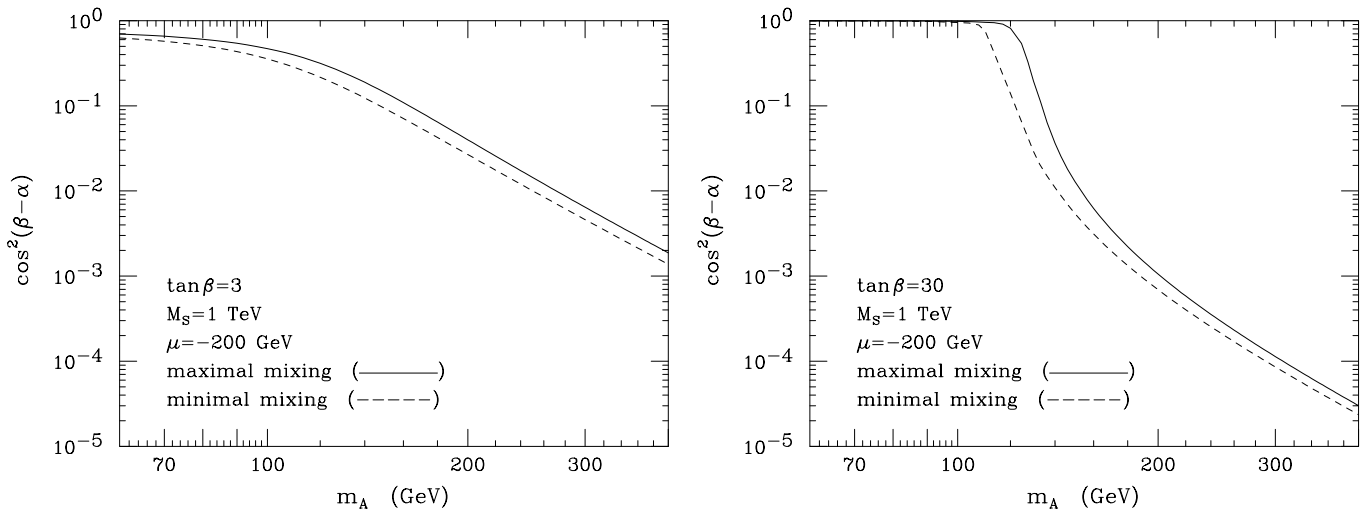

Figure 11: The value of $\cos^2(\beta-\alpha)$ is shown as a function of m_A for two choices of $\tan\beta = 3$ and $\tan\beta = 30$. When radiative-corrections are included, one can define an approximate loop-corrected angle α as a function of m_A, $\tan\beta$ and the MSSM parameters. In the figures above, we have incorporated radiative corrections, assuming that $M_{\rm SUSY} \equiv M_Q = M_U = M_D = 1$ TeV. In addition, two extreme cases for the squark mixing parameters are shown (see Sections 3.2 and 3.3 for further discussion of the radiative corrections and their dependence on the supersymmetric parameters). The decoupling effect expected from eq. (18), in which $\cos^2(\beta-\alpha) \propto m_Z^4/m_A^4$ for $m_A \gg m_Z$, continues to hold even when radiative corrections are included.

limit where $m_A \gg m_Z$, $\cos(\beta-\alpha) = \mathcal{O}(m_Z^2/m_A^2)$, which means that the h couplings to Standard Model particles approach values corresponding precisely to the couplings of the SM Higgs boson. There is a significant region of MSSM Higgs sector parameter space in which the decoupling limit applies, because $\cos(\beta-\alpha)$ approaches zero quite rapidly once m_A is larger than about 200 GeV, as shown in fig. 11. As a result, over a significant region of the MSSM parameter space, the search for the lightest CP-even Higgs boson of the MSSM is equivalent to the search for the Standard Model Higgs boson. This result is more general; in many theories of non-minimal Higgs sectors, there is a significant portion of the parameter space that approximates the decoupling limit. Consequently, simulations of the Standard Model Higgs signal are also relevant for exploring the more general Higgs sector.

3.2 Radiatively-Corrected MSSM Higgs Masses

The discussion of Section 3.1 was based on a tree-level analysis of the Higgs sector. However, radiative corrections can have a significant impact on the predicted values of Higgs masses and couplings. The radiative corrections involve both loops of Standard Model particles and loops of supersymmetric part-

ners. The dominant effects arise from loops involving the third generation quarks and squarks and are proportional to the corresponding Yukawa couplings. Thus, we first review the parameters that control the masses and mixing of the third-generation squarks. (We shall neglect intergenerational mixing effects, which have little impact on the discussion that follows.)

For each left-handed and right-handed quark of fixed flavor, q, there is a corresponding supersymmetric partner $\widetilde{q}_L$ and $\widetilde{q}_R$, respectively. These are the so-called interaction eigenstates, which mix according to the squark squared-mass matrix. The mixing angle that diagonalizes the squark mass matrix will be denoted by $\theta_{\widetilde{q}}$. The squark mass eigenstates, denoted by $\widetilde{q}_1$ and $\widetilde{q}_2$, are obtained by diagonalizing the following 2×2 matrix

$$\begin{pmatrix} M_Q^2 + m_f^2 + D_L & m_f X_f \\ m_f X_f & M_R^2 + m_f^2 + D_R \end{pmatrix} , \tag{36}$$

where $D_L \equiv (T_{3f} - e_f \sin^2\theta_W) m_Z^2 \cos 2\beta$ and $D_R \equiv e_f \sin^2\theta_W m_Z^2 \cos 2\beta$. In addition, $f = t$, $M_R \equiv M_U$, $e_t = 2/3$ and $T_{3f} = 1/2$ for the top-squark squared-mass matrix, and $f = b$, $M_R \equiv M_D$, $e_b = -1/3$ and $T_{3f} = -1/2$ for the bottom-squark squared-mass matrix. The squark mixing parameters are given by

$$X_t \equiv A_t - \mu \cot\beta \,, \qquad\qquad X_b \equiv A_b - \mu \tan\beta \,. \tag{37}$$

Thus, the top-squark and bottom-squark masses and mixing angles depend on the supersymmetric Higgsino mass parameter μ and the soft-supersymmetry-breaking parameters: M_Q, M_U, M_D, A_t and A_b. For simplicity, we shall initially assume that A_t, A_b and μ are real parameters. That is, we neglect possible CP-violating effects that can enter the MSSM Higgs sector via radiative corrections. The impact on new MSSM sources of CP-violation on the Higgs sector will be addressed in Section 3.2.3.

3.2.1 Radiatively-corrected Higgs masses in the CP-conserving MSSM

The radiative corrections to the Higgs squared-masses have been computed by a number of techniques, and using a variety of approximations such as the effective potential at one-loop [134,135,136] and two-loops [137,138,139,140] , and diagrammatic methods [141,142,143,144,145,146]. Complete one-loop diagrammatic computations of the MSSM Higgs masses have been presented by a number of groups [143,144]; and partial two-loop diagrammatic results are also known [145,146]. These include the $\mathcal{O}(m_t^2 h_t^2 \alpha_s)$ contributions to the neutral CP-even Higgs boson squared-masses in the on-shell scheme [146]. Finally, renormalization group methods (to be discussed further below) provide a powerful technique for identifying many of the most important contributions to the radiatively corrected Higgs masses [147,148,149,150]. Typical results for the radiatively corrected value of m_h as a function of the relevant supersymmetric parameters are shown in fig. 12.

One of the most striking effects of the radiative corrections to the MSSM Higgs sector is the modification of the upper bound of the light CP-even Higgs mass, as first noted in refs. [134] and [141]. Consider the region of parameter space where $\tan\beta$ is large and $m_A \gg m_Z$. In this limit, the *tree-level*

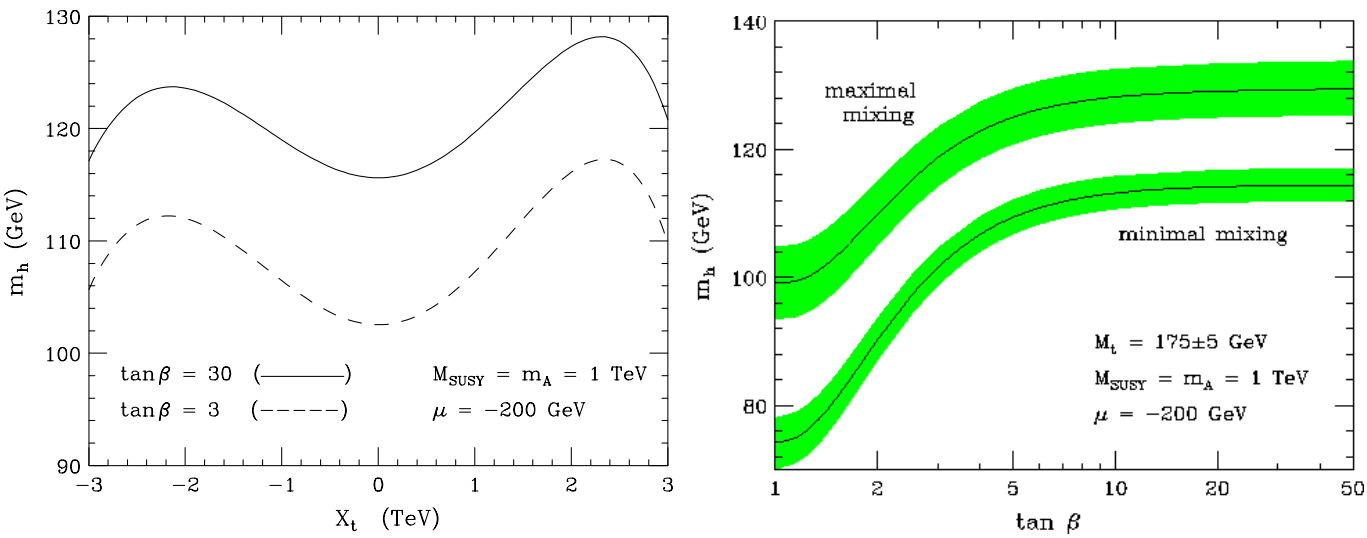

Figure 12: The radiatively corrected light CP-even Higgs mass is plotted (a) as a function of X_t, where $X_t \equiv A_t - \mu \cot\beta$, for $M_t = 174.3$ GeV and two choices of $\tan\beta = 3$ and 30, and (b) as a function of $\tan\beta$, for the maximal mixing [upper band] and minimal mixing [lower band] benchmark cases. In (b), the central value of the shaded bands corresponds to $M_t = 175$ GeV, while the upper [lower] edge of the bands correspond to increasing [decreasing] M_t by 5 GeV. In both (a) and (b), $m_A = 1$ TeV and the diagonal soft squark squared-masses are assumed to be degenerate: $M_{\rm SUSY} \equiv M_Q = M_U = M_D = 1$ TeV.

prediction for m_h corresponds to its theoretical upper bound, $m_h = m_Z$. Including radiative corrections, the theoretical upper bound is increased. The dominant effect arises from an incomplete cancellation[12] of the top-quark and top-squark loops (these effects cancel in the exact supersymmetric limit). The qualitative behavior of the radiative corrections can be most easily seen in the large top squark mass limit, where in addition, the splitting of the two diagonal entries and the off-diagonal entry of the top-squark squared-mass matrix are both small in comparison to the average of the two top-squark squared-masses:

$$M_{\rm S}^2 \equiv \tfrac{1}{2}(M_{\tilde{t}_1}^2 + M_{\tilde{t}_2}^2)\,. \tag{38}$$

In this case, the upper bound on the lightest CP-even Higgs mass is approximately given by

$$m_h^2 \lesssim m_Z^2 + \frac{3g^2 m_t^4}{8\pi^2 m_W^2}\left[\ln\left(\frac{M_S^2}{m_t^2}\right) + \frac{X_t^2}{M_S^2}\left(1 - \frac{X_t^2}{12 M_S^2}\right)\right]\,. \tag{39}$$

[12] In certain regions of parameter space (corresponding to large $\tan\beta$ and large values of μ), the incomplete cancellation of the bottom-quark and bottom-squark loops can be as important as the corresponding top sector contributions. For simplicity, we ignore this contribution in eq. (39).

The more complete treatments of the radiative corrections cited above show that eq. (39) somewhat overestimates the true upper bound of m_h. Nevertheless, eq. (39) correctly reflects some noteworthy features of the more precise result. First, the increase of the light CP-even Higgs mass bound beyond m_Z can be significant. This is a consequence of the m_t^4 enhancement of the one-loop radiative correction. Second, the dependence of the light Higgs mass on the top-squark mixing parameter X_t implies that (for a given value of $M_{\rm S}$) the upper bound of the light Higgs mass initially increases with X_t and reaches its *maximal* value for $X_t = \sqrt{6}M_{\rm S}$. This point is referred to as the *maximal mixing* case (whereas $X_t = 0$ corresponds to the *minimal mixing* case). In a more complete computation that includes both two-loop logarithmic and non-logarithmic corrections, the X_t values corresponding to maximal and minimal mixing are shifted and exhibit an asymmetry under $X_t \to -X_t$ as shown in fig. 12. In the numerical analysis presented in this and subsequent figures in this section, we assume for simplicity that the third generation diagonal soft-supersymmetry-breaking squark squared-masses are degenerate: $M_{\rm SUSY} \equiv M_Q = M_U = M_D$, which defines the parameter $M_{\rm SUSY}$.[13]

Third, note the logarithmic sensitivity to the top-squark masses. Naturalness arguments that underlie low-energy supersymmetry imply that the supersymmetric particle masses should not be larger than a few TeV. Still, the precise upper bound on the light Higgs mass depends on the specific choice for the upper limit of the top-squark masses. The dependence of the light Higgs mass obtained by the more complete computation as a function of $M_{\rm SUSY}$ is shown in fig. 13.[14]

As noted above, the largest contribution to the one-loop radiative corrections is enhanced by a factor of m_t^4 and grows logarithmically with the top squark mass. Thus, higher order radiative corrections can be non-negligible for large top squark masses, in which case the large logarithms must be resummed. Renormalization group (RG) techniques for resumming the leading logarithms have been developed by a number of authors [147,148,149]. The computation of the RG-improved one-loop corrections requires numerical integration of a coupled set of RG equations [148]. Although this procedure has been carried out in the literature, the analysis is unwieldy and not easily amenable to large-scale Monte-Carlo studies. It turns out that over most of the parameter range, it is sufficient to include the leading and sub-leading logarithms at two-loop order. (Some additional non-logarithmic terms, which cannot be ascertained by the renormalization group method, must also be included [151].) Compact analytic expressions have been obtained for the dominant one and two-loop contributions to the matrix elements of the radiatively-corrected CP-even Higgs squared-mass matrix:

$$\mathcal{M}^2 \equiv \begin{pmatrix} \mathcal{M}^2_{11} & \mathcal{M}^2_{12} \\ \mathcal{M}^2_{12} & \mathcal{M}^2_{22} \end{pmatrix} = \mathcal{M}^2_0 + \delta\mathcal{M}^2\,, \tag{40}$$

where the tree-level contribution $\mathcal{M}^2_0$ was given in eq. (11) and $\delta\mathcal{M}^2$ is the contribution from the

[13] We also assume that $M_{\rm SUSY} \gg m_t$, in which case it follows that $M_S^2 \simeq M^2_{\rm SUSY}$ up to corrections of $\mathcal{O}(m_t^2/M^2_{\rm SUSY})$.

[14] The flattening of the curves in fig. 13 as a function of $M_{\rm SUSY}$ in the maximal mixing scenario is due to the squark-mixing contributions at two-loops which partially cancel the contributions that grow logarithmically with $M_{\rm SUSY}$.

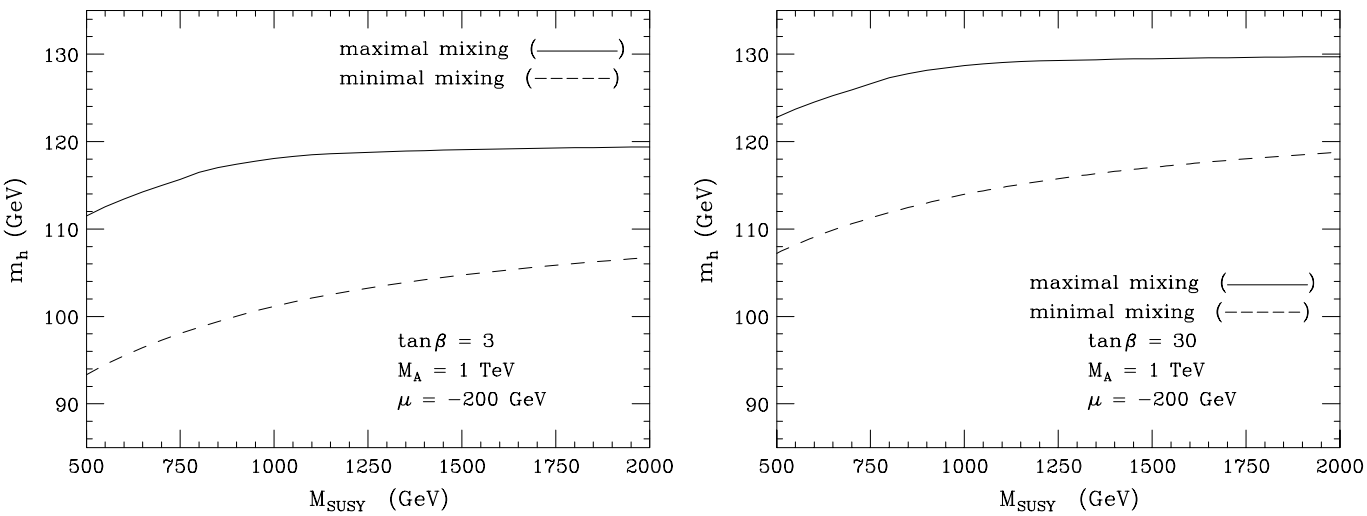

Figure 13: The radiatively corrected light CP-even Higgs mass is plotted as a function of $M_{\rm SUSY} \equiv M_Q = M_U = M_D$, for $M_t = 174.3$ GeV, $m_A = 1$ TeV and two choices of $\tan\beta = 3$ and $\tan\beta = 30$. Maximal mixing and minimal mixing are defined according to the value of X_t that yields the maximal and minimal Higgs mass as shown in fig. 12(a).

radiative corrections. The dominant corrections to $\mathcal{M}^2$, coming from the one-loop top and bottom quark and top and bottom squark contributions plus the two-loop leading logarithmic contributions, are given to $\mathcal{O}(h_t^4, h_b^4)$ by [149,150,152]

$$\delta\mathcal{M}^2_{11} \simeq -\bar{\mu}^2 x_t^2 \frac{h_t^4 v^2}{32\pi^2} s_\beta^2 \left[1 + c_{11} \ln\left(\frac{M_S^2}{m_t^2}\right)\right] - \bar{\mu}^2 a_b^2 \frac{h_b^4 v^2}{32\pi^2} s_\beta^2 \left[1 + c_{12} \ln\left(\frac{M_S^2}{m_t^2}\right)\right], \tag{41}$$

$$\delta\mathcal{M}^2_{12} \simeq -\bar{\mu} x_t \frac{h_t^4 v^2}{32\pi^2} (6 - x_t a_t) s_\beta^2 \left[1 + c_{31} \ln\left(\frac{M_S^2}{m_t^2}\right)\right] + \bar{\mu}^3 a_b \frac{h_b^4 v^2}{32\pi^2} s_\beta^2 \left[1 + c_{32} \ln\left(\frac{M_S^2}{m_t^2}\right)\right], \tag{42}$$

$$\begin{aligned}\delta\mathcal{M}^2_{22} \simeq\ & \frac{3 h_t^4 v^2}{8\pi^2} s_\beta^2 \ln\left(\frac{M_S^2}{m_t^2}\right) \left[1 + \tfrac{1}{2} c_{21} \ln\left(\frac{M_S^2}{m_t^2}\right)\right] \\ & + \frac{h_t^4 v^2}{32\pi^2} s_\beta^2 x_t a_t (12 - x_t a_t) \left[1 + c_{21} \ln\left(\frac{M_S^2}{m_t^2}\right)\right] - \bar{\mu}^4 \frac{h_b^4 v^2}{32\pi^2} s_\beta^2 \left[1 + c_{22} \ln\left(\frac{M_S^2}{m_t^2}\right)\right],\end{aligned} \tag{43}$$

where $s_\beta \equiv \sin\beta$, $c_\beta \equiv \cos\beta$, and the coefficients c_{ij} are:

$$c_{ij} \equiv \frac{t_{ij} h_t^2 + b_{ij} h_b^2 - 32 g_3^2}{32\pi^2}, \tag{44}$$

$(t_{11}, t_{12}, t_{21}, t_{22}, t_{31}, t_{32}) = (12, -4, 6, -10, 9, -7)$ and $(b_{11}, b_{12}, b_{21}, b_{22}, b_{31}, b_{32}) = (-4, 12, 2, 18, -1, 15)$. Above, h_t and h_b are the top and bottom quark Yukawa couplings [see eqs. (55)–(57)], g_3 is the strong QCD coupling, $v = 246$ GeV is the SM Higgs vacuum expectation value, and $M_S^2 = \frac{1}{2}(M_{\tilde{t}_1}^2 + M_{\tilde{t}_2}^2)$ is the average squared top squark mass.[15] The $\delta\mathcal{M}_{ij}^2$ also depend on the MSSM parameters A_t, A_b and μ that enter the off-diagonal top-squark and bottom-squark squared-mass matrices. We employ the following notation: $\bar{\mu} \equiv \mu/M_S$, $a_t \equiv A_t/M_S$, $a_b \equiv A_b/M_S$ and $x_t \equiv X_t/M_S$, where $X_t \equiv A_t - \mu\cot\beta$. Diagonalizing the CP-even Higgs squared-mass matrix yields radiatively-corrected values for m_h^2, m_H^2 and the mixing angle α.[16] The end result is a prediction for the Higgs mass in terms of running parameters in the $\overline{\rm MS}$ scheme. It is a simple matter to relate these parameters to the corresponding on-shell parameters used in the diagrammatic calculations [138,151].

Additional non-logarithmic two-loop contributions, which can generate a non-negligible shift in the Higgs mass (of a few GeV), must also be included.[17] A compact analytical expression that incorporates these effects at $\mathcal{O}(m_t^2 h_t^2 \alpha_s)$ was given in ref. [154] (with further refinements provided by ref. [155] to take into account the possibility of arbitrary top-squark splitting), and the corresponding corrections proportional to $h_b^2\alpha_s$ can be found in ref. [140]. An important source of such contributions are the one-loop supersymmetric threshold corrections to the relation between the Higgs–top-quark and Higgs–bottom-quark Yukawa couplings and the corresponding quark masses [eqs. (56) and (57)]. These generate a non-logarithmic two-loop shift of the radiatively corrected Higgs mass proportional to the corresponding squark mixing parameters. One consequence of these contributions [151] is the asymmetry in the predicted value of m_h under $X_t \to -X_t$ as noted in fig. 12(a). Recently, the computation of m_h has been further refined by the inclusion of genuine two-loop corrections of $\mathcal{O}(m_t^2 h_t^4)$ [139], and estimates of the two-loop corrections proportional to $h_b^2 h_t^2$ and h_b^4 [140] (which can be numerically relevant for values of $\tan\beta \gtrsim m_t/m_b$). These non-logarithmic corrections, which depend on the third generation squark mixing parameters, can slightly increase the value of the radiatively-corrected Higgs mass.

The numerical results displayed in figs. 11–14 are based on the calculations of refs. [149] and [150], with improvements as described in refs. [146] and [151]. The supersymmetric parameters in the maximal and minimal mixing cases have been chosen according to the first two benchmark scenarios of ref. [156]. Of particular interest is the upper bound for the lightest CP-even Higgs mass (m_h). At fixed $\tan\beta$, the maximal value of m_h is reached for $m_A \gg m_Z$ (see fig. 14). Taking m_A large, fig. 12(b) illustrates that the maximal value of the lightest CP-even Higgs mass bound is realized at large $\tan\beta$ in the case of

[15] Eqs. (41)–(43) have been derived under the assumption that $|M_{\tilde{t}_1}^2 - M_{\tilde{t}_2}^2|/(M_{\tilde{t}_1}^2 + M_{\tilde{t}_2}^2) \ll 1$. The approximate forms of eqs. (41)–(43) are sufficient to provide insight on the dependence of the radiatively-corrected Higgs masses and couplings on the MSSM parameters, although our numerical work is based on more exact forms for these expressions.

[16] Although $\mathcal{M}_{12}^2$ is *negative* at tree level (implying that $-\pi/2 \leq \alpha \leq 0$), it is possible that radiative corrections flip the sign of $\mathcal{M}_{12}^2$. Thus, the range of the radiatively corrected angle α can be taken to be $-\pi/2 \leq \alpha \leq \pi/2$.

[17] An improved procedure for computing the radiatively-corrected neutral Higgs mass matrix and the charged Higgs mass in a self-consistent way (including possible CP-violating effects), which incorporates one-loop supersymmetric threshold corrections to the Higgs–top-quark and Higgs–bottom-quark Yukawa couplings, can be found in ref. [153].

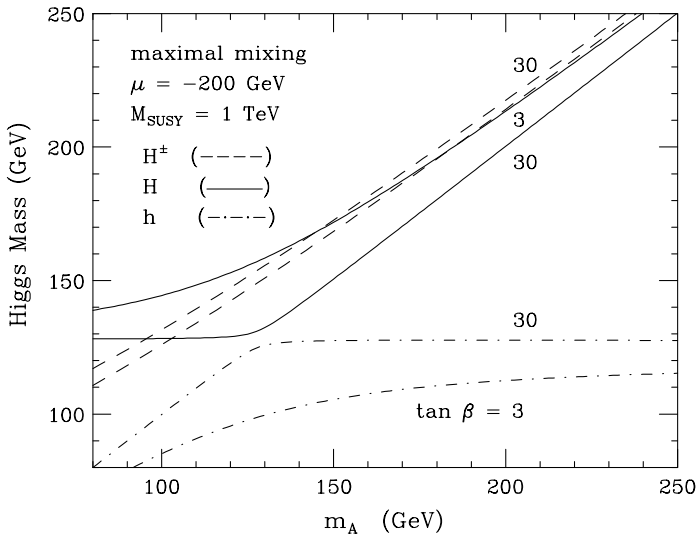

Figure 14: Lightest CP-even Higgs mass (m_h), heaviest CP-even Higgs mass (m_H) and charged Higgs mass ($m_{H^\pm}$) as a function of m_A for two choices of $\tan\beta = 3$ and $\tan\beta = 30$. Here, we have taken $M_t = 174.3$ GeV, and we have assumed that the diagonal soft squark squared-masses are degenerate: $M_{\rm SUSY} \equiv M_Q = M_U = M_D = 1$ TeV. In addition, we choose the other supersymmetric parameters corresponding to the maximal mixing scenario. The slight increase in the charged Higgs mass as $\tan\beta$ is increased from 3 to 30 is a consequence of the radiative corrections.

maximal mixing. For each value of $\tan\beta$, we denote the maximum value of m_h by $m_h^{\rm max}(\tan\beta)$ [this value also depends on the third-generation squark mixing parameters]. Allowing for the uncertainty in the measured value of m_t and the uncertainty inherent in the theoretical analysis, one finds for $M_{\rm SUSY} \lesssim 2$ TeV that $m_h \leq m_h^{\rm max} \equiv m_h^{\rm max}(\tan\beta \gg 1)$, where

$$\begin{aligned} m_h^{\rm max} &\simeq 122 \text{ GeV}, \quad \text{if top-squark mixing is minimal,} \\ m_h^{\rm max} &\simeq 135 \text{ GeV}, \quad \text{if top-squark mixing is maximal.} \end{aligned} \tag{45}$$

In practice, parameters leading to maximal mixing are not expected in typical models of supersymmetry breaking. Thus, in general, the upper bound on the lightest Higgs boson mass is expected to be somewhere between the two extreme limits quoted above. Cross-checks among various programs [157] and rough estimates of higher order corrections not yet computed suggest that the results for Higgs masses should be accurate to within about 2 to 3 GeV over the parameter ranges displayed in figs. 12–14.

In fig. 14, we exhibit the masses of the CP-even neutral and the charged Higgs masses as a function

of m_A. The squared-masses of the lighter and heavier neutral CP-even Higgs are related by[18]

$$m_H^2 \cos^2(\beta - \alpha) + m_h^2 \sin^2(\beta - \alpha) = [m_h^{\max}(\tan\beta)]^2 \,. \tag{46}$$

It is interesting to consider the behavior of the CP-even Higgs masses in the large $\tan\beta$ regime. For large values of $\tan\beta$ and for $m_A/\tan\beta \ll m_h^{\max}(\tan\beta)$, the off-diagonal elements of the Higgs squared-mass matrix $\mathcal{M}^2$ become small compared to the diagonal elements $|\mathcal{M}_{12}^2| \ll \mathcal{M}_{11}^2 + \mathcal{M}_{22}^2$; $\mathcal{M}_{12}^4 \ll \mathcal{M}_{11}^2 \mathcal{M}_{22}^2$. Hence the two CP-even Higgs squared-masses are approximately given by the diagonal elements of $\mathcal{M}^2$. As above, we employ the notation where $m_h^{\max}$ refers to the asymptotic value of m_h at large $\tan\beta$ and m_A (the actual numerical value of $m_h^{\max}$ depends primarily on the assumed values of the third generation squark mass and mixing parameters). If $m_A > m_h^{\max}$, then $m_h \simeq m_h^{\max}$ and $m_H \simeq m_A$, whereas if $m_A < m_h^{\max}$, then $m_h \simeq m_A$ and $m_H \simeq m_h^{\max}$. This behavior can be seen in fig. 14.

3.2.2 MSSM Higgs mass limits after LEP

No significant evidence for a Higgs signal has been detected at LEP [161]. As a result, one can obtain bounds on the possible MSSM Higgs parameters. These limits are often displayed in the m_A–$\tan\beta$ plane, although there is additional dependence on various MSSM parameters that effect the radiative corrections to the Higgs masses as discussed above. In representative scans of the MSSM parameters, the LEP Higgs Working Group [161] finds that $m_h > 91.0$ GeV and $m_A > 91.9$ GeV at 95% CL. These limits actually correspond to the large $\tan\beta$ region in which Zh production is suppressed, as shown in fig. 15. In this case, the quoted Higgs limits arise as a result of the non-observation of hA and HA production. As $\tan\beta$ is lowered, the limits on m_h and m_A become more stringent. In this regime, the hA production is suppressed while the Zh production rate approaches its SM value. Thus, in this case, the SM Higgs limit applies ($m_h \gtrsim 114$ GeV) as shown in fig. 15(a). The precise region of MSSM Higgs parameter space that is excluded depends on the values of the MSSM parameters that control the Higgs mass radiative corrections. For example, a conservative exclusion limit is obtained in the maximal mixing scenario, since in this case the predicted value of m_h as a function of m_A and $\tan\beta$ is maximal (with respect to changes in the other MSSM parameters). The excluded regions of the MSSM Higgs parameter space based on the maximal mixing benchmark scenario of ref. [156], are shown in fig. 15, and correspond to the exclusion of the range $0.5 < \tan\beta < 2.4$ at the 95% CL. However, the $\tan\beta$ exclusion region can still be significantly reduced (even to the point of allowing all $\tan\beta$ values) by, *e.g.*, taking $M_{\rm SUSY} = 2$ TeV and $m_t = 180$ GeV (which still lies within the error bars of the experimentally measured value), and allowing for the theoretical uncertainty in the prediction of $m_h^{\max}$ [162].

[18] At tree level, eq. (46) is a consequence of the sum rule: $\sum_n m_{\phi_n}^2 g_{\phi_n ZZ}^2 = \frac{4}{3} m_Z^4 g_{GGGG}$, first derived in ref. [131], where the ϕ_n are neutral Higgs bosons of a multi-Higgs-doublet model and g_{GGGG} is the quartic coupling of neutral Goldstone bosons. (In the MSSM, $g_{GGGG} = \frac{3}{4} g^2 \cos^2 2\beta / \cos^2\theta_W$ [2].) A general discussion of related tree-level Higgs mass sum rules and bounds can be found in ref. [158]. In fact, eq. (46) is more general and applies to the radiatively-corrected MSSM Higgs sector [159,160] in the approximation where the renormalized α is determined as discussed in Section 3.3.1.

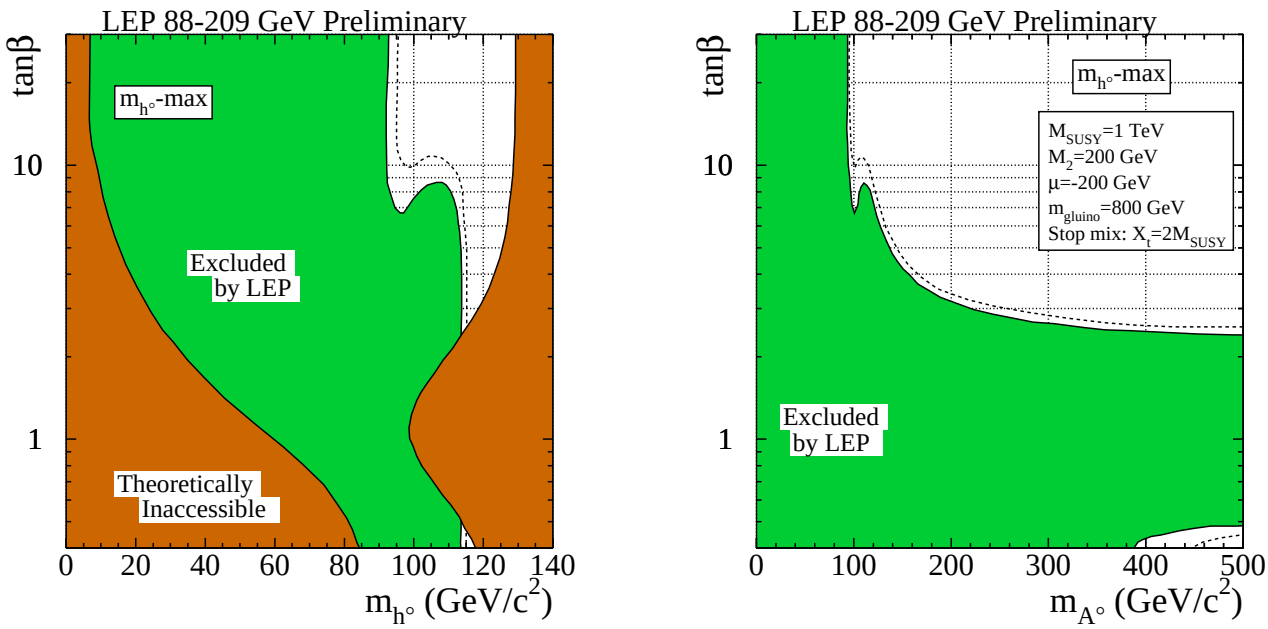

Figure 15: LEP2 contours of the 95% CL exclusion limits for MSSM Higgs sector parameters as a function of tan β and (a) m_h and (b) m_A (in GeV), taken from ref. [161]. The contours shown have been obtained for MSSM Higgs parameters chosen according to the maximal mixing benchmark of ref. [156].

No evidence for the charged Higgs boson has yet been found. The LEP Higgs Working Group quotes a limit of $m_{H^\pm} > 78.6$ GeV at 95% CL [163], which holds for a more general non-supersymmetric two-Higgs doublet model and assumes only that the H^+ decays dominantly into $\tau^+\nu_\tau$ and/or $c\bar{s}$. Although the MSSM tree-level bound $m_{H^\pm} \geq m_W$ can be relaxed somewhat by radiative corrections, the LEP bound quoted above provides no useful additional constraints on the MSSM Higgs sector.

3.2.3 Effect of explicit CP-violation on the radiatively-corrected MSSM Higgs masses

In the Standard Model, CP-violation is due to the existence of phases in the Yukawa couplings of the quarks to the Higgs field, which results in one non-trivial phase in the CKM mixing matrix. In the MSSM, there are additional sources of CP-violation, due to phases in the various supersymmetric mass parameters. In particular, the gaugino mass parameters (M_i, $i = 1, 2, 3$), the Higgsino mass parameter, μ, the bilinear Higgs squared-mass parameter, m_{12}^2, and the trilinear couplings of the squark and slepton fields ($\tilde{f}$) to the Higgs fields, A_f, may carry non-trivial phases. The existence of these CP phases can

significantly affect the MSSM Higgs sector through one-loop radiative corrections [164,165,166,153].

Note that if one sets $\mu = M_i = A_f = m_{12}^2$, then the MSSM Lagrangian possesses two independent global U(1) symmetries—a Peccei-Quinn (PQ) symmetry and an R symmetry. (The quantum numbers of the MSSM fields with respect to $\mathrm{U}(1)_{\mathrm{PQ}}$ and $\mathrm{U}(1)_{\mathrm{R}}$ can be found in refs. [167] and [166].) Consequently, in the MSSM with nonzero values for the above parameters, there are two independent phase redefinitions of the fields that can be used to remove two phases from μ, M_i, A_f and m_{12}^2. However, certain combinations of these parameters remain invariant under such phase redefinitions. The simplest way to determine these combinations is to treat the aforementioned parameters as spurions with quantum numbers under the $\mathrm{U}(1)_{\mathrm{PQ}}$ and $\mathrm{U}(1)_{\mathrm{R}}$ symmetries chosen such that the full MSSM Lagrangian is invariant. One can then easily check that the phases of the parameter combinations, $\arg[\mu A_f (m_{12}^2)^*]$ and $\arg[\mu M_i (m_{12}^2)^*]$, are indeed invariant under the $\mathrm{U}(1)_{\mathrm{PQ}}$ and $\mathrm{U}(1)_{\mathrm{R}}$ phase redefinitions of the MSSM fields [167,166]. Therefore, if one of these two quantities is different from zero (modulo π), one should expect new CP-violating effects induced by the production or exchange of supersymmetric particles.

We have already noted that the tree-level Higgs sector is CP-conserving. This is a consequence of the fact that m_{12}^2 is the only possible complex parameter that appears in the tree-level Higgs potential. Thus the phase of m_{12}^2 can be rotated away by redefining the phases of the complex Higgs doublets appearing in the Lagrangian. The same field redefinition implies that one can choose the vacuum expectation values of the two Higgs fields to be real and positive. However, at the one loop-level, the Higgs potential acquires a dependence on the parameters μA_t and μM_i through loops of third generation squarks and weak gauginos, respectively, which induce non-trivial CP-violating effects. The most important of these CP-violating effects is the generation of mixing between the neutral CP-odd and CP-even Higgs boson states. Therefore, the physical neutral Higgs bosons are no longer CP-eigenstates and the CP-odd Higgs boson mass m_A is no longer a physical parameter. The charged Higgs mass is still physical and can be used as an input for the computation of the neutral Higgs spectrum of the theory [153]. The Higgs mass spectrum can therefore be quite different from the CP-conserving case. For example, a large splitting between the masses of the next-to-lightest and the heaviest neutral Higgs bosons is possible if the charged Higgs boson is not too heavy.

For large values of the charged Higgs mass, the decoupling limit applies, and the properties of the lightest neutral Higgs boson state approach those of the SM Higgs boson. That is, for $m_{H^\pm} \gg m_W$, the lightest neutral Higgs boson is approximately a CP-even state, with CP-violating couplings that are suppressed by terms of $\mathcal{O}(m_W^2/m_{H^\pm}^2)$ [168]. In particular, the upper-bound on the lightest neutral Higgs boson mass, which is reached in the decoupling limit, takes the same value as in the CP-conserving case [166]. Nevertheless, there still can be significant mixing between the two heavier neutral mass eigenstates. Quantitatively, the leading contribution to the squared-mass terms that mix CP-even and CP-odd eigenstates, M_{SP}^2 (in a convention where m_{12}^2 is real) is of order

$$M_{SP}^2 \simeq \frac{3g^2 m_t^4 |\mu A_t|}{64\pi^2 m_W^2 M_S^2} \sin\left(\arg[\mu A_t]\right) . \tag{47}$$

Under the reasonable assumption that $|\mu A_t| < 10M_S^2$, it is clear that the mixing effects between the lightest neutral Higgs boson and the heavier Higgs states are small if the masses of the heavy Higgs bosons are larger than $2m_t$. In this limit, the two heavier states are highly degenerate in mass, and the CP-violating effects may still lead to non-trivial mixing of the two heavier CP-eigenstates. For a detailed study of the Higgs mass spectrum and parametric dependence of the Higgs mass radiative corrections, see ref. [153].

3.3 Radiatively-Corrected MSSM Higgs couplings

3.3.1 Renormalization of $\cos(\beta - \alpha)$

Radiative corrections also significantly modify the tree-level values of the Higgs boson couplings to fermion pairs and to vector boson pairs. As discussed in Section 3.1, the tree-level Higgs couplings depend crucially on the value of $\cos(\beta - \alpha)$. In first approximation, when radiative corrections of the Higgs squared-mass matrix are computed, the diagonalizing angle α is shifted from its tree-level value. Thus, one may compute a "radiatively-corrected" value for $\cos(\beta - \alpha)$. This provides one important source of the radiative corrections of the Higgs couplings. In fig. 11, we show the effect of radiative corrections on the value of $\cos(\beta - \alpha)$ as a function of m_A for different values of the squark mixing parameters and $\tan\beta$. One can then simply insert the radiatively corrected value of α into eqs. (20), (21) and (28)–(33) to obtain radiatively-improved couplings of Higgs bosons to vector bosons and to fermions.

The mixing angle α which diagonalizes the mass matrix in eq. (40) can be expressed as:

$$s_\alpha c_\alpha = \frac{\mathcal{M}_{12}^2}{\sqrt{(\mathrm{Tr}\mathcal{M}^2)^2 - 4\det\mathcal{M}^2}}\,, \qquad c_\alpha^2 - s_\alpha^2 = \frac{\mathcal{M}_{11}^2 - \mathcal{M}_{22}^2}{\sqrt{(\mathrm{Tr}\mathcal{M}^2)^2 - 4\det\mathcal{M}^2}}\,, \tag{48}$$

where $s_\alpha \equiv \sin\alpha$ and $c_\alpha \equiv \cos\alpha$. Note that if $\mathcal{M}_{12}^2 \to 0$, then either $\sin\alpha \to 0$ (if $\mathcal{M}_{11}^2 > \mathcal{M}_{22}^2$) or $\cos\alpha \to 0$ (if $\mathcal{M}_{11}^2 < \mathcal{M}_{22}^2$). At tree level, $\mathcal{M}_{12}^2$ is small for small m_A and/or large $\tan\beta$, but it cannot vanish. However, radiative corrections to $\mathcal{M}_{12}^2 \equiv -(m_A^2 + m_Z^2)s_\beta c_\beta + \delta\mathcal{M}_{12}^2$ can be of the same order as its tree level value for small values of m_A and large $\tan\beta$. Hence, it is possible for the one-loop contribution to approximately cancel the tree-level result (with two-loop corrections to $\mathcal{M}_{12}^2$ small compared to the corresponding one-loop result). For moderate or large values of $\tan\beta$, the vanishing of $\mathcal{M}_{12}^2$ [see eq. (42)] leads to the approximate numerical relation [152]:

$$\left[\frac{m_A^2}{m_Z^2} + 1\right] \simeq \frac{\mu x_t \tan\beta}{100 M_S}(2a_t x_t - 11)\left[1 - \frac{15}{16\pi^2}\ln\left(\frac{M_S^2}{m_t^2}\right)\right], \tag{49}$$

where h_t, α_s and the weak gauge couplings have been replaced by their approximate numerical values at the the electroweak scale. For low values of m_A or large values of the squark mixing parameters, a cancellation can easily take place.

If $\mathcal{M}^2_{12} \simeq 0$ and $\tan\beta$ is large (values of $\tan\beta \gtrsim 5$ are sufficient), the resulting pattern of Higgs couplings is easy to understand. In this limit, $\mathcal{M}^2_{11} \simeq m_A^2$ and $\mathcal{M}^2_{22} \simeq m_h^{\max}$, as noted at the end of Section 3.2.1. Two cases must be treated separately depending on the value of m_A. First, if $m_A < m_h^{\max}$, then $\sin\alpha \simeq -1$, $\cos\alpha \simeq 0$ and $\sin\beta \simeq -\cos(\beta-\alpha) \simeq 1$. In this case, the lighter CP-even Higgs boson h is roughly aligned along the Φ^0_d direction and the heavier CP-even Higgs boson H is roughly aligned along the Φ^0_u direction [see eq. (8)]. In particular, the coupling of H to $b\bar{b}$ and $\tau^+\tau^-$ is significantly diminished (since down-type fermions couple to Φ^0_d), while the HVV couplings [eq. (20)] are approximately equal to those of the Standard Model [since $\cos^2(\beta-\alpha) \simeq 1$]. Consequently, the branching ratios of H into gg, $\gamma\gamma$, $c\bar{c}$, and W^+W^- can be greatly enhanced over Standard Model expectations [152,160,169,170]. Second, if $m_A \gg m_h^{\max}$ then $\sin\alpha \simeq 0$ and $\sin\beta \simeq \cos\alpha \simeq \sin(\beta-\alpha) \simeq 1$ and the previous considerations for H apply now to h.

Although it is difficult to have an exact cancellation of the off-diagonal element $\mathcal{M}^2_{12}$, in many regions of the MSSM parameter space, a significant suppression of $\mathcal{M}^2_{12}$ may be present. Generically, the leading radiative corrections to $\mathcal{M}^2_{12}$ depend strongly on the sign of the product μX_t ($A_t \simeq X_t$ for large $\tan\beta$ and moderate μ) and on the value of $|A_t|$. For the same value of X_t, a change in the sign of μ can lead to observable variations in the branching ratio for the Higgs boson decay into bottom quarks. If $a_t^2 \lesssim 11/2$, then the absolute value of $\mathcal{M}^2_{12}$ tends to be suppressed [enhanced] for values of $\mu A_t < 0$ [$\mu A_t > 0$], which implies a similar suppression [enhancement] for the coupling of bottom quarks and τ-leptons to the SM-like Higgs boson. For larger values of $|a_t|$, the suppression [enhancement] occurs for the opposite sign of μA_t.

3.3.2 The decoupling limit revisited

Radiative corrections can also significantly affect the onset of the decoupling limit. Recall that at tree level [see eq. (18)], $|\cos(\beta-\alpha)| \ll 1$ for $m_A \gg m_Z$, in which case the couplings of h are nearly identical to those of the SM Higgs boson. Including the effects of $\delta\mathcal{M}^2$, we use eq. (48) to obtain

$$\begin{aligned}\cos(\beta-\alpha) &= \frac{(\mathcal{M}^2_{11}-\mathcal{M}^2_{22})\sin 2\beta - 2\mathcal{M}^2_{12}\cos 2\beta}{2(m_H^2-m_h^2)\sin(\beta-\alpha)} \\ &= \frac{m_Z^2\sin 4\beta + (\delta\mathcal{M}^2_{11}-\delta\mathcal{M}^2_{22})\sin 2\beta - 2\delta\mathcal{M}^2_{12}\cos 2\beta}{2(m_H^2-m_h^2)\sin(\beta-\alpha)}\,. \end{aligned} \tag{50}$$

Since $\delta\mathcal{M}^2_{ij} \sim \mathcal{O}(m_Z^2)$, and $m_H^2 - m_h^2 = m_A^2 + \mathcal{O}(m_Z^2)$, one finds

$$\cos(\beta-\alpha) = c\left[\frac{m_Z^2\sin 4\beta}{2m_A^2} + \mathcal{O}\left(\frac{m_Z^4}{m_A^4}\right)\right]\,, \tag{51}$$

in the limit of $m_A \gg m_Z$, where

$$c \equiv 1 + \frac{\delta\mathcal{M}^2_{11}-\delta\mathcal{M}^2_{22}}{2m_Z^2\cos 2\beta} - \frac{\delta\mathcal{M}^2_{12}}{m_Z^2\sin 2\beta}\,. \tag{52}$$

Eq. (51) exhibits the expected decoupling behavior for $m_A \gg m_Z$. However, eq. (50) illustrates another way in which $\cos(\beta-\alpha)=0$ can be achieved—simply choose the MSSM parameters (that govern the Higgs mass radiative corrections) such that the numerator of eq. (50) vanishes. That is,

$$2m_Z^2 \sin 2\beta = 2\,\delta\mathcal{M}_{12}^2 - \tan 2\beta \left(\delta\mathcal{M}_{11}^2 - \delta\mathcal{M}_{22}^2\right) . \tag{53}$$

Note that eq. (53) is independent of the value of m_A. For a typical choice of MSSM parameters, eq. (53) yields a solution at large $\tan\beta$. That is, by approximating $\tan 2\beta \simeq -\sin 2\beta \simeq -2/\tan\beta$, one can determine the value of β at which the decoupling occurs:

$$\tan\beta \simeq \frac{2m_Z^2 - \delta\mathcal{M}_{11}^2 + \delta\mathcal{M}_{22}^2}{\delta\mathcal{M}_{12}^2} . \tag{54}$$

The explicit expressions for $\delta\mathcal{M}_{ij}^2$ quoted in eq. (42) confirm that the assumption of $\tan\beta \gg 1$ used to derive this result is a consistent approximation because $\delta\mathcal{M}_{12}^2$ is typically small. We conclude that for the value of $\tan\beta$ specified in eq. (54), $\cos(\beta-\alpha)=0$ independently of the value of m_A. We shall refer to this phenomenon as m_A-independent decoupling. From eq. (42), it follows that explicit solutions to eq. (53) depend on ratios of MSSM parameters and are thus insensitive to the overall supersymmetric mass scale, modulo a mild logarithmic dependence on M_S/m_t.

3.3.3 Corrections to tree-level Higgs-fermion Yukawa couplings

We have seen in Section 3.3.1 that Higgs couplings are modified at one loop due to the renormalization of the CP-even Higgs mixing angle α. Additional contributions from the one-loop vertex corrections to tree-level Higgs couplings must also be considered [171,172,173,174]. These corrections are typically small and therefore do not alter significantly the pattern of Higgs couplings. However, at large $\tan\beta$, the corrections to Higgs-fermion Yukawa couplings can be enhanced, and thus require a careful analysis.

In the supersymmetric limit, bottom quarks only couple to Φ_d^0 and top quarks only couple to Φ_u^0. However, supersymmetry is broken and a small coupling of the bottom quark [top quark] to Φ_u^0 [Φ_d^0] will be generated from the one-loop Yukawa vertex corrections. These results can be summarized by an effective Lagrangian that describes the coupling of the Higgs bosons to the third generation quarks:[19]

$$-\mathcal{L}_{\rm eff} = \epsilon_{ij}\left[(h_b+\delta h_b)\bar{b}_R\mathbf{\Phi}_{\mathbf{d}}^i Q_L^j + (h_t+\delta h_t)\bar{t}_R Q_L^i \mathbf{\Phi}_{\mathbf{u}}^j\right] + \Delta h_t \bar{t}_R Q_L^k \mathbf{\Phi}_{\mathbf{d}}^{k*} + \Delta h_b \bar{b}_R Q_L^k \mathbf{\Phi}_{\mathbf{u}}^{k*} + \text{h.c.}, \tag{55}$$

[19] Due to weak isospin breaking, one should allow for different radiatively induced couplings to charged and neutral Higgs bosons. For example, one should write $\Delta h_b \bar{b}_R b_L \Phi_u^{0*} + \Delta\overline{h}_b \bar{b}_R t_L \Phi_u^-$ in place of $\Delta h_b \bar{b}_R Q_L^k \mathbf{\Phi}_{\boldsymbol{u}}^{k*}$, *etc.* To the extent that weak isospin breaking effects are small in the loop diagrams that generate Δh_b and $\Delta\overline{h}_b$, it follows that $\Delta h_b \approx \Delta\overline{h}_b$ (and similarly for the other radiatively generated coefficients), and we may use eq. (55) as written.

implying a modification of the tree-level relations between h_t, h_b and m_t, m_b as follows [175,176,172,144]:

$$m_b = \frac{h_b v}{\sqrt{2}} \cos\beta \left(1 + \frac{\delta h_b}{h_b} + \frac{\Delta h_b \tan\beta}{h_b}\right) \equiv \frac{h_b v}{\sqrt{2}} \cos\beta (1 + \Delta_b)\,, \tag{56}$$

$$m_t = \frac{h_t v}{\sqrt{2}} \sin\beta \left(1 + \frac{\delta h_t}{h_t} + \frac{\Delta h_t \cot\beta}{h_t}\right) \equiv \frac{h_t v}{\sqrt{2}} \sin\beta (1 + \Delta_t)\,. \tag{57}$$

The dominant contributions to Δ_b are $\tan\beta$-enhanced, with $\Delta_b \simeq (\Delta h_b/h_b)\tan\beta$; for $\tan\beta \gg 1$, $\delta h_b/h_b$ provides a small correction to Δ_b. In the same limit, $\Delta_t \simeq \delta h_t/h_t$, with the additional contribution of $(\Delta h_t/h_t)\cot\beta$ providing a small correction.[20] Explicitly, one finds that for $M_{\rm SUSY} \gg m_Z$ (where $M_{\rm SUSY}$ represents a typical supersymmetric mass that appears in the loops) and for $\tan\beta \gg 1$ [175,176,144],

$$\Delta_b \simeq \left[\frac{2\alpha_s}{3\pi}\mu M_{\tilde g}\, I(M^2_{\tilde b_1}, M^2_{\tilde b_2}, M^2_{\tilde g}) + \frac{h_t^2}{16\pi^2}\mu A_t\, I(M^2_{\tilde t_1}, M^2_{\tilde t_2}, \mu^2)\right]\tan\beta\,, \tag{58}$$

$$\Delta_t \simeq -\frac{2\alpha_s}{3\pi} A_t M_{\tilde g} I(M^2_{\tilde t_1}, M^2_{\tilde t_2}, M^2_{\tilde g}) - \frac{h_b^2}{16\pi^2}\mu^2 I(M^2_{\tilde b_1}, M^2_{\tilde b_2}, \mu^2)\,, \tag{59}$$

where $\alpha_s \equiv g_3^2/4\pi$, $M_{\tilde g}$ is the gluino mass, $M_{\tilde b_{1,2}}$ are the bottom squark masses, and smaller electroweak corrections have been ignored. The loop integral $I(a^2, b^2, c^2)$ is given by

$$I(a,b,c) = \frac{a^2 b^2 \ln(a^2/b^2) + b^2 c^2 \ln(b^2/c^2) + c^2 a^2 \ln(c^2/a^2)}{(a^2-b^2)(b^2-c^2)(a^2-c^2)}\,, \tag{60}$$

and is of order $1/\max(a^2, b^2, c^2)$ when at least one of its arguments is large compared to m_Z^2. Note that the Higgs coupling proportional to Δh_b is a manifestation of the broken supersymmetry in the low energy theory; hence, Δ_b does not decouple in the limit of large values of the supersymmetry breaking masses. Indeed, if all supersymmetry breaking mass parameters (and μ) are scaled by a common factor, the correction Δ_b remains constant.

Similarly to the case of the bottom quark, the relation between m_τ and the Higgs–tau-lepton Yukawa coupling h_τ is modified:

$$m_\tau = \frac{h_\tau v_d}{\sqrt{2}}(1 + \Delta_\tau). \tag{61}$$

The correction Δ_τ contains a contribution from a tau slepton–neutralino loop (depending on the two tau-slepton masses $M_{\tilde\tau_1}$ and $M_{\tilde\tau_2}$ and the mass parameter of the $\widetilde{B}$ component of the neutralino, M_1)

[20] Because the one-loop corrections δh_b, Δh_b, δh_t and Δh_t depend only on Yukawa and gauge couplings and the supersymmetric particle masses, they contain no hidden $\tan\beta$ enhancements [177].

and a tau sneutrino–chargino loop (depending on the tau sneutrino mass $M_{\tilde{\nu}_\tau}$, the mass parameter of the $\widetilde{W}^\pm$ component of the chargino, M_2, and μ). It is given by [176,144]:

$$\Delta_\tau = \left[\frac{\alpha_1}{4\pi} M_1 \mu\, I(M_{\tilde{\tau}_1}, M_{\tilde{\tau}_2}, M_1) - \frac{\alpha_2}{4\pi} M_2 \mu\, I(M_{\tilde{\nu}_\tau}, M_2, \mu)\right] \tan\beta\,, \tag{62}$$

where $\alpha_2 \equiv g^2/4\pi$ and $\alpha_1 \equiv g'^2/4\pi$ are the electroweak gauge couplings. Since corrections to h_τ are proportional to α_1 and α_2, they are expected to be smaller than the corrections to h_b.

From eq. (55) we can obtain the couplings of the physical Higgs bosons to third generation fermions. The resulting interaction Lagrangian is of the form:

$$\mathcal{L}_{\rm int} = -\sum_{q=t,b,\tau} \left[g_{hq\bar{q}} h q\bar{q} + g_{Hq\bar{q}} H q\bar{q} - i g_{Aq\bar{q}} A \bar{q}\gamma_5 q\right] + \left[\bar{b} g_{H^- t\bar{b}} t H^- + \text{h.c.}\right]\,. \tag{63}$$

Using eqs. (56) and (57), one obtains:

$$g_{hb\bar{b}} = -\frac{m_b}{v}\frac{\sin\alpha}{\cos\beta}\left[1 + \frac{1}{1+\Delta_b}\left(\frac{\delta h_b}{h_b} - \Delta_b\right)(1 + \cot\alpha\cot\beta)\right]\,, \tag{64}$$

$$g_{Hb\bar{b}} = \frac{m_b}{v}\frac{\cos\alpha}{\cos\beta}\left[1 + \frac{1}{1+\Delta_b}\left(\frac{\delta h_b}{h_b} - \Delta_b\right)(1 - \tan\alpha\cot\beta)\right]\,, \tag{65}$$

$$g_{Ab\bar{b}} = \frac{m_b}{v}\tan\beta\left[1 + \frac{1}{(1+\Delta_b)\sin^2\beta}\left(\frac{\delta h_b}{h_b} - \Delta_b\right)\right]\,, \tag{66}$$

$$g_{ht\bar{t}} = \frac{m_t}{v}\frac{\cos\alpha}{\sin\beta}\left[1 - \frac{1}{1+\Delta_t}\frac{\Delta h_t}{h_t}(\cot\beta + \tan\alpha)\right]\,, \tag{67}$$

$$g_{Ht\bar{t}} = \frac{m_t}{v}\frac{\sin\alpha}{\sin\beta}\left[1 - \frac{1}{1+\Delta_t}\frac{\Delta h_t}{h_t}(\cot\beta - \cot\alpha)\right]\,, \tag{68}$$

$$g_{At\bar{t}} = \frac{m_t}{v}\cot\beta\left[1 - \frac{1}{1+\Delta_t}\frac{\Delta h_t}{h_t}(\cot\beta + \tan\beta)\right]\,, \tag{69}$$

and the τ couplings are obtained from the above equations by replacing m_b, Δ_b and δh_b with m_τ, Δ_τ and δh_τ, respectively. In addition, one must employ the renormalized value of α in the above formulae to incorporate the radiative corrections discussed in section 3.3.1. In writing out the Higgs-top quark couplings above, we found it convenient to express the results in terms of Δ_t and $\Delta h_t/h_t$, since $\Delta_t \simeq \delta h_t/h_t$ and the corresponding contribution of $\Delta h_t/h_t$ is $\tan\beta$ suppressed [eq. (57)]. Alternatively, eqs. (64)–(69) can be rewritten in a more symmetrical form by using eqs. (56) and (57) to eliminate Δ_b and Δ_t from the numerators of the corresponding expressions.

At large $\tan\beta$, terms involving $\Delta_b \propto \tan\beta$ [eq. (58)] provide the dominant corrections to the neutral Higgs couplings to $b\bar{b}$. The corrections proportional to $\delta h_b/h_b$ [see eqs. (55) and (56) and the discussion that follows] are never $\tan\beta$-enhanced and are therefore numerically unimportant. The sign of Δ_b is governed by the sign of $M_{\tilde{g}}\mu$, since the bottom-squark gluino loop gives the dominant contribution to eq. (58). Thus, in a convention where $M_{\tilde{g}} > 0$, the radiatively corrected coupling $g_{Ab\bar{b}}$ is suppressed (enhanced) with respect to its tree level value for $\mu > 0$ ($\mu < 0$). In contrast, the radiative corrections to $g_{hb\bar{b}}$ and $g_{Hb\bar{b}}$ have a more complicated dependence on the supersymmetric parameters due to the dependence on the CP-even mixing angle α. Since α and Δ_b are governed by different combinations of the supersymmetry breaking parameters, it is difficult to exhibit in a simple way the behavior of the radiatively corrected couplings of the CP-even Higgs bosons to the bottom quarks as a function of the MSSM parameters.

One can check [using eq. (19)] that in the decoupling limit, $g_{hq\bar{q}} = g_{h_{\rm SM}q\bar{q}} = m_q/v$. Away from the decoupling limit, the Higgs couplings to bottom-type fermions can deviate significantly from their tree-level values due to enhanced radiative corrections at large $\tan\beta$ [where $\Delta_b \simeq \mathcal{O}(1)$]. In particular, because $\Delta_b \propto \tan\beta$, the leading one-loop radiative correction to $g_{hb\bar{b}}$ is of $\mathcal{O}(m_Z^2\tan\beta/m_A^2)$, which formally decouples only when $m_A^2 \gg m_Z^2\tan\beta$. This behavior is called *delayed decoupling* in ref. [174]. In addition, there are regions of MSSM parameter space in which there is a strong suppression of the Higgs coupling to $b\bar{b}$ (or $\tau^+\tau^-$) as compared to its tree-level value. As a result, there can be significant corrections to the tree-level relation $g_{hb\bar{b}}/g_{h\tau^+\tau^-} = m_b/m_\tau$ [169]. In particular, in some parameter regimes, the $\tau^+\tau^-$ decay mode can be the dominant h decay channel, a result that would be fatal to certain Higgs search strategies which assume that $h \to b\bar{b}$ is the dominant decay mode.

Assuming that weak isospin breaking effects in the loop corrections to the charged Higgs fermion Yukawa couplings are small (see footnote 19), then $g_{H^-t\bar{b}}$ [defined in eq. (63)] is given by

$$g_{H^-t\bar{b}} \simeq \frac{\sqrt{2}}{v}\left\{m_t\cot\beta\left[1-\frac{1}{1+\Delta_t}\frac{\Delta h_t}{h_t}(\cot\beta+\tan\beta)\right]P_R \right.$$
$$\left. +m_b\tan\beta\left[1+\frac{1}{(1+\Delta_b)\sin^2\beta}\left(\frac{\delta h_b}{h_b}-\Delta_b\right)\right]P_L\right\}, \tag{70}$$

with a similar form for $g_{H^-\nu_\tau\tau^+}$ with the replacements noted below eq. (69).

3.3.4 Effects of explicit CP-violation

In Section 3.2.3, we noted the possibility of mixing between the CP-even and CP-odd eigenstates due to CP-violating effects that enter via the one-loop radiative corrections. In this case, the neutral scalar mass eigenstates, denoted by H_i ($i = 1, 2, 3$), are determined by diagonalizing a 3×3 squared-mass matrix. Thus, one can no longer parameterize the various Higgs couplings in terms of the CP-even Higgs mixing angle α. It is convenient to work in a convention where the two vacuum expectation

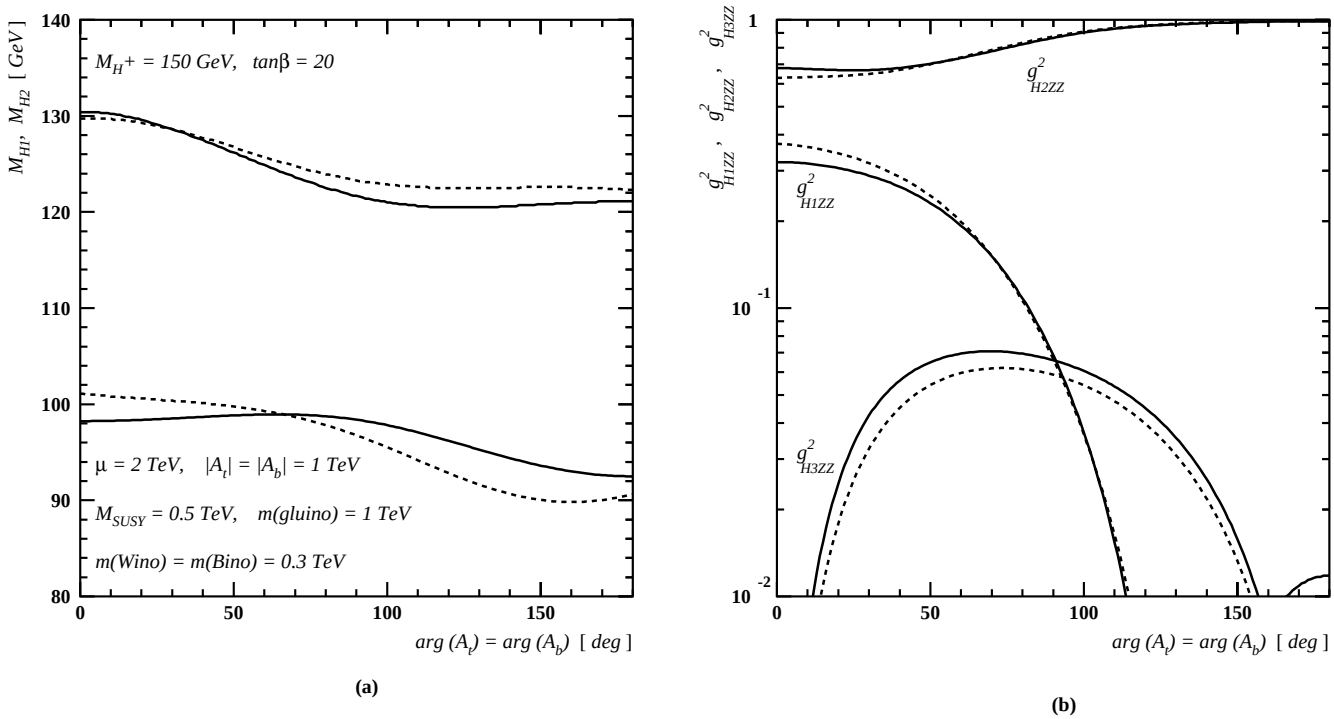

Figure 16: (a) Lightest and next-to-lightest neutral Higgs masses and (b) relative couplings (normalized to the SM) of the three neutral Higgs bosons to the Z (or W) as a function of the phase of A_t for the indicated choices of the MSSM parameters. Solid [dashed] lines are for $\arg(M_{\tilde{g}}) = 0^\circ$ [90°]. Taken from ref. [153].

values are real and positive (by absorbing any potential phases into the definition of the Higgs field) so that $\tan\beta = v_u/v_d$ as before. Then, eqs. (7) and (8) are replaced by

$$H_i = (\sqrt{2}\,\mathrm{Re}\,\Phi_d^0 - v_d)O_{1i} + (\sqrt{2}\,\mathrm{Re}\,\Phi_u^0 - v_u)O_{2i} + \sqrt{2}\left(\mathrm{Im}\,\Phi_d^0 \sin\beta + \mathrm{Im}\,\Phi_u^0 \cos\beta\right) O_{3i}\,, \tag{71}$$

where O is a 3×3 real orthogonal matrix.

In the CP-violating case, vector boson pairs VV ($V = W$ or Z) couple to all three neutral Higgs mass eigenstates, H_i, with [166]

$$g_{H_iVV} = O_{1i}\cos\beta + O_{2i}\sin\beta\,. \tag{72}$$

Fig. 16 shows the dependence of the Higgs masses and the H_iZZ squared-couplings on the phase of A_t for a particular choice of MSSM parameters [as indicated in fig. 16(a)]. Clearly, these couplings can depend sensitively on the phases of the complex supersymmetry-breaking parameters that generate the mixing of the CP-even and CP-odd scalar eigenstates through one-loop radiative effects.

The couplings of V to a pair of neutral Higgs bosons are given by $g_{H_iH_jZ}(p_{H_i} - p_{H_j})$, where the momenta p_{H_i} and p_{H_j} point into the vertex, $g_{H_iH_jZ}$ is antisymmetric under the interchange of H_i and

H_j, and [166]

$$g_{H_iH_jZ} = \frac{g}{2\cos\theta_W}\left[(O_{3i}O_{1j} - O_{1i}O_{1j})\sin\beta - (O_{3i}O_{2j} - O_{2i}O_{3j})\cos\beta\right] . \tag{73}$$

Using the orthogonality of O (and det $O = 1$), it is easy to derive the relation [166]:[21]

$$g_{H_iH_jZ} = \frac{m_Z^2}{2m_V^2}\,\epsilon_{ijk}\,g_{H_kVV} . \tag{74}$$

The sum rules of eqs. (22)–(24) are then easily extended:

$$\sum_i g^2_{H_iVV} = g_V^2 m_V^2 , \tag{75}$$

which when combined with eq. (74) yields

$$\sum_{i,j} g^2_{H_iH_jZ} = \frac{g^2}{2\cos^2\theta_W} , \tag{76}$$

$$g_{H_iVV}\,g_{H_jVV} + \frac{4m_V^4}{m_Z^2}\sum_k g_{H_iH_kZ}\,g_{H_jH_kZ} = \frac{m_V^4}{m_Z^2\cos^2\theta_W}\delta_{ij} . \tag{77}$$

The couplings of a neutral Higgs boson to H^-W^+ are given by $g_{H_iH^-W^+}(p_{H_i} - p_{H^-})$, where the momenta p_{H^-} and p_{H_i} point into the vertex, and [166]

$$g_{H_iH^-W^+} = [g_{H_iH^+W^-}]^* = \tfrac{1}{2}g\left[O_{1i}\sin\beta - O_{2i}\cos\beta - iO_{3i}\right] . \tag{78}$$

Another consequence of the CP-violating effects in the scalar sector is that all neutral Higgs scalars can couple to both scalar and pseudoscalar fermion bilinear densities ($\bar\psi\psi$ and $\bar\psi\gamma_5\psi$, respectively). The couplings of the mass eigenstate H_i to fermions depend on the loop-corrected fermion Yukawa couplings, $h_{b,t}$, $\delta h_{b,t}$, $\Delta h_{b,t}$, and on $\tan\beta$ and the O_{ji}. It is convenient to adjust the phases of the fields so that the quantities $h_b + \delta h_b + \Delta h_b \tan\beta$ and $h_t + \delta h_t + \Delta h_t \cot\beta$ are both real and positive [*i.e.*, the physical fermion masses are still given by eqs. (56) and (57)]. The resulting expressions are a straightforward generalization of those presented above for the CP-conserving case [153]:

$$\mathcal{L}_{H\bar f f} \;=\; -\sum_{i=1}^{3} H_i\left[\frac{m_b}{v}\,\bar b\left(g^S_{H_ibb} + ig^P_{H_ibb}\gamma_5\right)b \;+\; \frac{m_t}{v}\,\bar t\left(g^S_{H_itt} + ig^P_{H_itt}\gamma_5\right)t\right], \tag{79}$$

[21] One can easily check that eqs. (20) and (21) are recovered in the CP-conserving limit, where $(H_1, H_2, H_3) = (h, H, A)$, $O_{22} = -O_{11} = \sin\alpha$, $O_{12} = O_{21} = \cos\alpha$, $O_{33} = 1$, and all other elements O_{ji} vanish.

with

$$g^S_{H_i bb} = \frac{1}{h_b \,+\, \delta h_b \,+\, \Delta h_b \tan\beta} \left\{ \mathrm{Re}(h_b + \delta h_b)\, \frac{O_{1i}}{\cos\beta} \,+\, \mathrm{Re}(\Delta h_b)\, \frac{O_{2i}}{\cos\beta} \right.$$
$$\left. - \Big[\mathrm{Im}(h_b + \delta h_b) \tan\beta - \mathrm{Im}(\Delta h_b) \Big]\, O_{3i} \right\}, \tag{80}$$

$$g^P_{H_i bb} = \frac{1}{h_b \,+\, \delta h_b \,+\, \Delta h_b \tan\beta} \left\{ \Big[\mathrm{Re}\,(\Delta h_b) \,-\, \mathrm{Re}(h_b + \delta h_b) \tan\beta \Big]\, O_{3i} \right.$$
$$\left. - \mathrm{Im}(h_b + \delta h_b)\, \frac{O_{1i}}{\cos\beta} \,-\, \mathrm{Im}(\Delta h_b)\, \frac{O_{2i}}{\cos\beta} \right\}, \tag{81}$$

$$g^S_{H_i tt} = \frac{1}{h_t \,+\, \delta h_t \,+\, \Delta h_t \cot\beta} \left\{ \mathrm{Re}(h_t + \delta h_t)\, \frac{O_{2i}}{\sin\beta} + \,\mathrm{Re}(\Delta h_t)\, \frac{O_{1i}}{\sin\beta} \right.$$
$$\left. - \Big[\mathrm{Im}(h_t + \delta h_t) \cot\beta \,-\, \mathrm{Im}(\Delta h_t) \Big]\, O_{3i} \right\}, \tag{82}$$

$$g^P_{H_i tt} = \frac{1}{h_t \,+\, \delta h_t \,+\, \Delta h_t \cot\beta} \left\{ \Big[\mathrm{Re}(\Delta h_t) \,-\, \mathrm{Re}(h_t + \delta h_t) \cot\beta \Big]\, O_{3i} \right.$$
$$\left. - \mathrm{Im}(h_t + \delta h_t)\, \frac{O_{2i}}{\sin\beta} \,-\, \mathrm{Im}(\Delta h_t)\, \frac{O_{1i}}{\sin\beta} \right\}, \tag{83}$$

where the Higgs scalar couplings are normalized with respect to the corresponding SM values.

For large values of the charged Higgs boson mass and for heavy supersymmetric particles, the expressions of the lightest neutral Higgs boson coupling to fermions reduce to those of the (CP-conserving) SM Higgs boson, as expected for the decoupling limit. In contrast, the two heavy neutral Higgs bosons are still admixtures of CP-even and CP-odd eigenstates; hence, CP-violating effects are still present in the heavy neutral Higgs sector. However, due to the high degeneracy in mass of the heavy scalar sector (especially in the decoupling limit), CP-violating effects may be difficult to observe without precision measurements of the heavy neutral Higgs properties.

The couplings of the charged Higgs bosons to fermions are of the form $\mathcal{L}_{\rm int} = \bar{b}\, g_{H^- t\bar{b}}\, t H^- + \text{h.c.}$, with

$$g_{H^- t\bar{b}} \simeq \left(\frac{\sqrt{2}\, m_b}{v} \tan\beta - \frac{\Delta h_b}{\cos\beta} \right) P_L + \left(\frac{\sqrt{2}\, m_t}{v} \cot\beta - \frac{(\Delta h_t)^*}{\sin\beta} \right) P_R\,. \tag{84}$$

One can check that for real Δh_b and Δh_t, this result is equivalent to eq. (70) [with the same caveats noted in footnote 19]. An explicit computation of the CP-violating $H^- t\bar{b}$ vertex and its phenomenological implications can be found in ref. [178].

3.4 MSSM Higgs Boson Decay Modes

In the MSSM, we must consider the decay properties of three neutral Higgs bosons and one charged Higgs pair.[22] In the region of parameter space where $m_A \gg m_Z$ and the masses of supersymmetric particles are large, the decoupling limit applies, and we find that the properties of h are indistinguishable from the SM Higgs boson. If supersymmetric particles are light, then the decoupling limit does not strictly apply even in the limit of $m_A \gg m_Z$. In particular, the h branching ratios are modified, if the decays of h into supersymmetric particles are kinematically allowed. In addition, if light superpartners exist that can couple to photons and/or gluons, then the one-loop gg and $\gamma\gamma$ decay rates would also deviate from the corresponding Standard Model Higgs decay rates due to the extra contribution of the light superpartners appearing in the loops. In both cases, the heavier Higgs states, H, A and $H^{\pm}$, are roughly mass degenerate, and their decay branching ratios depend crucially on $\tan\beta$ as shown below.

For values of $m_A \sim \mathcal{O}(m_Z)$, all Higgs boson states lie below 200 GeV in mass. In this parameter regime, there is a significant area of the parameter space in which none of the neutral Higgs boson decay properties approximates that of the SM Higgs boson. For $\tan\beta \gg 1$, the resulting Higgs phenomenology shows marked differences from that of the SM Higgs boson [179]. In particular, radiative corrections can significantly modify the $b\bar{b}$ and/or the $\tau^+\tau^-$ decay rates with respect to those of the SM Higgs boson, as noted in Section 3.3.3. Additionally, the Higgs bosons can decay into new channels, either containing lighter Higgs bosons or supersymmetric particles. In the following, the decays of the neutral Higgs bosons h, H and A and the decays of charged Higgs bosons are discussed with particular emphasis on differences from Standard Model expectations. In the following discussion, we exhibit results for $\tan\beta = 3$ and 30 to illustrate the difference between "low" and "high" $\tan\beta$. The results shown below include the effects of the dominant radiative corrections, which affect both the masses and the couplings of the Higgs sector as described in Sections 3.2 and 3.3.

In order to display results for Higgs branching ratios, we must choose a set of MSSM parameters. We fix $\tan\beta$ (for two representative choices) and vary m_A from its LEP experimental lower bound of 90 GeV up to 1 TeV. In addition, the gluino and MSSM squark mass parameters have been chosen to be $M_{\rm SUSY} \equiv M_{\tilde{g}} = M_Q = M_U = M_D = 1$ TeV, the squark mixing parameter $X_t = A_t - \mu\cot\beta = 2.4 M_{\rm SUSY}$, and the gaugino mass matrix parameters, $\mu = M_2 \simeq 2M_1 = 1$ TeV. This differs somewhat from the maximal mixing benchmark scenario of ref. [156]. Nevertheless, the value of m_h is still close to maximal (for fixed m_A and $\tan\beta$), so we will continue to loosely refer to the above choice of MSSM parameters as a maximal mixing scenario. Our motivation for choosing the gaugino mass parameters large is to avoid possible supersymmetric decay modes for the Higgs bosons for Higgs masses below 1 TeV. We shall briefly comment on possible supersymmetric decay modes at the end of this section.

The branching ratios for h and H as a function of their masses are shown in fig. 17. As m_A varies from 90 GeV to 1 TeV, with the MSSM parameters as specified above, 135 GeV $\lesssim m_H \lesssim$ 1 TeV when

[22] Unless otherwise noted, we shall neglect CP-violating effects (*e.g.*, by assuming that CP-violating effects induced by radiative corrections are small).

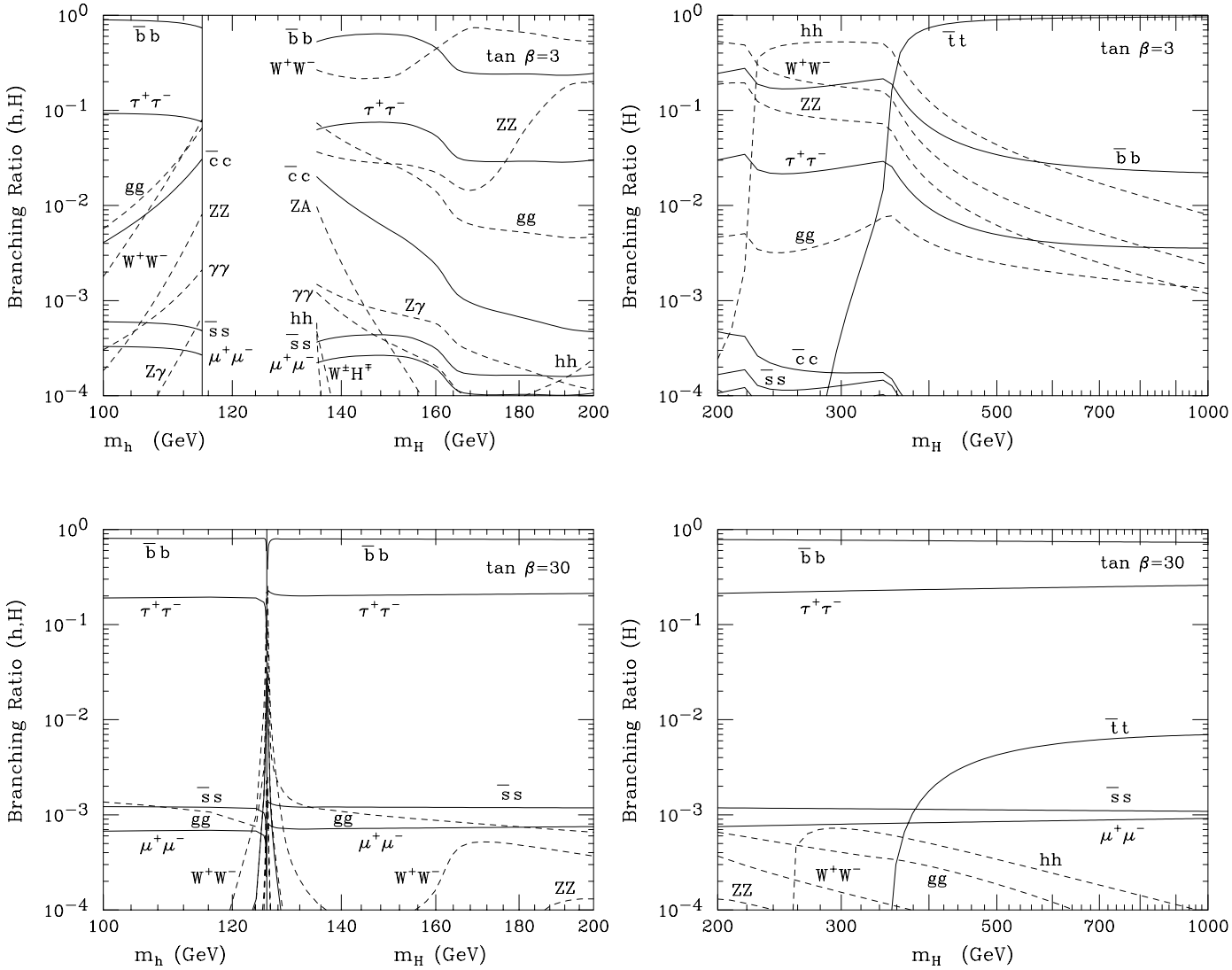

Figure 17: Branching ratios of the MSSM Higgs bosons h and H, with $\tan\beta = 3$ and 30, respectively. Final states labeled above include the possibility of one off-shell final state particle below the corresponding two-particle decay threshold. The above plots were made under the assumption that the average top and bottom squark masses are 1 TeV and top-squark mixing is maximal. In this case, $m_h^{\max} \simeq 115$ GeV (125.9 GeV) for $\tan\beta = 3$ (30), corresponding to the limit of large m_A, is indicated by the vertical line in the two left-side plots. The range of m_H shown corresponds to varying m_A between 90 GeV and 1 TeV, while $m_h > 100$ GeV corresponds to $m_A > 139$ GeV (104 GeV) for $\tan\beta = 3$ (30). Other supersymmetric parameters have been chosen such that there are no supersymmetric particle decay modes in the Higgs mass ranges shown above.

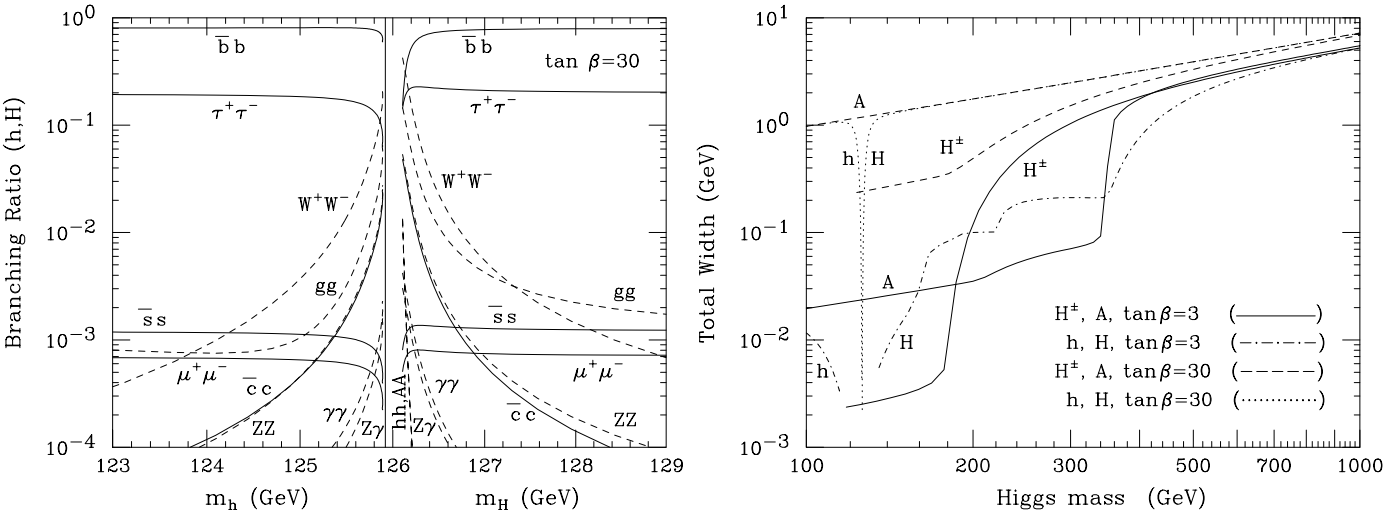

Figure 18: (a) Branching ratios of the MSSM Higgs bosons h and H, with $\tan\beta = 30$. Here, we zoom in on the Higgs mass regime within ± 3 GeV of $m_h^{\max} = 125.9$ GeV of fig. 17 in order to get a clearer picture of the various decay modes. The range of m_H shown corresponds to 90 GeV $< m_A <$ 130 GeV, whereas the range of m_h shown corresponds to 128 GeV $< m_A <$ 1 TeV. (b) Total widths of the MSSM Higgs boson as a function of the corresponding Higgs mass for $\tan\beta = 3$ and 30, with the same parameter assumptions employed in fig. 17.

$\tan\beta = 3$ and 126.1 GeV $\lesssim m_H \lesssim$ 1 TeV when $\tan\beta = 30$. In contrast, most of the variation in m_A occurs for values of m_h a few GeV below $m_h^{\max}$. Thus, we also exhibit in fig. 18(a) the branching ratios for h and H for $\tan\beta = 30$ and Higgs mass values of $m_h^{\max} \pm 3$ GeV. This reveals a detailed pattern of branching ratios that is not easily visible in fig. 17. The branching ratios for A and H^+ as a function of their masses are shown in fig. 19.

The total Higgs decay widths as a function of the corresponding Higgs mass are shown in fig. 18(b) for the two cases of $\tan\beta = 3$ and 30 (and the other relevant MSSM parameters as described above). Note that for large values of the Higgs mass, the corresponding widths are considerably smaller than that of the SM Higgs boson. This is due to the suppressed HVV couplings at large Higgs mass and to the absence of tree-level AVV and H^+W^-Z couplings. One can also check that in the decoupling limit ($m_A \gg m_Z$), the total width of h coincides with that of $h_{\rm SM}$. This is illustrated by replotting the h (and H) widths on the same plot as the $h_{\rm SM}$ width [see fig. 4(b)]. In particular, note that the dashed and dot-dashed h contours in fig. 4(b) approach the $h_{\rm SM}$ contour as m_h reaches its maximal value. (which corresponds to the limit of large m_A at fixed $\tan\beta$). It is interesting to note that in the opposite limit of small m_A (especially at large $\tan\beta$), $\cos(\beta-\alpha) \to 1$ and it is H that assumes many of the properties of $h_{\rm SM}$. However, there can still be deviations in the $Hb\bar{b}$ coupling from the corresponding Standard Model value at large $\tan\beta$, as noted below eq. (35). This explains why the H contours in fig. 4(b)

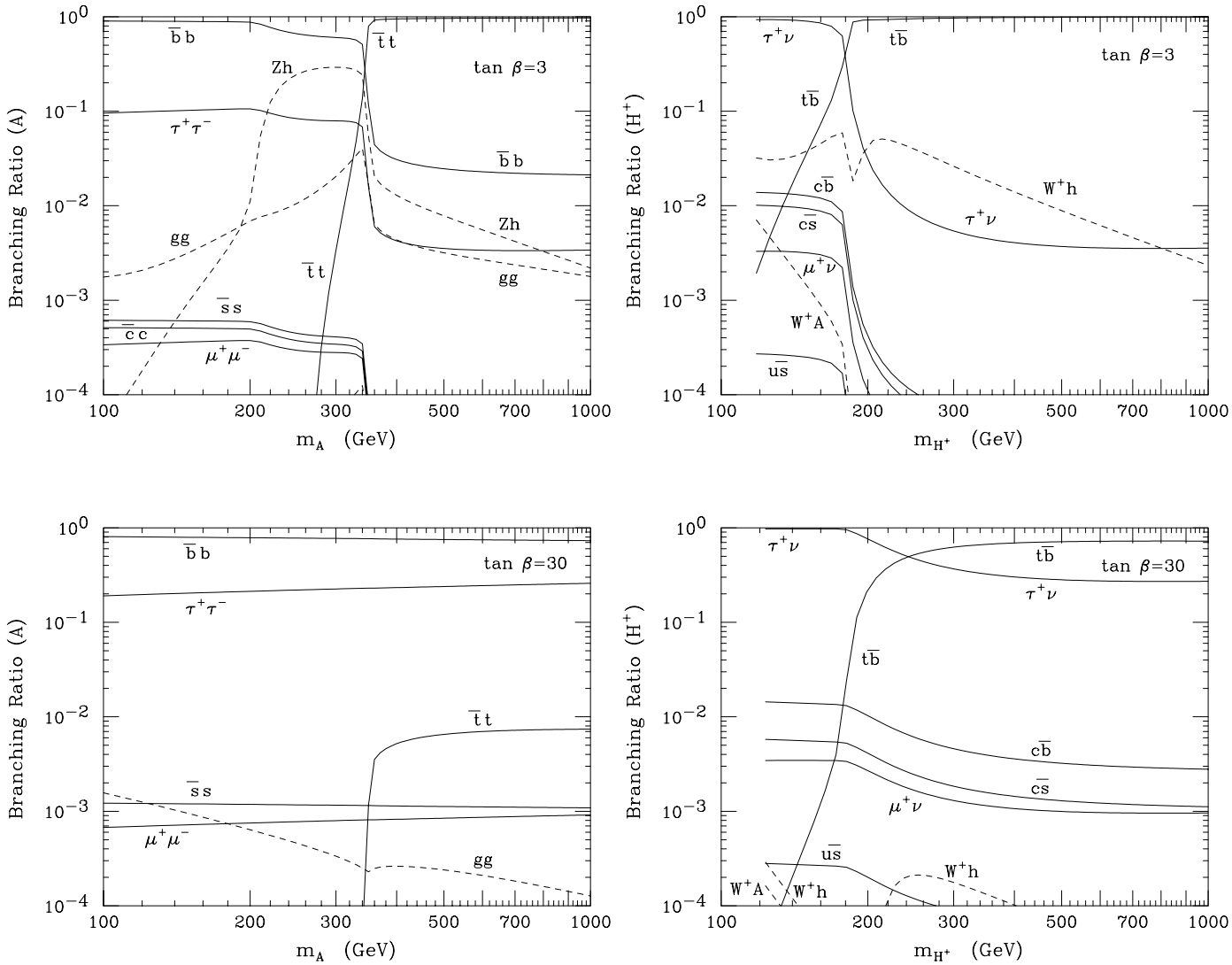

Figure 19: Branching ratios of the MSSM Higgs bosons A and H^+, with $\tan\beta = 3$ and 30, respectively. Final states labeled above include the possibility of one off-shell final state particle below the corresponding two-particle decay threshold. The above plots were made under the assumption that the average top and bottom squark masses are 1 TeV and top-squark mixing is maximal. The range of $m_{H^\pm}$ shown corresponds to varying m_A between 90 GeV and 1 TeV. Other supersymmetric parameters have been chosen such that there are no supersymmetric particle decay modes in the Higgs mass ranges shown above.

do not quite coincide with the result of the $h_{\rm SM}$ contour as m_H approaches its lower limit (with the discrepancy between the H and $h_{\rm SM}$ contours more pronounced at large $\tan\beta$).

The branching ratios and widths in figs. 17–19 have been computed using a modified version of the HDECAY program [180] that incorporates the leading radiative corrections to the Higgs couplings discussed in Section 3.3.[23] The decay modes $h, H, A \to b\bar{b}$, $\tau^+\tau^-$ dominate the neutral Higgs decay modes when $\tan\beta$ is large for all values of the Higgs masses. For small $\tan\beta$, these modes are significant for neutral Higgs masses below $2m_t$ (although there are other competing modes in this mass range), whereas the $t\bar{t}$ decay mode dominates above the $t\bar{t}$ decay threshold. In contrast to the SM Higgs boson, the vector boson decay modes of H are strongly suppressed at large m_H due to the suppressed HVV couplings in the decoupling limit. For the charged Higgs boson, $H^+ \to \tau^+\nu$ dominates below $t\bar{b}$ threshold, while $H^+ \to t\bar{b}$ dominates for large values of $m_{H^\pm}$. Note that final states labeled in figs. 17 and 19 include the possibility of one off-shell final state particle below the corresponding two-particle decay threshold [181]. For example, for $m_{H^\pm} < m_t + m_b$, the $t\bar{b}$ contour shown in fig. 19 actually corresponds to an off-shell t quark that decays to bW^+. That is, in this mass region, the $t\bar{b}$ contour corresponds to the branching ratio for the three-body decay $H^+ \to W^+b\bar{b}$. This decay mode can be especially significant at moderate values of $\tan\beta$ due to the large Higgs-top Yukawa coupling.

As in the Standard Model case, the partial decay widths of the neutral Higgs bosons into $b\bar{b}$ and $c\bar{c}$ are reduced by about 50–75% when QCD corrections are included (*e.g.*, by employing running quark masses in the decay width formulae), whereas the QCD corrections are less significant for Higgs decays into $t\bar{t}$ [29]. The effects of the QCD radiative corrections on the charged Higgs branching ratios [182] are significant in the region of $\tan\beta$ where the $c\bar{s}$ and $\tau^+\nu_\tau$ decay modes are competitive or for large values of $\tan\beta$ for the decay mode $H^+ \to t\bar{b}$ (and for $H^+ \to W^+b\bar{b}$ below $t\bar{b}$ threshold [183]). Additional supersymmetric radiative corrections discussed in Section 3.3 can also significantly affect the Higgs boson partial widths. Some of these corrections can be absorbed into the effective mixing angle α [173] as shown in Section 3.3.1. As a consequence of this universal correction, the coupling of h to $b\bar{b}$ and $\tau^+\tau^-$ can be suppressed for small m_A and large $\tan\beta$. For the $h \to b\bar{b}$ decay width, the supersymmetric corrections [152,171,172,173,174] proportional to the strong coupling constant α_s and the Higgs-top quark Yukawa coupling h_t can be significant for large values of μ and $\tan\beta$. As shown in Section 3.3.3, this effect can be interpreted as a correction to the tree-level relation between m_b and h_b.

In addition to the decay modes of the neutral Higgs bosons into fermion and gauge boson final states, there exist new Higgs decay channels that involve scalars of the extended Higgs sector and supersymmetric final states. The unambiguous observation of these modes (as well as any decay mode of a charged scalar) would clearly constitute direct evidence of new physics beyond the Standard Model. Higgs decays into charginos, neutralinos and third-generation squarks and sleptons can become impor-

[23] For the maximal mixing choice of MSSM parameters used in figs. 17–19, we find $\Delta_b \simeq 0.55$ for $\tan\beta = 30$. For large m_A and $\tan\beta$, the partial widths of H, $A \to b\bar{b}$ and $H^+ \to t\bar{b}$ (and likewise the corresponding total widths) are suppressed by a factor of about $(1+\Delta_b)^2$ with respect to the corresponding tree-level results.

tant, once they are kinematically allowed [184]. One interesting possibility is a significant branching ratio for the decay of a neutral Higgs boson to the invisible mode $\widetilde{\chi}_1^0\widetilde{\chi}_1^0$ (where $\widetilde{\chi}_1^0$ is the lightest supersymmetric particle). In such a scenario, the discovery of this neutral Higgs boson would be difficult at a hadron collider [185]. In contrast, at lepton colliders, methods exist for detecting an invisibly decaying Higgs boson by observing a peak in the missing mass recoiling against the produced Z.

3.5 MSSM Higgs Boson Production at Hadron Colliders

3.5.1 Cross-sections at hadron colliders

The production mechanisms for the SM Higgs boson at hadron colliders can also be relevant for the production of the MSSM neutral Higgs bosons. However, we must take into account the possibility of enhanced or suppressed couplings (with respect to those of the Standard Model). For example, the HVV couplings are very suppressed in the decoupling limit, and tree-level AVV couplings are completely absent. On the other hand, at large $\tan\beta$, typically two of the three neutral Higgs couplings to bottom-type quarks are enhanced. These effects can significantly modify the neutral Higgs production cross-sections. New production mechanisms must be considered for charged Higgs production.

As in the case of Higgs branching ratios, the predicted cross-sections are sensitive to the MSSM Higgs parameters. Again, we consider two representative values of $\tan\beta$: a low value of $\tan\beta = 3$ and a high value of $\tan\beta = 30$. We then vary m_A, evaluate the other Higgs masses, and compute each Higgs cross-section as a function of the corresponding Higgs mass. The Higgs masses and cross-sections depend on other MSSM parameters through radiative corrections. As in Section 3.4, we work in a maximal squark mixing scenario in which the value of m_h for a fixed choice of $\tan\beta$ and m_A is maximal. In addition, because the squark masses are assumed to be heavy (of order 1 TeV), potential supersymmetric contributions to the one-loop Higgs-gluon-gluon vertex (due to squark loops) are suppressed. Cross-sections for neutral MSSM Higgs production at the Tevatron and the LHC are shown in figs. 20 and 21 respectively. The dominant Higgs production mechanism over much of the MSSM parameter space is gluon-gluon fusion, which is mediated by heavy top and bottom quark triangle loops and the corresponding supersymmetric partners [186,187,188]. The gluon-gluon fusion results shown in figs. 20 and 21 include NLO QCD corrections [189].[24]

The cross-sections for the production of the neutral CP-even Higgs bosons ($\phi = h$ or H) via gauge boson fusion $V^*V^* \to \phi$ ($V = W$ or Z) [45] and via the process $q\bar{q} \to V^* \to V\phi$ [42], including first-order QCD corrections,[25] are also exhibited in figs. 20 and 21. Recall that the CP-even scalar ϕ has SM-like couplings to the vector bosons in two cases: (i) in the decoupling regime for the lightest Higgs boson, where $\phi = h$ and (ii) for large $\tan\beta$ and low m_A, where $\phi = H$. In either case, the SM-like

[24] A recent computation of the NNLO QCD corrections to A production via gluon fusion exhibits a 20–30% increase over the corresponding NLO cross-section [190].

[25] The supersymmetric-QCD corrections due to the exchange of virtual squarks and gluinos are known to be small [188].

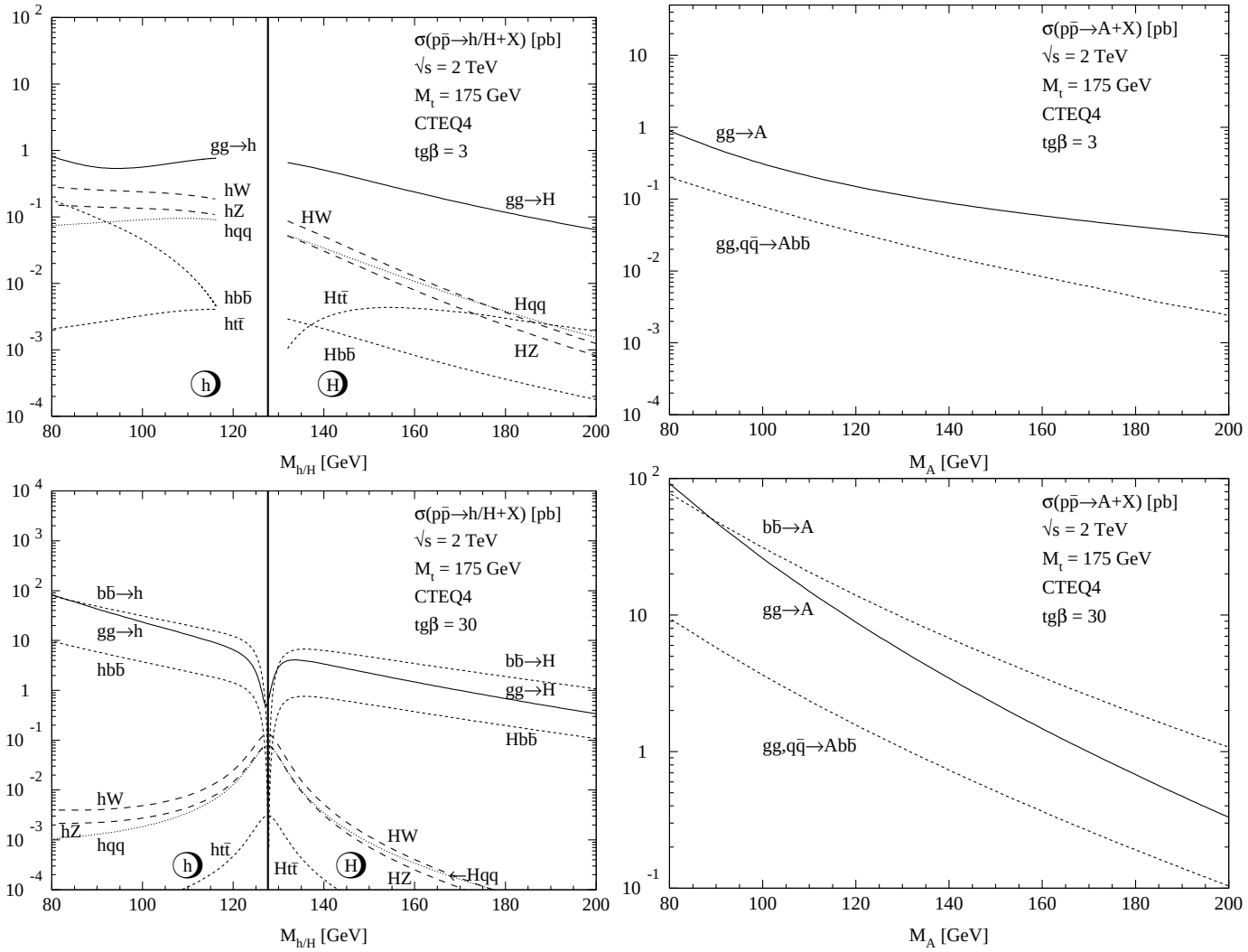

Figure 20: Neutral MSSM Higgs production cross-sections at the Tevatron [$\sqrt{s} = 2$ TeV] for gluon fusion $gg \to \phi$, vector-boson fusion $qq \to qqV^*V^* \to qqh$, qqH, vector-boson bremsstrahlung $q\bar{q} \to V^* \to hV/HV$ and the associated production $gg, q\bar{q} \to \phi b\bar{b}/\phi t\bar{t}$ including all known QCD corrections, where $\phi = h$, H or A [32,34]. As in fig. 5, in the vector boson fusion process, qq refers to both ud and $q\bar{q}$ scattering. The four panels exhibited above show (a) h, H production for $\tan\beta = 3$, (b) A production for $\tan\beta = 3$, (c) h, H production for $\tan\beta = 30$, (d) A production for $\tan\beta = 30$.

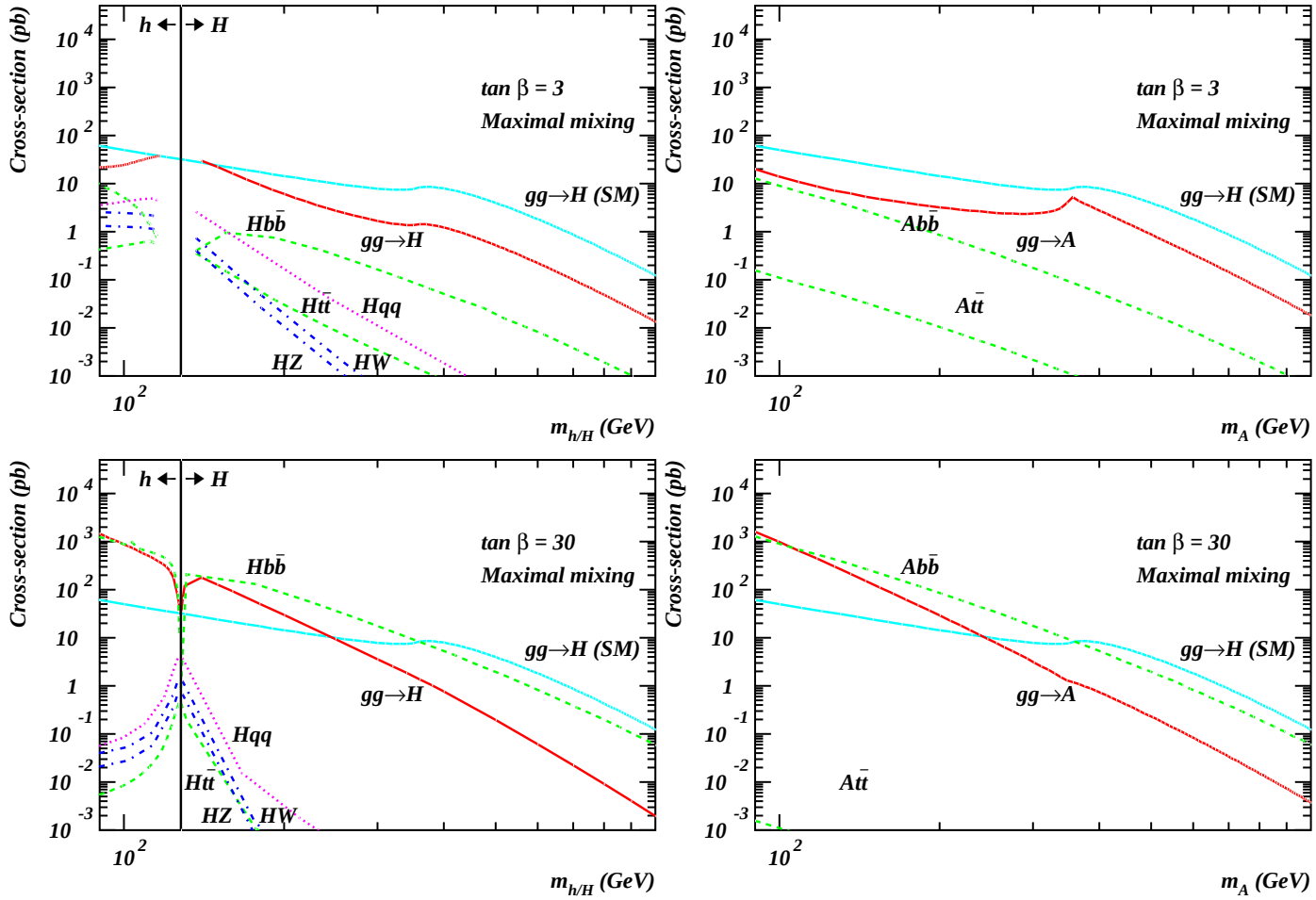

Figure 21: Neutral MSSM Higgs production cross-sections at the LHC [$\sqrt{s} = 14$ TeV] for gluon fusion $gg \to \phi$, vector-boson fusion $qq \to qqV^*V^* \to qqh$, qqH, vector-boson bremsstrahlung $q\bar{q} \to V^* \to hV/HV$ and the associated production $gg, q\bar{q} \to \phi b\bar{b}/\phi t\bar{t}$ including all known QCD corrections, where $\phi = h$, H or A [34,44]. The four panels exhibited above show the cross-section in pb *vs.* the Higgs mass, ranging from 90 GeV to 1 TeV, for (a) h, H production for $\tan\beta = 3$, (b) A production for $\tan\beta = 3$, (c) h, H production for $\tan\beta = 30$, (d) A production for $\tan\beta = 30$. For comparison, the cross-section for gluon-gluon fusion to a SM Higgs boson is also shown.

Higgs scalar, ϕ, has a mass less than or about equal to 130 GeV, and the corresponding cross-sections for $V^*V^* \to \phi$ and $q\bar{q} \to V^* \to V\phi$ are phenomenologically relevant. The other (non-SM-like) CP-even scalar has suppressed couplings to VV, and the corresponding cross-sections are generally too small to be observed.

Higgs boson radiation off bottom quarks becomes important for large $\tan\beta$ in the MSSM, where the Higgs coupling to bottom-type fermions is enhanced. Thus, the theoretical predictions, including full NLO computations, are crucial for realistic simulations of the MSSM Higgs signals in these channels.[26] Moreover, as discussed in Section 3.3.3, vertex corrections to the $b\bar{b}\phi$ coupling play a very important role in enhancing or suppressing (depending on the MSSM parameters) these production cross-sections at large $\tan\beta$ [152,160,170].

We now turn to charged Higgs production. If $m_{H^\pm} < m_t - m_b$, then $H^\pm$ can be produced in the decay of the top quark via $t \to bH^+$ (and $\bar{t} \to \bar{b}H^-$) [192]. The $t \to bH^+$ decay mode can be competitive with the dominant Standard Model decay mode, $t \to bW^+$, depending on the value of $\tan\beta$, as shown in fig. 22(a) for $m_{H^\pm} = 120$ GeV. This figure, taken from ref. [193] illustrates the effects of including one-loop radiative corrections. The curved labeled $\mathrm{BR}_{\mathrm{QCD}}$, which incorporates the one-loop QCD corrections (first computed in ref. [194]), is applicable to a more general (non-supersymmetric) Type-II two-Higgs doublet model [based on the tree-level Higgs-fermion couplings of eqs. (28)–(35)]. Note that the supersymmetric corrections can be particularly significant at large $\tan\beta$ due to the effect of Δ_b [see eq. (70)] depending on the choice of MSSM parameters. A full one-loop calculation of $\Gamma(t \to H^+ b)$ in the MSSM including all sources of large Yukawa couplings can be found in refs. [195] and [193]. A treatment including resummation of the leading QCD quantum effects and the dominant contributions from loop effects arising from supersymmetric particle exchange can be found in ref. [196].

For $m_{H^\pm} < m_t - m_b$, the total cross-section for charged Higgs production (in the narrow-width approximation) is then given by:[27]

$$\sigma(p\bar{p} \to H^\pm + X) = \Big(1 - [\mathrm{BR}(t \to bW^+)]^2\Big)\, \sigma(p\bar{p} \to t\bar{t} + X)\,. \tag{85}$$

With $\sigma(p\bar{p} \to t\bar{t}) \simeq 7$ pb at $\sqrt{s} = 2$ TeV and $\sigma(pp \to t\bar{t}) \simeq 1$ nb at $\sqrt{s} = 14$ TeV [197], roughly 1400 $t\bar{t}$ pairs per detector will be produced per year in Run 2a of the Tevatron (assuming a yearly luminosity of 2 fb^{-1}), while about 10^7–10^8 $t\bar{t}$ pairs will be produced at the LHC (assuming a yearly luminosity of 10–100 fb^{-1}). Folding in the top quark branching ratio, it is a simple matter to compute the inclusive

[26] As mentioned in the corresponding discussion for $q\bar{q}$, $gg \to b\bar{b}h_{\mathrm{SM}}$ [see Section 2.2.1], one also needs to evaluate $gb \to b\phi$ and $b\bar{b} \to \phi$ with suitable subtraction of the logarithms due to quasi-on-shell quark exchange (to avoid double counting) in order to obtain the total inclusive cross-section for ϕ production. For example, the $\tan\beta$ enhancement can lead to copious s-channel production of Higgs bosons via b-quark fusion [36,191].

[27] Note that if one evaluates $\sigma(p\bar{p} \to H^+\bar{t}b + X)$ in the region of $m_{H^\pm} < m_t - m_b$, one obtains the *single* charged Higgs inclusive cross-section, $\sigma(p\bar{p} \to H^+ + X) = \mathrm{BR}(t \to bH^+)\sigma(p\bar{p} \to t\bar{t} + X)$, rather than full charged Higgs inclusive cross-section of eq. (85). The latter is not quite a factor of two larger than the former since X can contain a charged Higgs boson; one must subtract off $[\mathrm{BR}(t \to bH^+)]^2\sigma(p\bar{p} \to t\bar{t} + X)$ to avoid double-counting.

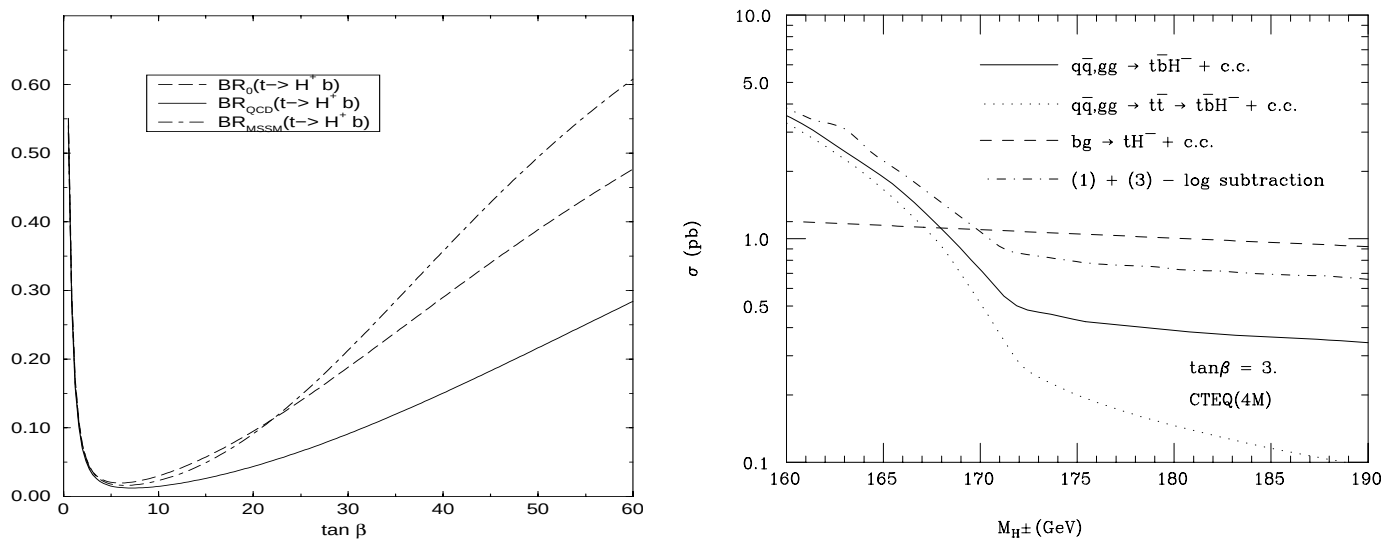

Figure 22: (a) Branching ratio for $t \to bH^+$ in the MSSM as a function of $\tan\beta$ for $m_{H^\pm} = 120$ GeV. The three curves shown are the results of a computation that (i) is at tree-level; (ii) includes one-loop QCD corrections; and (iii) incorporates both one-loop QCD, electroweak and the effects of MSSM particle exchange (taken from ref. [193]); the parameters chosen in (iii) correspond to a rather light supersymmetric spectrum: $M_{\tilde{g}} = 300$ GeV, $M_{\tilde{t}_1} = 100$ GeV, $M_{\tilde{b}_1} = 150$ GeV, $A_t = A_b = 300$ GeV, $M_2 = 150$ GeV, and $M_{\tilde{u}} = M_{\tilde{\nu}} = 200$ GeV. Curves (i) and (ii) are also applicable to a Model-II two-Higgs doublet model without supersymmetry. (b) The charged Higgs production cross-section at the LHC near the threshold for $t \to bH^+$ for $\tan\beta = 3$ (taken from ref. [199]).

charged Higgs cross-section. For values of $m_{H^\pm}$ near m_t, the width effects are important. In addition, the full $2 \to 3$ processes $p\bar{p} \to H^+\bar{t}b + X$ and $p\bar{p} \to H^-t\bar{b} + X$ must be considered. In this case eq. (85) no longer provides an accurate estimate of the charged Higgs cross-section [198], as illustrated in fig. 22(b) (taken from ref. [199]). The results of fig. 22(a) imply that for $m_{H^\pm} < m_t - m_b$, the discovery of the charged Higgs boson at the Tevatron and/or LHC (given sufficient luminosity) is possible if $\tan\beta \gg 1$ or $\tan\beta \lesssim 1$ (the latter is theoretically disfavored). The precise bound on $\tan\beta$ (as a function of $m_{H^\pm}$) depends somewhat on the details of the other MSSM Higgs parameters.

If $m_{H^\pm} > m_t - m_b$, then charged Higgs boson production occurs mainly through radiation off a third generation quark. Single charged Higgs associated production proceeds via the $2 \to 3$ partonic processes gg, $q\bar{q} \to t\bar{b}H^-$ (and the charge conjugate final state). As in the case of $b\bar{b}h_{\rm SM}$ production, large logarithms $\ln(m^2_{H^\pm}/m^2_b)$ arise for $m_{H^\pm} \gg m_b$ due to quasi-on-shell t-channel quark exchanges, which can be resummed by absorbing them into the b-quark parton densities. Thus, the proper procedure for computing the charged Higgs production cross-section is to add the cross-sections for $gb \to tH^-$ and $gg \to t\bar{b}H^-$ and subtract out the large logarithms accordingly from the calculation of the $2 \to 3$

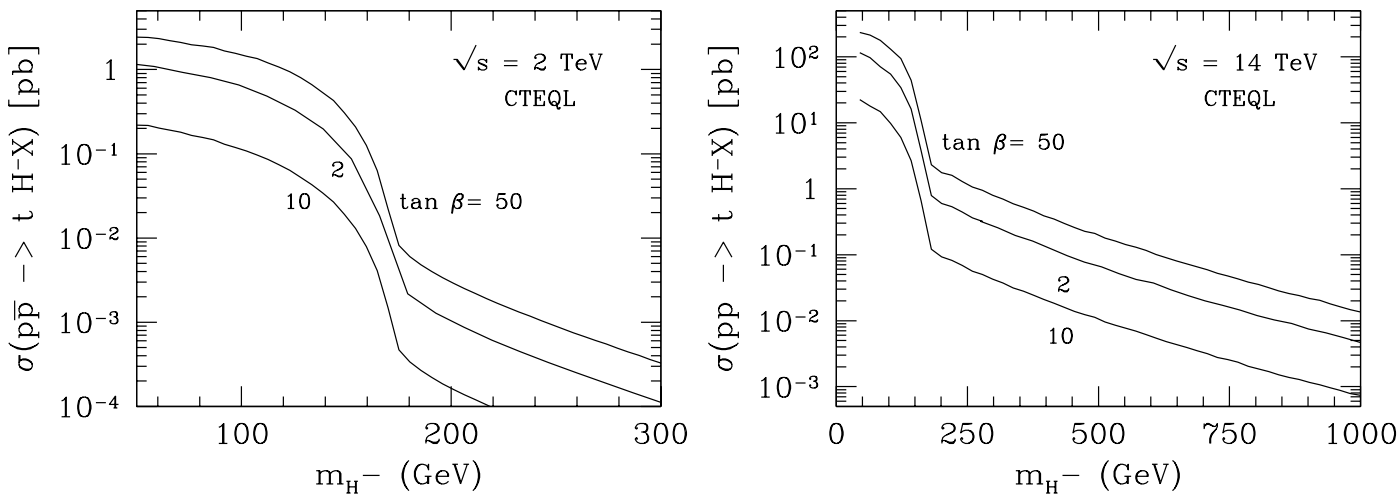

Figure 23: The leading-order production cross-sections for charged Higgs production at (a) the Tevatron ($p\bar{p} \to t\bar{b}H^- + X$) and (b) the LHC ($p\bar{p} \to t\bar{b}H^- + X$) are shown as a function of $m_{H^\pm}$ for three values of $\tan\beta = 2$, 10 and 50. The cross-sections are obtained by adding the contribution of the $2 \to 2$ processes, $gb \to tH^-$, to those of the $2 \to 3$ processes, $gg \to t\bar{b}H^-$ and $q\bar{q} \to t\bar{b}H^-$ (suitably subtracted to avoid double counting). Renormalization and factorization scales have been both set to $m_t + m_{H^\pm}$. These results are taken from ref. [201].

process [48,200]. This procedure avoids double-counting of the large logarithms at $\mathcal{O}(\alpha_s)$, and correctly resums the leading logs to all orders. In particular, the contribution to the total cross-section coming from the kinematical region of the gluon-initiated $2 \to 3$ process in which one of the two gluons splits into a pair of b-quarks (one of which is collinear with the initial proton or antiproton), is incorporated into the b-quark parton density. A cruder calculation would omit the contribution of the $2 \to 2$ process and simply include the results of the unsubtracted $2 \to 3$ process. The latter procedure would miss the resummed leading logs that are incorporated into the b-quark density. However, the numerical difference between the two procedures is significant only for $m_{H^\pm} \gg m_t$.

The single inclusive charged Higgs cross-sections at the Tevatron and LHC are exhibited in fig. 23 as a function of the charged Higgs mass, for $\tan\beta = 2$, 10 and 50. Note that the cross-sections shown include the region of charged Higgs mass below $m_{H^\pm} = m_t - m_b$ corresponding to the case discussed above where the charged Higgs cross-section is dominated by $t\bar{t}$ production followed by $t \to bH^-$. These results are based on the calculations of ref. [201] and include the contributions of the $2 \to 2$ process and suitably subtracted $2 \to 3$ process as described above. Similar results have also been obtained in ref. [202]. The impact of the leading electroweak and MSSM radiative corrections has been studied in ref. [203]. In addition, the NLO QCD corrections to the $2 \to 2$ process $gb \to H^+t$ have recently been

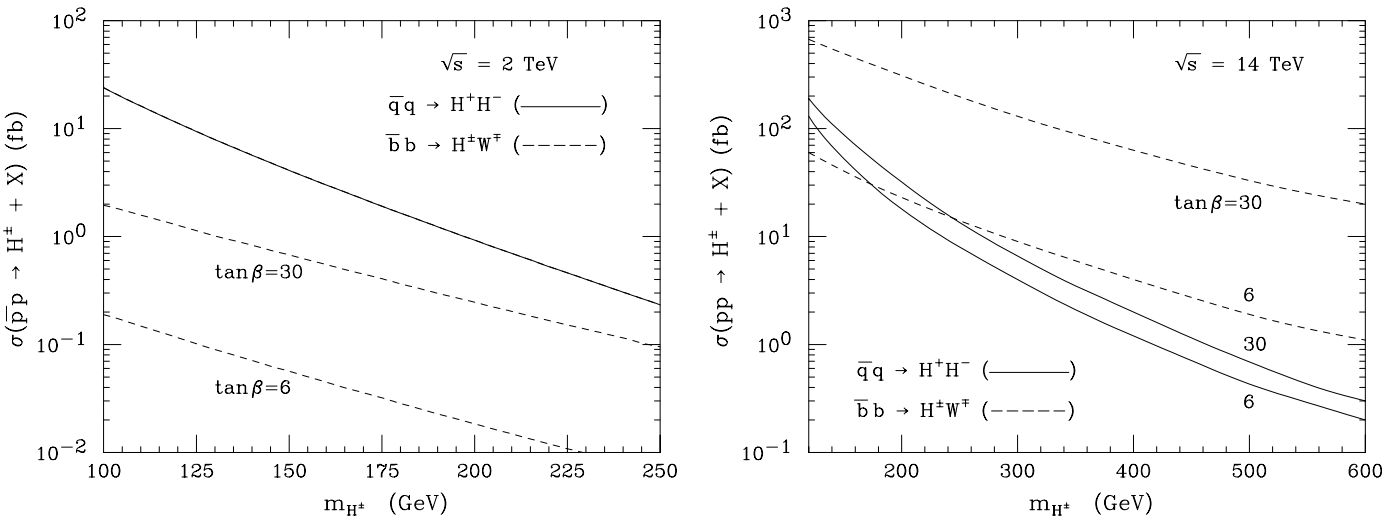

Figure 24: Total cross-section (in fb) for inclusive production of (i) $H^+H^- + X$ [207] (solid line) and (ii) $H^\pm W^\mp + X$ [205] (dashed lines) as a function of $m_{H^\pm}$ for $\tan\beta = 6$ and 30. Curves for (a) $p\bar{p} \to H^+H^- + X$ at the Tevatron and (b) $pp \to H^+H^- + X$ at the LHC are exhibited. Note that the dependence of process (i) on $\tan\beta$ is negligible at the Tevatron, while there is some $\tan\beta$ dependence at the LHC due to the enhancement of $b\bar{b} \to H^+H^-$ at large $\tan\beta$. The contribution of $b\bar{b}$ annihilation to process (ii) dominates over the gg fusion scattering mechanism. $M_t = 174.3$ GeV and a fixed b-quark pole mass of $M_b = 4.7$ GeV are used to fix the Higgs–fermion Yukawa coupling. The leading-order CTEQ5L parton distribution functions are used.

evaluated [204]. These corrections typically increase the tree-level cross-section by a factor of 1.3 to 1.6, depending on the value of the charged Higgs mass and $\tan\beta$, with some additional dependence on the choice of renormalization and factorization scales.

Associated production of a charged Higgs boson and a $W^\pm$ can occur via $b\bar{b}$ annihilation and gg-fusion [205]. The contribution of $b\bar{b}$ annihilation to $\sigma(p\bar{p} \to H^\pm W^\mp + X)$ [$\sigma(pp \to H^\pm W^\mp + X)$] at the Tevatron [LHC] (both charge combinations are included) are shown as function of the charged Higgs mass for $\tan\beta = 6$ and 30 in fig. 24. The loop-induced gg fusion contribution is significantly suppressed relative to the tree-level $b\bar{b}$ annihilation if $\tan\beta \gtrsim 6$, independently of the value of $m_{H^\pm}$ [206].

Charged Higgs bosons can also be produced in pairs via Drell-Yan $q\bar{q}$ annihilation. The dominant contribution, which arises from $u\bar{u}$ and $d\bar{d}$ annihilation into a virtual photon or Z, is independent of $\tan\beta$. Some $\tan\beta$ dependence enters through $b\bar{b}$ annihilation via t-channel top-quark exchange, although this effect is more than one order of magnitude suppressed relative to the dominant contribution at the Tevatron. The $b\bar{b}$ annihilation is more significant at the LHC (at large $\tan\beta$ where the $H^-t\bar{b}$ coupling is enhanced). The tree-level results for $\sigma(p\bar{p} \to H^+H^- + X)$ at the Tevatron and $\sigma(pp \to H^+H^- + X)$ at the LHC are shown in fig. 24. These results are obtained [207] with the Higgs–fermion Yukawa

coupling based on a fixed b-quark pole mass of $M_b = 4.7$ GeV. The contribution of the loop-induced $gg \to H^+H^-$ is typically less important than that of $q\bar{q}$ annihilation [208,209], and is not included in fig. 24. However, the gg fusion contribution can become significant at large $\tan\beta$, with further enhancements in some regions of MSSM parameter space in which the squarks (which appear in the loop) are light and strongly mixed [209]. Nevertheless, the inclusive H^+H^- cross-section lies below the cross-section for single charged Higgs associated production (*c.f.* figs. 23 and 24).

Finally, one can compute the cross-sections for double neutral Higgs production at hadron colliders. These include the inclusive production of hh, hH, HH, hA, HA and AA. Cross-sections can be found in refs. [54,55,56] and [210,211] (QCD corrections to these cross-sections are evaluated in ref. [55]). In general, the rates for these processes are considerably smaller than for the corresponding single Higgs production rates. However, in certain regions of supersymmetric parameter space, squark loops can enhance the cross-section for pair production of two CP-even Higgs bosons by as much as two orders of magnitude [210]. In some cases, observation of double Higgs production provides some information on three-Higgs couplings. For example, for low to moderate values of $\tan\beta$, gluon fusion to a virtual Higgs boson, which splits into hh, is dominant over $b\bar{b} \to hh$. Thus, the overall rate for $pp \to hh + X$ would provide a measure of the hhh vertex.

Additional sources for Higgs boson production can arise from the decay of supersymmetric particles into final states containing one or more Higgs boson in the decay chain [212]. These processes depend in detail on the details of the supersymmetric particle spectrum and their couplings. For example, the production of h in supersymmetric particle decay followed by the decay $h \to b\bar{b}$ can yield a signal above background at LHC [213]. Processes of this type provide additional channels for possible Higgs discovery and precision study, and deserve further analysis.

3.5.2 Benchmarks for Higgs searches

In the search for the MSSM Higgs bosons, one must first search for the lightest Higgs scalar, which is expected (in almost all cases) to be the neutral CP-even scalar, h. In the decoupling region of the MSSM Higgs parameter space (where $m_A \gg m_Z$), the search techniques already outlined for $h_{\rm SM}$ are relevant for h, since the properties of h approximately coincide with those of the SM Higgs boson. The h discovery reach can be mapped out as a region of m_A–$\tan\beta$ parameter space, since these two parameters (along with the MSSM parameters that determine the size of the radiative corrections) fix the value of m_h. Next, it is critical to identify deviations of the properties of h from those of $h_{\rm SM}$. Positive evidence for such a deviation would signal the existence of additional scalar states of the non-minimal Higgs sector. The difficulty of this step depends on how close the model is to the decoupling limit. After the discovery of h, the Higgs boson search will focus on the non-minimal Higgs states of the model.

For values of $m_A \sim m_Z$, all the Higgs bosons of the MSSM are of a similar order of magnitude, and the properties of h will no longer resemble those of $h_{\rm SM}$. In principle, one can then discover multiple scalar states in one experiment. Since the two CP-even scalars share the coupling to vector boson pairs

[eq. (22)], one may identify the CP-even scalar whose squared-coupling to VV is larger than $0.5g^2_{h_{\rm SM}VV}$. The Tevatron and LHC production cross-sections of this scalar (compared to that of $h_{\rm SM}$) are reduced by no more than 50% (by assumption), while the Higgs branching ratio into $b\bar{b}$ is similar to that of $h_{\rm SM}$ over most of the MSSM parameter space. Thus, the Tevatron and LHC SM Higgs search results also apply here modulo minor modifications (which account for the somewhat suppressed production cross-section and the effects of supersymmetric corrections to the third generation Yukawa couplings).

The general MSSM parameter space involves many *a priori* unknown parameters. In practice, only a small subset of these parameters govern the properties of the Higgs sector. Nevertheless, a full scan of this reduced subset is still a formidable task. However, a detailed study of a few appropriately chosen points of the parameter space can help determine the ultimate MSSM Higgs discovery reach of the Tevatron and LHC. It is convenient to choose a set of benchmark MSSM parameters that govern the Higgs radiative corrections [156,214]. These include the supersymmetric Higgs mass parameter μ, the third generation squark mixing parameters, A_t and A_b, the gluino mass $M_{\tilde{g}}$, the diagonal soft-supersymmetry-breaking third generation squark squared-masses (which we take for simplicity to be degenerate and equal to $M_{\rm SUSY}$), and the top quark mass (which is held fixed at $m_t = 174.3$ GeV). The *maximal mixing* benchmark scenario, is defined as the one in which the squark mixing parameters are such that they maximize the value of the lightest CP-even Higgs boson mass for fixed values of m_A, $\tan\beta$ and $M_{\rm SUSY}$. Here, we choose $X_t \equiv A_t - \mu\cot\beta \simeq \sqrt{6}$, $A_b = A_t$, $M_2 = -\mu = 200$ GeV and $M_{\tilde{g}} = M_{\rm SUSY} = 1$ TeV [corresponding to $m_h^{\rm max} = 129$ GeV].

The maximal mixing scenario poses a challenge for Higgs searches, since the predicted Higgs mass takes on its maximal value for a given set of MSSM parameters. However, different regions of the MSSM Higgs parameter space pose new challenges. For example, regions of parameter space exist in which the CP-even neutral Higgs boson with SM-like couplings to the W, Z and t has suppressed couplings to $b\bar{b}$. The benchmark scenario denoted by "suppressed $V\phi \to Vb\bar{b}$ production" is an example of this behavior. In this case, we take $\mu = -A_t = 1.5$ TeV, $A_b = 0$, $M_2 = 200$ GeV and $M_{\tilde{g}} = M_{\rm SUSY} = 1$ TeV [corresponding to $m_h^{\rm max} = 120$ GeV]. The regions of strongly suppressed BR($\phi \to b\bar{b}$) correspond to a suppressed $Hb\bar{b}$ coupling at lower m_A and a suppressed $hb\bar{b}$ coupling at larger m_A. In particular, the suppression for large $\tan\beta$ extends to relatively large values of $m_A \sim 300$ GeV, indicating a delay in the onset of the decoupling limit. Moreover, in the suppressed $V\phi \to Vb\bar{b}$ benchmark scenario, *all* the Higgs couplings to $b\bar{b}$ are generally suppressed, since $0 < \Delta_b \ll 1$ and $\sin 2\alpha \simeq 0$. From the analytic formulae, it can be deduced that $\mu A_t < 0$ and large values of $|A_t|$, $|\mu|$ and $\tan\beta$ are needed.

The coverage in the m_A–$\tan\beta$ plane by different Higgs production and decay channels can vary significantly, depending on the choice of MSSM parameters. In the last example in which the CP-even Higgs boson with the larger coupling to the W and Z has a strongly suppressed coupling to bottom quarks, the Higgs searches at the Tevatron will become more problematical, while the LHC search for Higgs production followed by its decay into photons becomes more favorable [160]. At the same time the LHC Higgs discovery reach via vector bosons fusion to Higgs production followed by its decay into $\tau^+\tau^-$ pairs can be significant [215].

3.5.3 MSSM Higgs Boson searches at the Tevatron

We first consider the Tevatron MSSM Higgs search. Specifically, we make use of the Tevatron $h_{\rm SM}$ search techniques, where $h_{\rm SM}$ is replaced by either h or H. If $\tan\beta \gg 1$, a new search mode becomes viable, due to the possibility of enhanced couplings of the neutral Higgs boson states to $b\bar{b}$ [216,170]. Thus, we also consider the possibility of the $b\bar{b}\phi \to b\bar{b}b\bar{b}$ signature, where $\phi = h$, H, and/or A. If $\tan\beta$ is large, two of the neutral Higgs boson states, $\phi = A$ and h $[H]$ are produced with enhanced rates if $m_A \lesssim m_Z$ $[m_A \gg m_Z]$, as noted below eq. (35). We may combine the results for the various channels to provide summary plots of the MSSM Higgs discovery reach of the upgraded Tevatron collider. We consider here the results based on a generic MSSM analysis [62]; see ref. [217] for a similar analysis in the context of a variety of models of supersymmetry breaking. In the latter case, the results obtained will be somewhat more constraining than the generic analysis, since the supersymmetry-breaking parameters that control the radiative corrections to Higgs masses and couplings are no longer arbitrary.

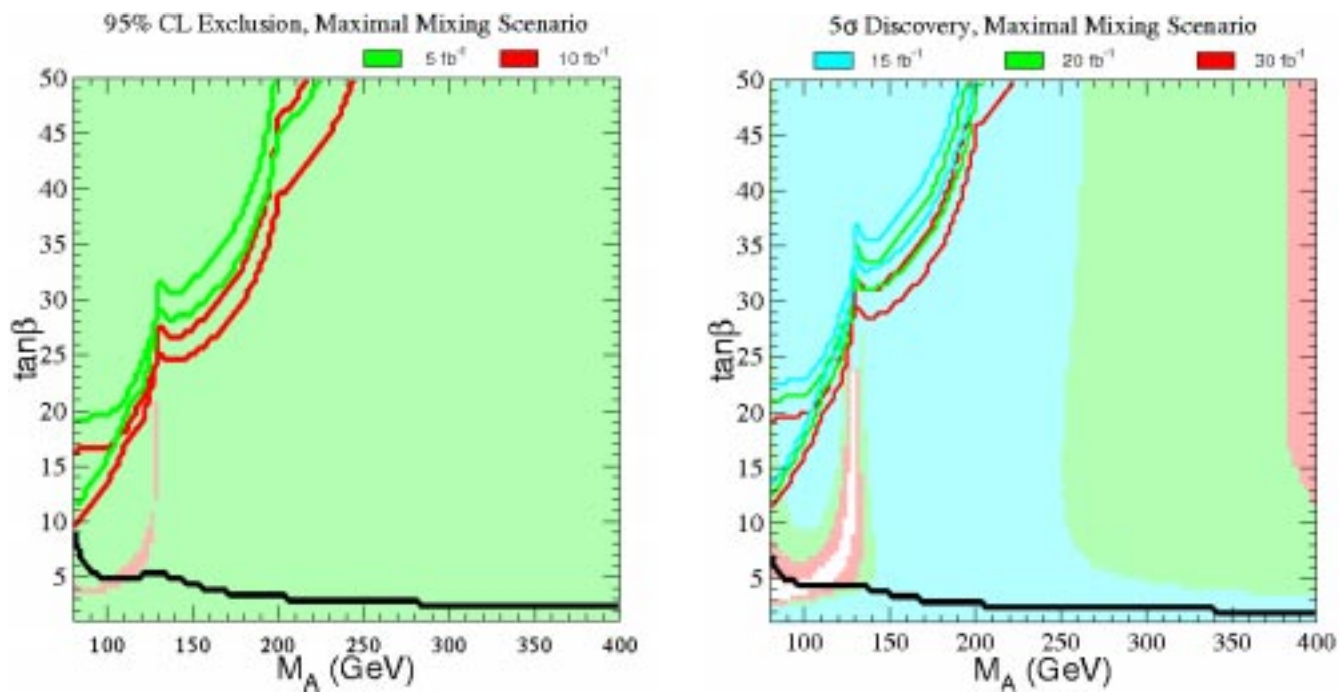

Figure 25: (a) 95% CL exclusion region and (b) 5σ discovery region in the m_A–$\tan\beta$ plane, for the maximal mixing benchmark scenario (see Section 3.5.2) and two different search channels: $q\bar{q} \to V\phi$ $[\phi = h,\, H]$, $\phi \to b\bar{b}$ (shaded regions) and gg, $q\bar{q} \to b\bar{b}\phi$ $[\phi = h,\, H,\, A]$, $\phi \to b\bar{b}$ (region in the upper left-hand corner bounded by the solid lines; the two sets of lines correspond to CDF and DØ simulations). The region below the solid black line near the bottom of the plot is excluded by the absence of $e^+e^- \to Z\phi$ events at LEP. Taken from ref. [62].

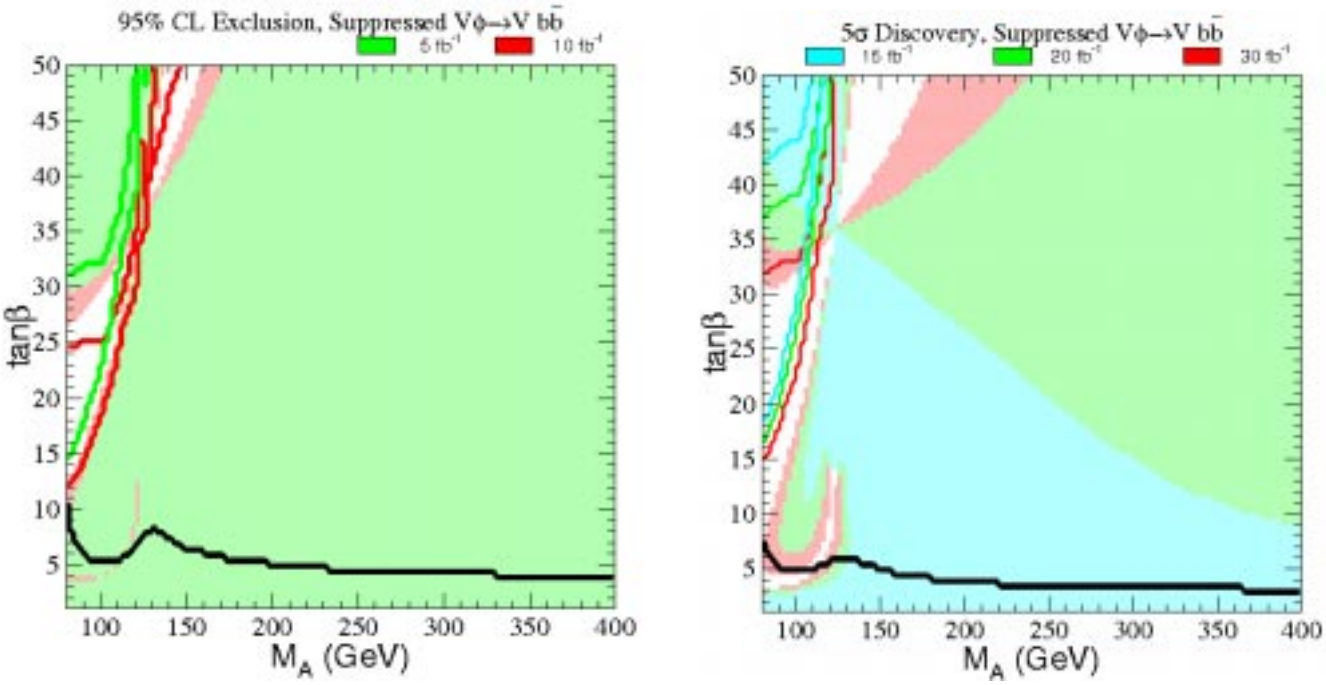

Figure 26: The same as fig. 25 but for the suppressed $V\phi \to Vb\bar{b}$ production benchmark scenario of Section 3.5.2. Taken from ref. [62].

In figs. 25 and 26, we show the regions of 95% CL Higgs exclusion and 5σ Higgs discovery on the m_A–$\tan\beta$ plane, for two representative MSSM parameter choices, via the search of neutral Higgs bosons in the channels: $q\bar{q} \to V\phi$ [$\phi = h$, H], $\phi \to b\bar{b}$ (shaded regions) and gg, $q\bar{q} \to b\bar{b}\phi$ [$\phi = h$, H, A], $\phi \to b\bar{b}$ (region in the upper left-hand corner bounded by the solid lines), for different integrated luminosities as indicated by the color coding. The shaded regions presented in these figures reflect the results of the SHW simulation of $q\bar{q} \to V\phi$ improved by neutral network techniques [62]. The two sets of lines (for a given color) bounding the regions accessible by the $b\bar{b}\phi$ search correspond to the CDF and DØ simulations, respectively. The solid black line near the bottom of each plot indicates the lower limit of $\tan\beta$ (as a function of m_A) based on the absence of observed $e^+e^- \to Z\phi$ events at LEP [161]. Note the importance of the complementarity between the $q\bar{q} \to V\phi$ and $q\bar{q} \to b\bar{b}\phi$ channels for improving the coverage of the MSSM parameter space in the low m_A region in fig. 26(a). The results of figs. 25(a) and 26(a) demonstrate that 5 fb^{-1} of integrated luminosity per experiment will be sufficient to cover nearly all of the MSSM Higgs parameter space at 95% CL in the benchmark scenarios specified above.

To assure discovery of a CP-even Higgs boson at the 5σ level, the luminosity requirement becomes very important. Figs. 25(b) and 26(b) show that a total integrated luminosity of about 20 fb^{-1} per

experiment is necessary in order to assure a significant, although not exhaustive, coverage of the MSSM parameter space. In general, we observe that the complementarity between the two channels, $q\bar{q} \to V\phi$ and $q\bar{q} \to b\bar{b}\phi$, is less effective in assuring discovery of a Higgs boson as compared with a 95% CL Higgs exclusion. This is due to the much higher requirement of total integrated luminosity combined with the existence of MSSM parameter regimes which can independently suppress both Higgs production channels. Fig. 26 exhibits one of the most difficult regions of MSSM parameter space for Higgs searches at the Tevatron collider. Nevertheless, even in this case, a very high luminosity experiment can cover a significant fraction of the available MSSM parameter space.

If explicit CP violation occurs through nonzero phases of the supersymmetry breaking parameters, then the three neutral Higgs bosons are a combination of CP-even and CP-odd states and the phenomenology can become much more complicated. In particular the couplings of the neutral Higgs bosons to the W and Z bosons are now shared by the three Higgs bosons and it may well be that the lightest Higgs has such a weak coupling to the vector bosons that it would have been missed at LEP and will be elusive at the Tevatron. Fig. 16 shows an interesting example where the effects of CP violation are such that for CP-violating phases of the parameter A_t of about 90°, the lightest Higgs boson cannot be detected at the Tevatron even though its mass is below 100 GeV, but the second lightest Higgs has SM-like couplings to the W and Z and thus can be detected if sufficient luminosity is provided.

3.5.4 MSSM Higgs Searches at the LHC

If no Higgs boson is discovered at the Tevatron, the LHC will cover the remaining unexplored regions of the m_A–$\tan\beta$ plane, as shown in figs. 27 and 28. That is, in the maximal mixing scenario (and probably in most regions of MSSM Higgs parameter space), at least one of the Higgs bosons is guaranteed to be discovered at either the Tevatron and/or the LHC. A large fraction of the parameter space can be covered by the search for a neutral CP-even Higgs boson by employing the SM Higgs search techniques, where the SM Higgs boson is replaced by h or H with the appropriate re-scaling of the couplings. Moreover, in some regions of the parameter space, both h and H can be simultaneously observed, and additional Higgs search techniques can be employed to discover A, and/or $H^\pm$ at the LHC.

A CP-even Higgs boson, ϕ, can be observed in a number of different decay modes. If $m_A > m_h^{\max}$, then $\phi = h$ is SM-like (near the decoupling limit), whereas at large $\tan\beta$ and $m_A < m_h^{\max}$, $\phi = H$ is the SM-like Higgs boson.[28] It is possible to observe $\phi \to \gamma\gamma$ when ϕ is produced singly via gg and V^*V^* fusion, or when produced in association with $W^\pm$ and/or $t\bar{t}$. A second decay mode, $h \to b\bar{b}$, can be observed in $\phi t\bar{t}$ production. Finally, it may be possible to observe $\phi \to \tau^+\tau^-$ when ϕ is produced via V^*V^* fusion, where the forward jets are used to help reduce backgrounds [215]. Hence, by using the complementarity of the various Higgs signatures described above, one can discover ϕ over

[28] For $m_A < m_h^{\max}$ and moderate $\tan\beta$ values, neither CP-even Higgs boson is SM-like, although both Higgs masses lie below about 150 GeV and will appear (albeit with reduced couplings to VV) in the Higgs searches described above.

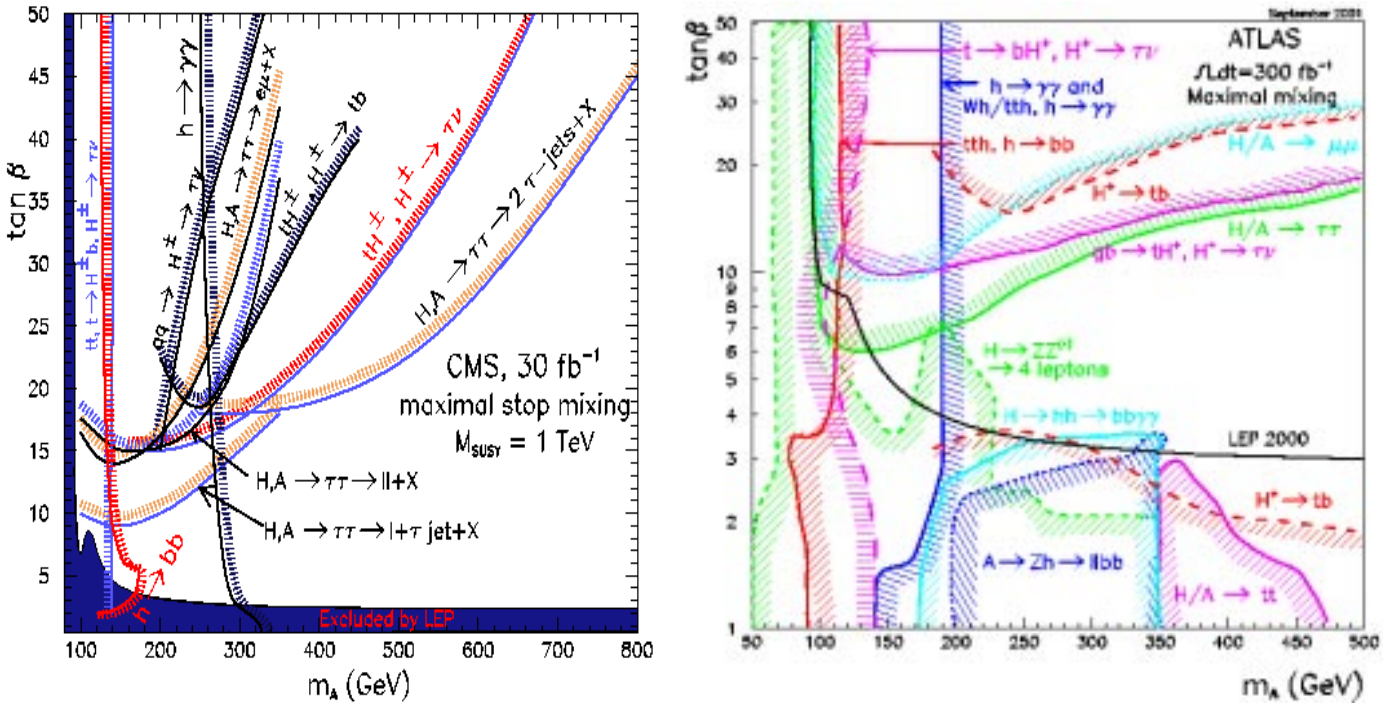

Figure 27: (a) 5σ discovery contours for MSSM Higgs boson detection in various channels in the m_A–$\tan\beta$ plane, in the maximal mixing scenario, assuming an integrated luminosity of $L = 30$ fb^{-1} for the CMS detector [218]. (b) As in (a), but for an integrated luminosity of $L = 300$ fb^{-1} for the ATLAS detector [222].

nearly the entire MSSM parameter space, given sufficient integrated luminosity.[29] In order to illustrate the complementarity of the $\gamma\gamma$ and $b\bar{b}$ decay modes, we exhibit in fig. 29 the regions of MSSM Higgs parameter space that can be covered for the two benchmark scenarios of MSSM parameters described in Section 3.5.2. The behavior illustrated in this figure can be understood by noting that the $\phi b\bar{b}$ coupling can be significantly suppressed (or enhanced), depending on the impact of the radiative corrections discussed in Section 3.3. As a result, the branching ratio for $\phi \to \gamma\gamma$ is correspondingly larger (or smaller), with obvious implications for the $\phi \to b\bar{b}$ and $\phi \to \gamma\gamma$ searches.

We next focus on the potential for observing the heavier Higgs states ($H^\pm$, A and H). A number of recent studies [74,75,218,219,220,221] show that the following modes will be effective in searching for the heavier MSSM Higgs bosons. For the heavy neutral Higgs bosons, the most relevant decay signatures

[29] One must still demonstrate that it is possible at the LHC to discover the lightest CP-even Higgs boson, even if its branching ratios into $b\bar{b}$ and/or $\gamma\gamma$ are significantly suppressed (either due to the effects of radiative corrections or due to the existence of a significant branching fraction into invisible modes). Such suppressions can occur in regions of the MSSM parameter space not yet considered by the LHC Higgs search simulations.

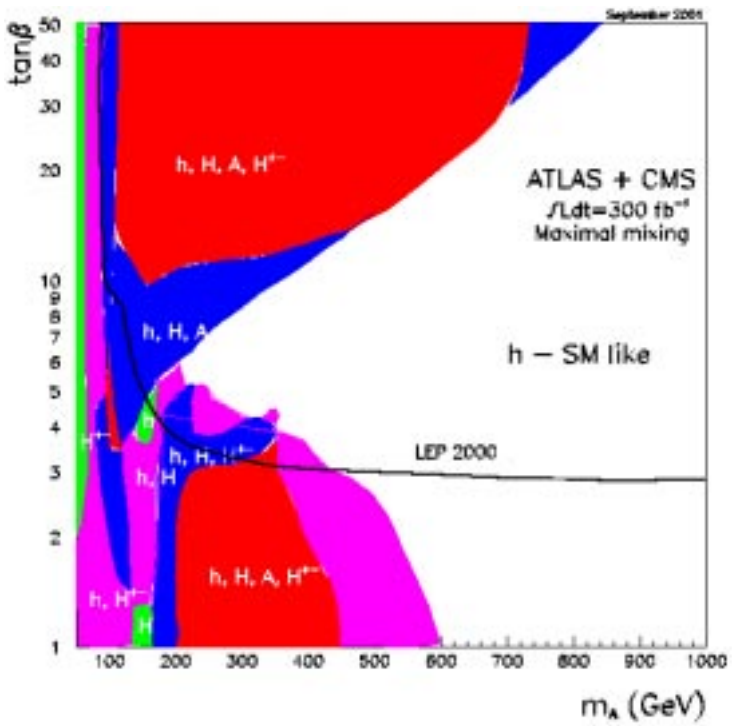

Figure 28: Regions in the m_A–$\tan\beta$ plane in the maximal mixing scenario in which up to four Higgs boson states of the MSSM can be discovered at the LHC with 300 fb^{-1} of data, based on a simulation that combines data from the ATLAS and CMS detectors. Taken from ref. [87].

are: $A, h \to \tau^+\tau^-$ (where the τ is detected either via its leptonic or hadronic decay) and $A, h \to \mu^+\mu^-$, which yield promising signals if $\tan\beta$ is large. The $\tau^+\tau^-$ channel provides the largest discovery reach in the heavy Higgs mass. Other possible neutral Higgs decays: $A, H \to t\bar{t}$; $H \to ZZ^* \to 4\ell$; $H \to hh$ and $A \to Zh$ are significant in regions of the parameter space that are (nearly) ruled out by the LEP Higgs search. For the charged Higgs boson, we must again consider whether $H^\pm$ can be produced in (on-shell) top-quark decays. If this decay is forbidden, the positively charged Higgs boson will be produced primarily by $gb \to H^+t$ (see Section 3.5.1). In either case, the observation of the charged Higgs boson is possible if $\tan\beta \gg 1$ or $\tan\beta \lesssim \mathcal{O}(1)$ [221]. For large $\tan\beta$, the decays $H^+ \to \tau^+\nu$ and $t\bar{b}$ (if kinematically allowed) provide the most favorable signatures. In particular, the $\tau\nu$ decay mode, followed by the hadronic decay of the τ provides the largest discovery reach for large $m_{H^\pm}$. The ultimate charged Higgs mass reach can depend significantly on the choice of MSSM parameters that control the radiative corrections to the Higgs-bottom quark Yukawa coupling [196] [see, *e.g.*, eq. (70)].

Putting all of the above results together, it may be possible at the LHC to either *exclude* the entire m_A–$\tan\beta$ plane (thereby eliminating the MSSM Higgs sector as a viable model), or achieve a

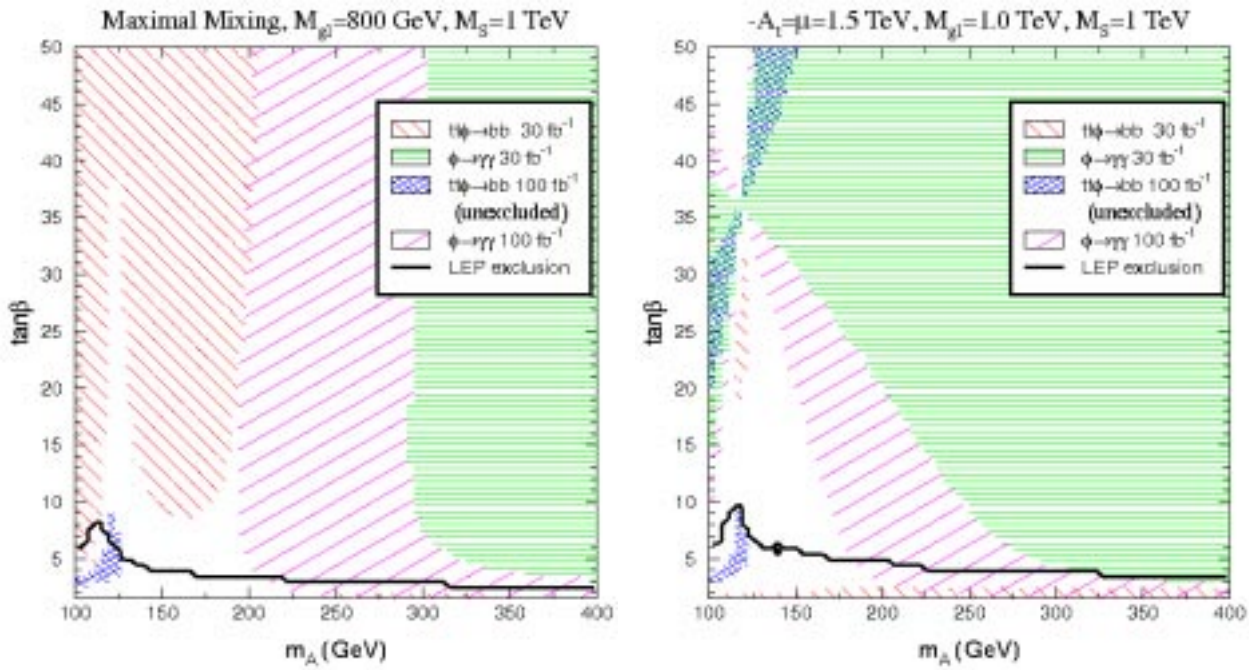

Figure 29: Complementarity between the LHC searches for the decay modes $\phi \to b\bar{b}$ and $\phi \to \gamma\gamma$, where $\phi = h$ or H corresponds to the CP-even Higgs boson with the larger coupling to VV. Two different choices of MSSM parameters are exhibited: (a) the maximal mixing scenario and (b) the suppressed $Vb \to Vb\bar{b}$ production scenario. In both cases, the region corresponding to 5σ discovery of $\phi \to \gamma\gamma$ with 30 fb^{-1} of data is shaded with parallel horizontal lines. With 100 fb^{-1} of data, these regions expand to include areas shaded with diagonal parallel lines with positive slope. The region corresponding to 5σ discovery of $t\bar{t}\phi \to t\bar{t}b\bar{b}$ with 30 fb^{-1} of data is shaded with diagonal parallel lines with negative slope. With 100 fb^{-1} of data, these regions expand to include the entire m_A–$\tan\beta$ plane *excluding* the blue cross-hatched region. The "unexcluded" region (where no discovery of $t\bar{t}\phi \to t\bar{t}b\bar{b}$ is possible) occupies a small region at low $\tan\beta$ and m_A in both (a) and (b). In addition, in case (b), the excluded region also includes the two narrow wedge regions at large $\tan\beta$ and low m_A. Taken from ref. [223].

5σ discovery of at least one of the MSSM Higgs bosons, independently of the value of $\tan\beta$ and m_A. For example, Fig. 27 shows what can be achieved by the CMS detector with 30 fb^{-1} [218] and by the ATLAS detector with 300 fb^{-1} [222], assuming the maximal mixing scenario. Note that over a significant fraction of the MSSM Higgs parameter space, at least two Higgs bosons can be observed as shown in fig. 28. Nevertheless, there is still a sizable wedge-shaped region at moderate values of $\tan\beta$ opening up from about $m_A = 200$ GeV to higher values in which the heavier Higgs bosons cannot be discovered at the LHC. In this parameter regime, only the lightest CP-even Higgs boson can be discovered, and its properties are nearly indistinguishable from those of the SM Higgs boson. Precision measurements of Higgs branching ratios and other properties will be required in order to detect deviations from SM Higgs predictions and demonstrate the existence of a non-minimal Higgs sector.

Finally, we noted at the end of Section 3.5.3 that CP-violating effects in the Higgs sector can modify the usual CP-conserving Higgs phenomenology. As a result, the LHC discovery reach of various Higgs channels discussed above may be altered in a significant way. It is therefore essential to make complementary measurements in as many Higgs channels as possible in order to cover the most general MSSM parameter space [223].

3.6 MSSM Higgs Boson Searches at the LC

The main production mechanisms for the MSSM Higgs bosons are [224]

$$\begin{aligned}
&(i)\quad e^+e^- \to Zh\,, ZH \quad \text{via Higgs-strahlung}\,,\\
&(ii)\quad e^+e^- \to \nu\bar{\nu}h\,, \nu\bar{\nu}H \quad \text{via } W^+W^- \text{ fusion}\,,\\
&(iii)\quad e^+e^- \to hA\,, HA \quad \text{via } s\text{-channel } Z \text{ exchange}\,,\\
&(iv)\quad e^+e^- \to H^+H^- \quad \text{via } s\text{-channel } \gamma\,, Z \text{ exchange}\,.
\end{aligned} \tag{86}$$

As in the SM Higgs search, process *(i)* followed by $Z \to \ell^+\ell^-$ allows the Higgs boson recoiling against the Z to be reconstructed, independently of the Higgs decay channel. Thus, h [or H if $\sin(\beta-\alpha) \ll 1$] can be discovered at the LC even if it has a large branching fraction into invisible modes.[30]

Processes *(i)* and *(iii)* are complementary to each other as a consequence of unitarity sum rules for tree-level Higgs couplings [131,132]. In particular, eq. (24) implies that both $g^2_{\phi ZZ}$ and $g^2_{\phi AZ}$ ($\phi = h$ or H) cannot simultaneously vanish. If $m_A \lesssim m_h^{\max}$, then all the MSSM Higgs boson states have mass below 150 GeV, and can be cleanly reconstructed at the LC (with $\sqrt{s} \geq 350$ GeV) via the four production mechanisms listed above [92]. On the other hand, when $m_A \gtrsim 200$ GeV, one finds that $m_A \sim m_H \sim m_{H^\pm}$ and $g_{HZZ} \sim g_{hAZ} \sim 0$, and the couplings of h are nearly identical to those of $h_{\rm SM}$ as a consequence of the decoupling limit. Since $m_h \lesssim 135$ GeV, the LC with a center-of-mass energy of 300 GeV is more than sufficient to observe the h [via processes *(i)* and *(ii)*] and thus cover the entire MSSM parameter space with certainty. Moreover, the cross-sections for HZ, $H\nu\bar{\nu}$ and hA are strongly suppressed [since $|\cos(\beta-\alpha)| \ll 1$]. The cross-sections for HA and H^+H^- production are unsuppressed if kinematically allowed.[31] That is, the heavy Higgs bosons, H, A and $H^\pm$ can only be observed in pair production processes where both Higgs states are heavy (and the minimum $\sqrt{s}$ required is somewhat above $2m_A$). These features are evident in fig. 30, which depicts cross-sections for Higgs-strahlung [process *(i)*] and associated Higgs pair production [processes *(iii)* and *(iv)*] as a function of the corresponding Higgs mass for two different choices of $\sqrt{s}$ and $\tan\beta$. The cross-section

[30] The processes $e^+e^- \to e^+e^-h$, e^+e^-H (via ZZ fusion) also allow for Higgs detection, independently of its decay channel, by reconstruction of the Higgs boson recoiling against the final state e^+e^- pair. However, the ZZ fusion rates are an order of magnitude smaller than the corresponding W^+W^- fusion rates [process *(ii)*].

[31] Due to the p-wave suppression at threshold, the HA and H^+H^- cross-sections fall off rapidly as the corresponding Higgs masses approach $\sqrt{s}/2$.

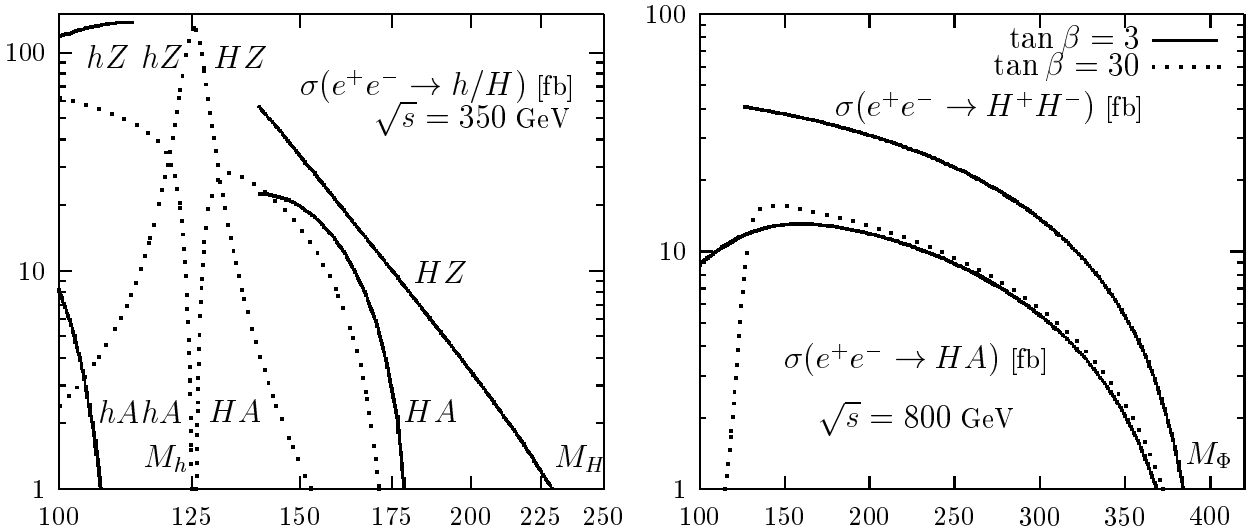

Figure 30: MSSM Higgs boson production rates at the LC for two choices of $\tan\beta = 3$ (solid) and 30 (dotted) for (a) $\sqrt{s} = 350$ GeV as a function of the mass of the produced CP-even neutral Higgs boson (either h or H); and for (b) $\sqrt{s} = 800$ GeV as a function of $m_{H^\pm}$ and m_A, respectively. Taken from ref. [225].

for Higgs production via W^+W^- fusion [process *(ii)*] is not shown. The $\nu\bar{\nu}\phi$ production cross-section is suppressed relative to the corresponding SM cross-section (shown in fig. 9) by a factor of $\sin^2(\beta-\alpha)$ [$\cos^2(\beta-\alpha)$] for $\phi = h$ [$\phi = H$].

In addition to H^+H^- production, there are a number of mechanisms in which the charged Higgs boson is singly produced. Charged Higgs bosons can be produced in top decays via $t \to b + H^+$ if $m_{H^\pm} < m_t - m_b$, as discussed previously in Section 3.5.1. The process $e^+e^- \to W^\pm H^\mp$, which arises at one-loop [226,227], allows for the possibility of producing a charged Higgs boson with $m_{H^\pm} > \sqrt{s}/2$, when H^+H^- production is kinematically forbidden. With favorable MSSM parameters and moderate values of $\tan\beta$, more than ten $W^\pm H^\mp$ events can be produced at the LC for $m_{H^\pm} \lesssim 350$ GeV with $\sqrt{s} = 500$ GeV and 500 fb^{-1} of data, or for $m_{H^\pm} \lesssim 600$ GeV with $\sqrt{s} = 1$ TeV and 1 ab^{-1} [227]. Other single charged Higgs production mechanisms include $t\bar{b}H^-/\bar{t}bH^+$ production [101], $\tau^+\nu H^-/\tau^-\bar{\nu}H^+$ production [228], and a variety of processes in which $H^\pm$ is produced in association with a one or two other gauge and/or Higgs bosons [229].

The heavier Higgs states could lie beyond the discovery reach of the LC ($\sqrt{s} \leq 1$ TeV) and the LHC [*cf.* fig. 28]. In this case, the precision measurements of the h decay branching ratios and couplings achievable at the LC are critical for distinguishing between $h_{\rm SM}$ and h of a non-minimal Higgs sector with properties close to that of the SM Higgs boson. To illustrate the challenge of probing the decoupling limit, suppose that $m_A > \sqrt{s}/2$ so that only the light Higgs boson, h, can be observed directly at the

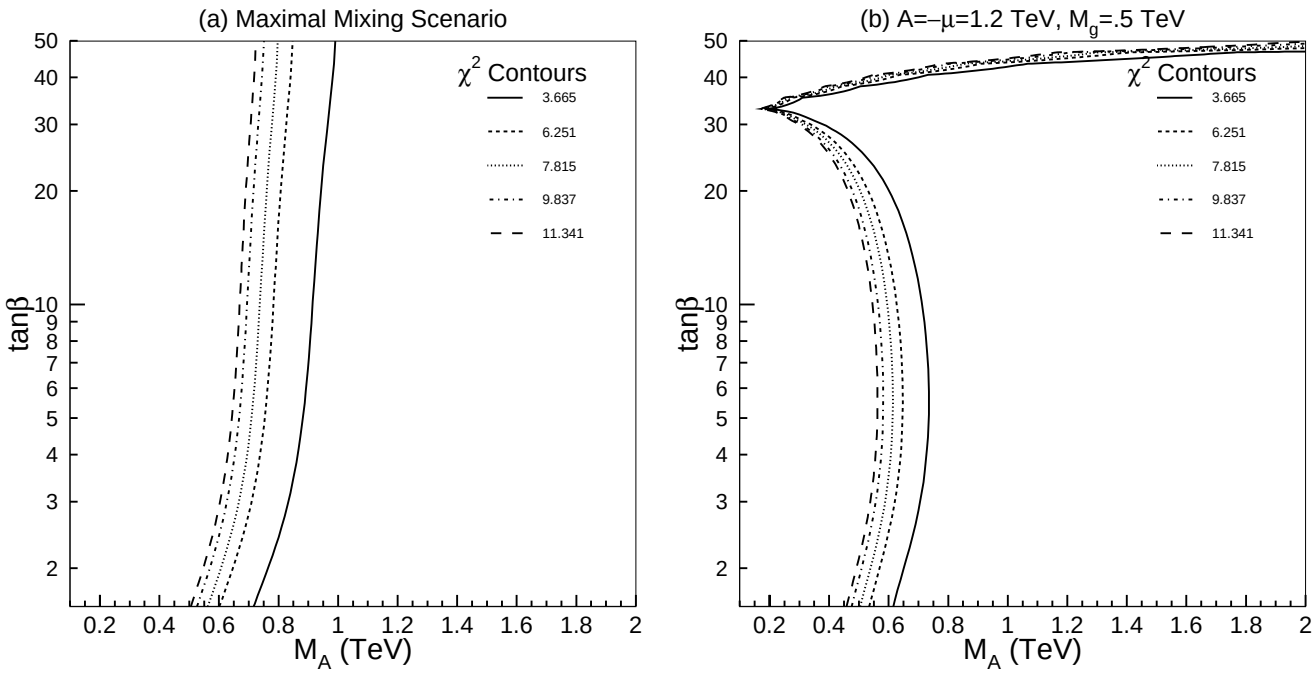

Figure 31: Contours of χ^2 for Higgs boson decay observables for (a) the maximal mixing scenario; and (b) a choice of MSSM parameters for which the loop-corrected $hb\bar{b}$ coupling is suppressed (relative to the corresponding tree-level coupling) at large $\tan\beta$ and low m_A. These results are based on Higgs partial width measurements anticipated at the LC (shown in Table 1) with $\sqrt{s} = 500$ GeV and an integrated luminosity of 500 fb^{-1}. The contours correspond to 68, 90, 95, 98 and 99% confidence levels (right to left) for the observables g^2_{hbb}, $g^2_{h\tau\tau}$, and g^2_{hgg}. See ref. [112] for additional details.

LC. In this case, the fractional deviation of the couplings of h relative to those of the SM Higgs boson scales as m_Z^2/m_A^2. Thus, if precision measurements reveal a non-zero deviation, one could in principle derive a constraint (*e.g.*, upper and lower bounds) on the heavy Higgs masses of the model. In the MSSM, the constraint is sensitive to the MSSM parameters that control the radiative corrections to the Higgs couplings. This is illustrated in fig. 31, where the constraints on m_A are derived for two different sets of MSSM parameter choices [112]. Here, a simulation of a global fit of measured hbb, $h\tau\tau$ and hgg couplings is made (based on the results of Table 1) and χ^2 contours are plotted indicating the constraints in the m_A–$\tan\beta$ plane, assuming a deviation from SM Higgs boson couplings is seen.[32] In the maximal mixing scenario shown in fig. 31(a), the constraints on m_A are significant and rather insensitive to the value of $\tan\beta$. Similar results, in which deviations of $\mathrm{BR}(h \to b\bar{b})/\mathrm{BR}(h \to \tau^+\tau^-)$ from the

[32] These results are similar to those of ref. [107], in which $m_h = 120$ GeV and an integrated LC luminosity of 1000 fb^{-1} were assumed. The upper bound on m_A as a function of $\tan\beta$ was determined in which 68%, 90% and 95% of the MSSM parameter space, respectively, yield h branching ratio predictions that differ from those of the SM at the 95% CL. However, the MSSM parameter regimes in which the sensitivity to m_A are weakest were not identified in ref. [107].

SM prediction yield limits on the allowed values of m_A as a function of $\tan\beta$, have been obtained in ref. [230]. However in some cases, as shown in fig. 31(b), a region of $\tan\beta$ may yield almost no constraint on m_A. This is due to the phenomenon of m_A-independent decoupling noted below eq. (54), in which $\cos(\beta-\alpha)$ [which controls the departure from the decoupling limit] vanishes at a particular value of $\tan\beta$ independently of the value of m_A. Thus, one cannot extract a fully model-independent upper bound on the value of m_A (beyond what can be deduced if no direct A production is observed at the LC). Of course, after supersymmetric particles are discovered, information about the MSSM spectrum can be used to obtain a more stringent bound on m_A, using the techniques described above.

The e^+e^- linear collider running in the $\gamma\gamma$ collider mode presents additional opportunities for the study of the MSSM Higgs sector. Resonance production $\gamma\gamma \to H$ and A can be used to extend the reach in Higgs masses beyond the limit set by HA pair production in the e^+e^- mode [231,123,124]. Typically, one can probe the heavy Higgs masses out to $m_A \sim 0.8\sqrt{s}$ (where $\sqrt{s}$ is the center of mass energy of the LC). This expands the MSSM Higgs discovery reach further into regions of the m_A–$\tan\beta$ parameter space for which the LHC is not sensitive in general (the so-called "blind wedge" of large m_A and moderate values of $\tan\beta$ seen in fig. 28).

As noted above, at least one Higgs boson must be observable at the LC in the MSSM. In non-minimal supersymmetric models, additional Higgs bosons appear in the spectrum, and the "no-lose" theorem of the MSSM must be reconsidered. For example, in the non-minimal supersymmetric extension of the Standard Model (the so-called NMSSM where a Higgs singlet is added to the model [232]), the lightest Higgs boson decouples from the Z boson if its wave function is dominated by the Higgs singlet component. However, in this case the second lightest neutral CP-even Higgs boson usually plays the role of h of the MSSM. That is, the mass of the second lightest Higgs boson is typically below 150 GeV with significant couplings to ZZ, so that it can be produced by the Higgs-strahlung process with an observable cross-section [233,158]. If the second lightest Higgs boson also decouples from the Z, then the third lightest Higgs boson will play the role of h of the MSSM for which the observation is ensured, and so on. Even in bizarre scenarios where all the neutral Higgs boson share equally in the coupling to ZZ (with the sum of all squared couplings constrained to equal the square of the $h_{\rm SM}ZZ$ coupling [131,132]), the "no-lose" theorem still applies—Higgs production at the LC must be observable [234]. In contrast, despite significant progress, there is no complete guarantee that at least one Higgs boson of the NMSSM must be discovered at the LHC for all choices of the model parameters [235].

One of the key parameters of the MSSM Higgs sector is the value of the ratio of Higgs vacuum expectation values, $\tan\beta$. In addition to providing information about the structure of the non-minimal Higgs sector, the measurement of this parameter also provides an important check of supersymmetric structure, since this parameter also enters the chargino, neutralino and third generation squark mass matrices and couplings. Thus, $\tan\beta$ can be measured independently using supersymmetric processes and compared to the value obtained from studying the Higgs sector. Near the decoupling limit, the properties of h are almost indistinguishable from those of $h_{\rm SM}$, and thus no information can be extracted on the value of $\tan\beta$. However, the properties of the heavier Higgs bosons are $\tan\beta$-dependent. Far

from the decoupling limit, all Higgs bosons of the MSSM will be observable at the LC and exhibit strong $\tan\beta$-dependence in their couplings. Thus, to extract a value of $\tan\beta$ from Higgs processes, one must observe the effects of the heavier Higgs bosons of the MSSM at the LC.

The ultimate accuracy of the $\tan\beta$ measurement at the LC depends on the value of $\tan\beta$. In Ref. [236], it is argued that one must use a number of processes, including $b\bar{b}b\bar{b}$ final states arising from $b\bar{b}H$, $b\bar{b}A$, and HA production, and $t\bar{t}b\bar{b}$ final states arising from $t\bar{b}H^+$, $b\bar{t}H^-$ and H^+H^- production. One subtlety that arises here is that in certain processes, the determination of $\tan\beta$ may be sensitive to loop corrections that depend on the values of other supersymmetric parameters. One must settle on a consistent definition of $\tan\beta$ when loop corrections are included [237]. A comprehensive analysis of the extraction of $\tan\beta$ from collider data, which incorporates loop effects, has not yet been given.

The study of the properties of the heavier MSSM Higgs bosons (mass, width, branching ratios, quantum numbers, *etc.*) provides a number of additional challenges. For example, in the absence of CP-violation, the heavy CP-even and CP-odd Higgs bosons, H and A, are expected to be nearly mass-degenerate. Their CP quantum numbers and their separation can be investigated at the same time in the $\gamma\gamma$ collider mode of the LC. If the polarization states of the two incoming linearly-polarized photons are parallel [perpendicular] then only the CP-even Higgs boson H [CP-odd Higgs boson A] will be produced [238]. Thus, the determination of the Higgs boson CP quantum numbers and the separation of the two different states can be achieved. In the case of a CP-violating Higgs sector, the observation and measurement of Higgs boson properties become much more challenging. The $\gamma\gamma$ collider can provide new opportunities to test the nature of the couplings of the Higgs neutral eigenstates (with indefinite CP quantum numbers) to gauge bosons and fermions [124,239].

Finally, once the heavy Higgs spectrum is revealed, one would like to reconstruct the two-Higgs-doublet scalar potential [240]. This is not likely to be accomplished at a first generation LC, although one can make a start if the heavy Higgs masses are not too large. To probe aspects of the Higgs potential one must observe multiple Higgs production in order to extract the Higgs self-couplings [113,114,240,241]. Ultimately, such a program would require an LC with very high energy and luminosity such as CLIC.

4 Conclusions

The physical origin of electroweak symmetry breaking is not yet known. In all theoretical approaches and models, the dynamics of electroweak symmetry breaking must be revealed at the TeV-scale or below. This energy scale will be thoroughly explored by hadron colliders, starting with the Tevatron and followed later in this decade by the LHC. Even though the various theoretical alternatives can only be confirmed or ruled out by future collider experiments, a straightforward interpretation of the electroweak precision data suggests that electroweak symmetry breaking dynamics is weakly-coupled, and a Higgs boson with mass between 100 and 200 GeV must exist. With the supersymmetric extension of the Standard Model, this interpretation opens the route to grand unification of all the fundamental

forces, with the eventual incorporation of gravity in particle physics.

In this review we have summarized the theoretical properties of the Standard Model Higgs boson and the Higgs bosons of the MSSM, and surveyed the search strategies for discovering the Higgs boson at hadron and lepton colliders. We have assessed the Higgs boson discovery reach of present and future colliders, and described methods for measuring the various Higgs boson properties (mass, width, CP quantum numbers, branching ratios and coupling strengths).

The observation of a Higgs boson in the theoretically preferred mass range below 200 GeV may be possible at the Tevatron, whereas experiments at the LHC can discover the SM Higgs boson over the full Higgs mass range up to 1 TeV. The Tevatron can also extend the LEP search for Higgs bosons of the MSSM by either discovering the lightest CP-even MSSM Higgs boson, h (or in some special cases discovering additional Higgs scalars of the model), or by further constraining the MSSM Higgs parameter space. The LHC is sensitive to nearly the entire MSSM Higgs parameter space, in which either h alone can be discovered or multiple Higgs states can be observed. A program of Higgs measurements will be initiated at the LHC to measure Higgs partial widths with an accuracy in the range of 10–30%.

The discovery of the Higgs boson at the Tevatron and/or the LHC is a crucial first step. The measurement of Higgs properties at the LHC will begin to test the dynamics of electroweak symmetry breaking. However, a high-luminosity e^+e^- linear collider, now under development, is needed for a systematic program of precision Higgs measurements. For example, depending on the value of the Higgs mass, branching ratios and Higgs couplings can be determined in some cases at the level of a few percent. In this way, one can extract the properties of the Higgs sector in a comprehensive way, and establish (or refute) the existence of scalar sector dynamics as the mechanism responsible for generating the masses of the fundamental particles.

Acknowledgments

We would like to thank Ulrich Baur, Sally Dawson, Jack Gunion, Heather Logan, Carlos Wagner, Georg Weiglein, Scott Willenbrock and Peter Zerwas for enlightening discussions. We are especially grateful to Steve Mrenna and Michael Spira for many useful suggestions and for their dedicated work in providing a number of plots shown in this review. Finally, much of this work would not have been possible without the collective wisdom gathered from our colleagues of the 1998 Tevatron Higgs Working Group and the 2001 Snowmass Electroweak Symmetry Breaking Working Group.

Fermilab is operated by Universities Research Association, under contract no. DE-AC02-76CH03000 with the U.S. Department of Energy. H.E.H. is supported in part by the U.S. Department of Energy under grant no. DE-FG03-92ER40689.

References

[1] P.W. Higgs, *Phys. Rev. Lett.* **12** (1964) 132; *Phys. Rev.* **145** (1966) 1156; F. Englert and R. Brout, *Phys. Rev. Lett.* **13** (1964) 321; G.S. Guralnik, C.R. Hagen, and T.W.B. Kibble, *Phys. Rev. Lett.* **13** (1964) 585.

[2] J.F. Gunion, H.E. Haber, G. Kane and S. Dawson, *The Higgs Hunter's Guide* (Perseus Publishing, Cambridge, MA, 1990).

[3] H.P. Nilles, *Phys. Reports* **110** (1984) 1; H.E. Haber and G.L. Kane, *Phys. Reports* **117** (1985) 75; S.P. Martin, hep-ph/9709356; P. Fayet, *Nucl. Phys. B (Proc. Suppl.)* **101** (2001) 81.

[4] G. 't Hooft, in *Recent Developments in Gauge Theories,* Proceedings of the NATO Advanced Summer Institute, Cargèse, 1979, edited by G. 't Hooft *et al.* (Plenum, New York, 1980) p. 135; M. Veltman, *Act. Phys. Pol.* **B12** (1981) 437.

[5] E. Witten, *Nucl. Phys.* **B188** (1981) 513; R.K. Kaul, *Phys. Lett.* **109B**, 19 (1982); *Pramana* **19**, 183 (1982); L. Susskind, *Phys. Reports* **104** (1984) 181.

[6] K. Inoue, A. Kakuto, H. Komatsu, and S. Takeshita, *Prog. Theor. Phys.* **68** (1982) 927 [E: **70** (1983) 330]; **71** (1984) 413; R. Flores and M. Sher, *Ann. of Phys.* **148** (1983) 95; J.F. Gunion and H.E. Haber, *Nucl. Phys.* **B272** (1986) 1 [E: **B402** (1993) 567].

[7] S. Weinberg, *Phys. Rev.* **D13** (1979) 974; **D19** (1979) 1277; L. Susskind, *Phys. Rev.* **D20** (1979) 2619; E. Farhi and L. Susskind, *Phys. Reports* **74** (1981) 277; R.K. Kaul, *Rev. Mod. Phys.* **55** (1983) 449; C.T. Hill and E.H. Simmons, FERMI-PUB-02/045-T [hep-ph/0203079], to be published in *Phys. Reports.*

[8] N. Arkani-Hamed, A.G. Cohen and H. Georgi, *Phys. Lett.* **B513** (2001) 232; N. Arkani-Hamed, A.G. Cohen, E. Katz and A.E. Nelson, *JHEP* **0207** (2002) 034. N. Arkani-Hamed, A.G. Cohen, T. Gregoire and J.G. Wacker, *JHEP* **0208** (2002) 020. N. Arkani-Hamed, A.G. Cohen, E. Katz, A.E. Nelson, T. Gregoire and J.G. Wacker, *JHEP* **0208** (2002) 021; I. Low, W. Skiba and D. Smith, *Phys. Rev.* **D66** (2002) 072001.

[9] I. Antoniadis, *Phys. Lett.* **B246** (1990) 377; N. Arkani-Hamed, S. Dimopoulos and G.R. Dvali, *Phys. Lett.* **B429** (1998) 263; L. Randall and R. Sundrum, *Phys. Rev. Lett.* **83** (1999) 3370. For a recent review, see V.A. Rubakov, *Phys. Usp.* **44** (2001) 871.

[10] D. Abbaneo *et al.* [LEP Electroweak Working Group] and A. Chou *et al.* [SLD Heavy Flavor and Electroweak Groups], LEPEWWG/2002-01 (8 May 2002) and additional updates at `http://lepewwg.web.cern.ch/LEPEWWG/`.

[11] ALEPH, DELPHI, L3 and OPAL Collaborations, The LEP working group for Higgs boson searches, LHWG Note 2002-01 (July 2002), and additional updates at `http://lephiggs.web.cern.ch/LEPHIGGS/www/Welcome.html`.

[12] J. Erler, *Phys. Rev.* **D63** (2001) 071301; talk given at *50 Years of Electroweak Physics*, A Symposium in Honor of Professor Alberto Sirlin's 70th Birthday, New York, NY, 27-28 October 2000 [hep-ph/0102143].

[13] R. Barbieri and A. Strumia, *Phys. Lett.* **B462** (1999) 144; R.S. Chivukula and N. Evans, *Phys. Lett.* **B464** (1999) 244; L.J. Hall and C. Kolda, *Phys. Lett.* **B459** (1999) 213; B.A. Kniehl and A. Sirlin, *Eur. Phys. J.* **C16** (2000) 635; J.A. Bagger, A.F. Falk and M. Swartz, *Phys. Rev. Lett.* **84** (2000) 1385.

[14] C. Kolda and H. Murayama, *JHEP* **0007** (2000) 035.

[15] R. Casalbuoni, S. De Curtis, D. Dominici, R. Gatto and M. Grazzini, *Phys. Lett.* **B435** (1998) 396; R.S. Chivukula, B.A. Dobrescu, H. Georgi and C.T. Hill, *Phys. Rev.* **D59** (1999) 075003; T.G. Rizzo and J.D. Wells, *Phys. Rev.* **D61** (2000) 016007; R.S. Chivukula, C. Hoelbling and N. Evans, *Phys. Rev. Lett.* **85** (2000) 511; P. Chankowski, T. Farris, B. Grzadkowski, J.F. Gunion, J. Kalinowski and M. Krawczyk, *Phys. Lett.* **B496** (2000) 195; H.C. Cheng, B.A. Dobrescu and C.T. Hill, *Nucl. Phys.* **B589** (2000) 249; H.J. He, N. Polonsky and S.F. Su, *Phys. Rev.* **D64** (2001) 053004; M.E. Peskin and J.D. Wells, *Phys. Rev.* **D64** (2001) 093003; H.J. He, C.T. Hill and T.M. Tait, *Phys. Rev.* **D65** (2002) 055006; V.A. Novikov, hep-ph/0205320.

[16] M.E. Peskin and T. Takeuchi, *Phys. Rev. Lett.* **65** (1990) 964, *Phys. Rev.* **D46** (1992) 381.

[17] G. Altarelli, F. Caravaglios, G.F. Giudice, P. Gambino and G. Ridolfi, *JHEP* **0106** (2001) 018; M.S. Chanowitz, *Phys. Rev. Lett.* **87** (2001) 231802; *Phys. Rev.* **D66** (2002) 073002; D. Choudhury, T.M. Tait and C.E.M. Wagner, *Phys. Rev.* **D65** (2002) 053002; S. Davidson, S. Forte, P. Gambino, N. Rius and A. Strumia, *JHEP* **0202** (2002) 037; W. Loinaz, N. Okamura, T. Takeuchi and L.C. Wijewardhana, hep-ph/0210193.

[18] L.E. Ibáñez and G.G. Ross, *Phys. Lett.* **B105** (1981) 439; S. Dimopoulos, S. Raby, F. Wilczek, *Phys. Rev.* **D24** (1981) 1681; M.B. Einhorn and D.R.T. Jones, *Nucl. Phys.* **B196** (1982) 475; W.J. Marciano and G. Senjanovic, *Phys. Rev.* **D25** (1982) 3092.

[19] J. Ellis, S. Kelley and D.V. Nanopoulos, *Phys. Lett.* **B249** (1990) 441; P. Langacker and M. Luo, *Phys. Rev.* **D44** (1991) 817; U. Amaldi, W. de Boer and H. Fürstenau, *Phys. Lett.* **B260** (1991) 447; P. Langacker and N. Polonsky, *Phys. Rev.* **D52** (1995) 3081; S. Pokorski, *Act. Phys. Pol.* **B30** (1999) 1759. For a recent review, see: R.N. Mohapatra, in *Particle Physics 1999*, Proceedings

of the ICTP Summer School in Particle Physics, Trieste, Italy, 21 June–9 July, 1999, edited by G. Senjanovic and A.Yu. Smirnov. (World Scientific, Singapore, 2000) pp. 336–394.

[20] T. Hambye and K. Riesselmann, *Phys. Rev.* **D55** (1997) 7255.

[21] See, *e.g.*, G. Altarelli and G. Isidori, *Phys. Lett.* **B337** (1994) 141; J.A. Casas, J.R. Espinosa and M. Quirós, *Phys. Lett.* **B342** (1995) 171; **B382** (1996) 374.

[22] K. Riesselmann, DESY-97-222 (1997) [hep-ph/9711456].

[23] G. Isidori, G. Ridolfi and A. Strumia, *Nucl. Phys.* **B609** (2001) 387.

[24] J.M. Cornwall, D.N. Levin and G. Tiktopoulos, *Phys. Rev. Lett.* **30** (1973) 1268; *Phys. Rev.* **D10** (1974) 1145; C.H. Llewellyn Smith, *Phys. Lett.* **46B** (1973) 233.

[25] B.W. Lee, C. Quigg and H.B. Thacker, *Phys. Rev.* **D16** (1977) 1519.

[26] B.A. Kniehl, *Phys. Reports* **240** (1994) 211.

[27] A. Djouadi, J. Kalinowski and M. Spira, *Comp. Phys. Commun.* **108** (1998) 56. The HDECAY program is available from `http://home.cern.ch/~mspira/proglist.html`.

[28] E. Braaten and J.P. Leveille, *Phys. Rev.* **D22** (1980) 715; N. Sakai, *Phys. Rev.* **D22** (1980) 2220; T. Inami and T. Kubota, *Nucl. Phys.* **B179** (1981) 171; S.G. Gorishniĭ, A.L. Kataev and S.A. Larin, *Sov. J. Nucl. Phys.* **40** (1984) 329 [*Yad. Fiz.* **40** (1984) 517]; M. Drees and K. Hikasa, *Phys. Lett.* **B240** (1990) 455 [E: **B262** (1991) 497].

[29] A. Djouadi, M. Spira and P.M. Zerwas, *Z. Phys.* **C70** (1996) 427.

[30] D.Yu. Bardin, B.M. Vilenskiĭ and P. Kh. Khristov, *Sov. J. Nucl. Phys.* **53** (1991) 152 [*Yad. Fiz.* **53** (1991) 240]; B.A. Knihel, *Nucl. Phys.* **B376** (1992) 3; A. Dabelstein and W. Hollik, *Z. Phys.* **C53** (1992) 507; L. Durand, K. Riesselmann and B.A. Kniehl, *Phys. Rev. Lett.* **72** (1994) 2534 [E: **74** (1995) 1699]; *Phys. Rev.* **D51** (1995) 5007.

[31] A.L. Kataev, *JETP Lett.* **66** (1997) 327 [*Pis'ma Zh. Éksp. Teor. Fiz.* **66** (1997) 308].

[32] M. Spira, hep-ph/9810289.

[33] See, *e.g.*, H. Fusaoka and Y. Koide, *Phys. Rev.* **D57** (1998) 3986.

[34] A computer program library with cross-sections for the Higgs production processes (in the Standard Model and the MSSM) that are relevant for hadron collider Higgs searches is available from `http://home.cern.ch/~mspira/proglist.html`.

[35] M. Spira, private communication. Fig. 5 updates the result presented in ref. [32] by including the NLO QCD-corrected cross-section for $h_{\rm SM}t\bar{t}$ production.

[36] D. Dicus, T. Stelzer, Z. Sullivan and S. Willenbrock, *Phys. Rev.* **D59** (1999) 094016.

[37] H. Georgi, S. Glashow, M. Machacek and D.V. Nanopoulos, *Phys. Rev. Lett.* **40** (1978) 692.

[38] A. Djouadi, M. Spira and P.M. Zerwas, *Phys. Lett.* **B264** (1991) 440; S. Dawson, *Nucl. Phys.* **B359** (1991) 283; D. Graudenz, M. Spira and P.M. Zerwas, *Phys. Rev. Lett.* **70** (1993) 1372; M. Spira, A. Djouadi, D. Graudenz and P.M. Zerwas, *Nucl. Phys.* **B453** (1995) 17.

[39] M. Krämer, E. Laenen and M. Spira, *Nucl. Phys.* **B511** (1998) 523; C. Balázs and C.-P. Yuan, *Phys. Lett.* **B478** (2000) 192.

[40] V. Ravindran, J. Smith and W.L. Van Neerven, *Nucl. Phys.* **B634** (2002) 247.

[41] R.V. Harlander and W.B. Kilgore, *Phys. Rev. Lett.* **88** (2002) 201801; C. Anastasiou and K. Melnikov, *Nucl. Phys.* **B646** (2002) 220.

[42] T. Han and S. Willenbrock, *Phys. Lett.* **B273** (1991) 167.

[43] S. Mrenna and C.P. Yuan, *Phys. Lett.* **B416** (1998) 200.

[44] M. Spira, *Fortschr. Phys.* **46** (1998) 203.

[45] T. Han, G. Valencia and S. Willenbrock, *Phys. Rev. Lett.* **69** (1992) 3274.

[46] L. Reina and S. Dawson, *Phys. Rev. Lett.* **87** (2001) 201804; L. Reina, S. Dawson and D. Wackeroth, *Phys. Rev.* **D65** (2002) 053017.

[47] W. Beenakker, S. Dittmaier, M. Kramer, B. Plumper, M. Spira and P.M. Zerwas, *Phys. Rev. Lett.* **87** (2001) 201805.

[48] R.M. Barnett, H.E. Haber and D.E. Soper, *Nucl. Phys.* **B306** (1988) 697.

[49] D.A. Dicus and S. Willenbrock, *Phys. Rev.* **D39** (1989) 751.

[50] D. Rainwater, M. Spira and D. Zeppenfeld, hep-ph/0203187.

[51] D. Choudhury, A. Datta and S. Raychaudhuri, hep-ph/9809552; C.S. Huang and S.H. Zhu, *Phys. Rev.* **D60** (1999) 075012.

[52] J. Campbell, R.K. Ellis, F. Maltoni and S. Willenbrock, hep-ph/0204093.

[53] E.W. Glover and J.J. van der Bij, *Nucl. Phys.* **B309** (1988) 282.

[54] T. Plehn, M. Spira and P.M. Zerwas, *Nucl. Phys.* **B479** (1996) 46 [E: **B531** (1998) 655].

[55] S. Dawson, S. Dittmaier and M. Spira, *Phys. Rev.* **D58** (1998) 115012.

[56] A. Djouadi, W. Kilian, M. Mühlleitner and P.M. Zerwas, *Eur. Phys. J.* **C10** (1999) 45.

[57] V.A. Khoze, A.D. Martin and M.G. Ryskin, *Eur. Phys. J.* **C14** (2000) 525; **C23** (2002) 311; B. Cox, J. Forshaw and B. Heinemann, *Phys. Lett.* **B540** (2002) 263; R. Enberg, G. Ingelman, A. Kissavos and N. Timneanu, *Phys. Rev. Lett.* **89** (2002) 081801.

[58] V.A. Khoze, A.D. Martin and M.G. Ryskin, IPPP/02/44 and DCPT/02/88 [hep-ph/0207313].

[59] A. De Roeck, V.A. Khoze, A.D. Martin, R. Orava and M.G. Ryskin, *Eur. Phys. J.* **C25** (2002) 391.

[60] T. Han, A.S. Turcot and R.-J. Zhang, *Phys. Rev.* **D59** (1999) 093001.

[61] A. Stange, W. Marciano and S. Willenbrock, *Phys. Rev.* **D49** (1994) 1354; **D50** (1994) 4491.

[62] M. Carena, J.S. Conway, H.E. Haber, J. Hobbs *et al.*, Report of the Tevatron Higgs Working Group, hep-ph/0010338.

[63] P.C. Bhat, R. Gilmartin and H.B. Prosper, *Phys. Rev.* **D62** (2000) 074022.

[64] C. Nelson, *Phys. Rev.* **D37** (1988) 1220.

[65] M. Dittmar and H. Dreiner, *Phys. Rev.* **D55** (1997) 167; and in *The Higgs Puzzle—What can We Learn from LEP2, LHC, NLC, and FMC?*, Proceedings of the 1996 Ringberg Workshop, Ringberg Castle, Tegernsee, Germany, 8–13 December, 1996, edited by B.A. Kniehl (World Scientific, Singapore, 1997) pp. 113–121.

[66] A. Belyaev, T. Han and R. Rosenfeld, FSU-HEP-020417 [hep-ph/0204210].

[67] J. Goldstein, C.S. Hill, J. Incandela, S. Parke, D. Rainwater and D. Stuart, *Phys. Rev. Lett.* **86** (2001) 1694.

[68] J. Conway, K. Desch, J.F. Gunion, S. Mrenna and D. Zeppenfeld, Report of the P1-WG2 subgroup, "The Precision of Higgs Boson Measurements and their Implications," in *Proceedings of the APS/DPF/DPB Summer Study on the Future of Particle Physics* (Snowmass 2001), edited by R. Davidson and C. Quigg, SNOWMASS-2001-P1WG2 [hep-ph/0203206].

[69] S. Dawson, "Higgs boson production rates in hadronic collisions," in *Proceedings of the APS/DPF/DPB Summer Study on the Future of Particle Physics* (Snowmass 2001), edited by R. Davidson and C. Quigg, SNOWMASS-2001-P124 [hep-ph/0111226].

[70] See *e.g.*, ATLAS Collaboration, *ATLAS Detector and Physics Performance: Technical Design Report*, Volume 2, ATLAS TDR 15, CERN/LHCC 99-15. The LHC Higgs search is discussed in Chapter 19; D. Costanzo, "Higgs Physics at the Large Hadron Collider," presented at the 36th Rencontres de Moriond on Electroweak Interactions and Unified Theories, Les Arcs, France, 10–17 March 2001 [hep-ex/0105033].

[71] K. Lassila-Perini, dissertation, ETH No. 12961 (1998) [CERN-THESIS-99-3]; "Higgs Physics at the LHC," presented at the III International Symposium on LHC Physics and Detectors, Chia, 25–27 October 2001, CMS Conference Report CMS CR 2001/018.

[72] M. Dittmar, Pramana **55** (2000) 151; M. Dittmar and A.-S. Nicollerat, "High Mass Higgs Studies using $gg \to h_{\rm SM}$ and $qq \to qqh_{\rm SM}$ at the LHC," CMS-NOTE 2001/036.

[73] T. Trefzger, *Fortschr. Phys.* **49** (2001) 1147.

[74] J.G. Branson, D. Denegri, I. Hinchliffe, F. Gianotti, F.E. Paige and P. Sphicas, editors [The ATLAS and CMS Collaborations], *EPJdirect* **CN1** (2002) 1.

[75] D. Cavalli *et al.*, Report of the Higgs working group for the Workshop "Physics at TeV Colliders," Les Houches, France, 21 May–1 June 2001, hep-ph/0203056.

[76] T. Trefzger, "Search for Higgs Bosons at LHC," in *Proceedings of the APS/DPF/DPB Summer Study on the Future of Particle Physics* (Snowmass 2001), edited by R. Davidson and C. Quigg, SNOWMASS-2001-P111.

[77] V. Drollinger, Th. Muller and D. Denegri, CMS NOTE 2002/006 [hep-ph/0201249].

[78] D. Zeppenfeld, R. Kinnunen, A. Nikitenko and E. Richter-Was, *Phys. Rev.* **D62** (2000) 013009; D. Zeppenfeld, "Higgs Couplings at the LHC," in *Proceedings of the APS/DPF/DPB Summer Study on the Future of Particle Physics* (Snowmass 2001), edited by R. Davidson and C. Quigg, SNOWMASS-2001-P123 [hep-ph/0203123].

[79] T. Plehn, D. Rainwater and D. Zeppenfeld, *Phys. Rev. Lett.* **88** (2002) 051801.

[80] T. Han and B. McElrath, *Phys. Lett.* **B528** (2002) 81.

[81] D. Rainwater and D. Zeppenfeld, *Phys. Rev.* **D60** (1999) 113004 [E: **D61**, 099901 (1999)]; N. Kauer, T. Plehn, D. Rainwater and D. Zeppenfeld, *Phys. Lett.* **B503** (2001) 113.

[82] E. Richter-Was and M. Sapinski, *Act. Phys. Pol.* **B30** (1999) 1001; M. Sapinski and D. Cavalli, *Act. Phys. Pol.* **B32** (2001) 1317.

[83] D. Green, K. Maeshima, R. Vidal and W. Wu, CMS NOTE 2001/039; D. Green, K. Maeshima, R. Vidal, W. Wu and S. Kunori, FERMILAB-FN-0705 (2001); V. Drollinger, Th. Müller and D. Denegri, CMS NOTE 2001/054 [hep-ph/0111312].

[84] A. Belyaev and L. Reina, *JHEP* **0208** (2002) 041.

[85] F. Maltoni, D. Rainwater and S. Willenbrock, *Phys. Rev.* **D66** (2002) 034022.

[86] U. Baur, T. Plehn and D. Rainwater, *Phys. Rev. Lett.* **89** (2002) 151801.

[87] F. Gianotti, M.L. Mangano and T. Virdee conveners, *Physics Potential and Experimental Challenges of the LHC Luminosity Upgrade*, CERN-TH/2002-078 [hep-ph/0204087].

[88] N. Akasaka *et al.*, "JLC design study," KEK-REPORT-97-1.

[89] C. Adolphsen *et al.* [International Study Group Collaboration], "International study group progress report on linear collider development," SLAC-R-559 and KEK-REPORT-2000-7 (April, 2000).

[90] R. Brinkmann, K. Flottmann, J. Rossbach, P. Schmuser, N. Walker and H. Weise [editors], "TESLA: The superconducting electron positron linear collider with an integrated X-ray laser laboratory. Technical design report, Part 2: The Accelerator," DESY-01-011 (March, 2001), [`http://tesla.desy.de/tdr/`].

[91] R.W. Assmann *et al.* [The CLIC Study Team], "A 3 TeV e^+e^- linear collider based on CLIC technology," edited by G. Guignard, SLAC-REPRINT-2000-096 and CERN-2000-008.

[92] R.D. Heuer, D.J. Miller, F. Richard and P.M. Zerwas [editors], "TESLA: The superconducting electron positron linear collider with an integrated X-ray laser laboratory. Technical design report, Part 3: Physics at an e^+e^- Linear Collider," DESY-01-011 (March, 2001), `http://tesla.desy.de/tdr/` [hep-ph/0106315].

[93] T. Abe *et al.* [American Linear Collider Working Group Collaboration], SLAC-R-570 (2001) [hep-ex/0106055–58].

[94] ACFA Linear Collider Working Group, K. Abe *et al.*, KEK-REPORT-2001-11 (2001) [hep-ph/0109166].

[95] J. Ellis, M.K. Gaillard, D.V. Nanopoulos, *Nucl. Phys.* **B106** (1976) 292; B.L. Ioffe, V.A. Khoze. *Sov. J. Nucl. Phys.* **9** (1978) 50.

[96] D.R.T. Jones and S. Petcov, *Phys. Lett.* **B84** (1979) 440; R.N. Cahn and S. Dawson, *Phys. Lett.* **B136** (1984) 196; G.L. Kane, W.W. Repko and W.B. Rolnick, *Phys. Lett.* **B148** (1984) 367; G. Altarelli, B. Mele and F. Pitolli. *Nucl. Phys.* **B287** (1987) 205; W. Kilian, M. Krämer and P.M. Zerwas, *Phys. Lett.* **B373** (1996) 135.

[97] B.A. Kniehl, *Z. Phys.* **C55** (1992) 605.

[98] J. Fleischer and F. Jegerlehner, *Nucl. Phys.* **B216** (1983) 469; A. Denner, J. Kublbeck, R. Mertig and M. Bohm, *Z. Phys.* **C56** (1992) 261.

[99] B.A. Kniehl, *Int. J. Mod. Phys.* **A17** (2002) 1457.

[100] D. Choudhury, T.M. Tait and C.E.M. Wagner, *Phys. Rev.* **D65** (2002) 115007.

[101] K.J. Gaemers and G.J. Gounaris, *Phys. Lett.* **77B** (1978) 379; A. Djouadi, J. Kalinowski and P. M. Zerwas, *Z. Phys.* **C54** (1992) 255; B.A. Kniehl, F. Madricardo and M. Steinhauser, *Phys. Rev.* **D66** (2002) 054016.

[102] S. Dittmaier, M. Kramer, Y. Liao, M. Spira and P.M. Zerwas, *Phys. Lett.* **B441** (1998) 383; **B478** (2000) 247; S. Dawson and L. Reina, *Phys. Rev.* **D59** (1999) 054012.

[103] D.J. Miller, S.Y. Choi, B. Eberle, M. Mühlleitner and P.M. Zerwas, *Phys. Lett.* **B505** (2001) 149; P. Garcia, W. Lohmann and A. Raspereza, LC-Note LC-PHSM-2001-054.

[104] V.D. Barger, K. Cheung, A. Djouadi, B.A. Kniehl and P.M. Zerwas, *Phys. Rev.* **D49** (1994) 79.

[105] D. Chang, W.-Y. Keung and I. Phillips, *Phys. Rev.* **D48** (1993) 3225; A. Soni and R.M. Xu, *Phys. Rev.* **D48** (1993) 5259; A. Skjold and P. Osland, *Phys. Lett.* **B329** (1994) 305; *Nucl. Phys.* **B453** (1995) 3; B. Grzadkowski and J.F. Gunion, *Phys. Lett.* **B350** (1995) 218; T. Han and J. Jiang, *Phys. Rev.* **D63** (2001) 096007.

[106] J.F. Gunion, B. Grzadkowski and X.-G. He, *Phys. Rev. Lett.* **77** (1996) 5172; K. Hagiwara, S. Ishihara, J. Kamoshita and B.A. Kniehl, *Eur. Phys. J.* **C14** (2000) 457.

[107] K. Desch and M. Battaglia, in *Physics and experiments with future linear e^+e^- colliders*, Proceedings of the 5th International Linear Collider Workshop, Batavia, IL, USA, 2000, edited by A. Para and H.E. Fisk (American Institute of Physics, New York, 2001), pp. 312–316; M. Battaglia and K. Desch, in *ibid.*, pp. 163–182 [hep-ph/0101165].

[108] E. Boos, J.C. Brient, D.W. Reid, H.J. Schreiber and R. Shanidze, *Eur. Phys. J.* **C19** (2001) 455.

[109] M. Battaglia and A. De Roeck, "Determination of the muon Yukawa coupling at high energy e^+e^- linear colliders," in *Proceedings of the APS/DPF/DPB Summer Study on the Future of Particle Physics* (Snowmass 2001), edited by R. Davidson and C. Quigg SNOWMASS-2001-E3066 [hep-ph/0111307].

[110] C.T. Potter, J.E. Brau and M. Iwasaki, "Standard Model Higgs Boson Branching Ratio Measurements at a Linear Collider," in *Proceedings of the APS/DPF/DPB Summer Study on the Future of Particle Physics* (Snowmass 2001), edited by R. Davidson and C. Quigg, SNOWMASS-2001-P118.

[111] J.F. Gunion, B. Grzadkowski and X.G. He, *Phys. Rev. Lett.* **77** (1996) 5172; A. Juste and G. Merino, hep-ph/9910301; H. Baer, S. Dawson and L. Reina, *Phys. Rev.* **D61** (2000) 013002.

[112] M. Carena, H.E. Haber, H.E. Logan and S. Mrenna, *Phys. Rev.* **D65** (2002) 055005 [E: **D65** (2002) 099902].

[113] A. Djouadi, H.E. Haber and P.M. Zerwas, *Phys. Lett.* **B375** (1996) 203; F. Boudjema and E. Chopin, *Z. Phys.* **C73** (1996) 85; J. Kamoshita, Y. Okada, M. Tanaka and I. Watanabe, hep-ph/9602224; D.J. Miller and S. Moretti, *Eur. Phys. J.* **C13** (2000) 459.

[114] A. Djouadi, W. Kilian, M. Mühlleitner and P.M. Zerwas, *Eur. Phys. J.* **C10** (1999) 27; C. Castanier, P. Gay, P. Lutz and J. Orloff, LC Note LC-PHSM-2000-061 [hep-ex/0101028].

[115] M. Battaglia, E. Boos and W. Yao, "Studying the Higgs Potential at the e^+e^- Linear Collider," in *Proceedings of the APS/DPF/DPB Summer Study on the Future of Particle Physics* (Snowmass 2001), edited by R. Davidson and C. Quigg, SNOWMASS-2001-E3016 [hep-ph/0111276].

[116] K. Desch and N. Meyer, LC Note LC-PHSM-2001-25.

[117] P.F. Derwent *et al.*, "Linear collider physics," a report prepared for Fermilab Directorate [hep-ex/0107044].

[118] J. Alcaraz and E. Ruiz Morales, *Phys. Rev. Lett.* **86** (2001) 3726.

[119] I.F. Ginzburg, G.L. Kotkin, S.L. Panfil, V.G. Serbo and V.I. Telnov, *Nucl. Inst. Meth.* **A219** (1984) 5.

[120] E. Boos *et al.*, *Nucl. Inst. Meth.* **A472** (2001) 100.

[121] D.L. Borden, D.A. Bauer and D.O. Caldwell, *Phys. Rev.* **D48** (1993) 4018; J.F. Gunion and H.E. Haber, *Phys. Rev.* **D48** (1993) 5109.

[122] S. Söldner-Rembold and G. Jikia, *Nucl. Inst. Meth.* **A472** (2001) 133; M. Melles, *Nucl. Inst. Meth.* **A472** (2001) 128.

[123] D.M. Asner, J.B. Gronberg and J.F. Gunion, hep-ph/0110320.

[124] M.M. Velasco *et al.*, "Photon-Photon and Electron-Photon Colliders with Energies Below a TeV," in *Proceedings of the APS/DPF/DPB Summer Study on the Future of Particle Physics* (Snowmass 2001), edited by R. Davidson and C. Quigg, SNOWMASS-2001-E3005 [hep-ex/0111055].

[125] D.L. Borden, V.A. Khoze, W.J. Stirling and J. Ohnemus, *Phys. Rev.* **D50** (1994) 4499; V.S. Fadin, V.A. Khoze and A.D. Martin, *Phys. Rev.* **D56** (1997) 484; M. Melles, W.J. Stirling and V.A. Khoze, *Phys. Rev.* **D61** (2000) 054015.

[126] L.E. Ibáñez and G.G. Ross, *Phys. Lett.* **B110** (1982) 215; L.E. Ibáñez, *Phys. Lett.* **B118** (1982) 73; J. Ellis, D.V. Nanopoulos and K. Tamvakis, *Phys. Lett.* **B121** (1983) 123; L. Alvarez-Gaumé, J. Polchinski and M.B. Wise, *Nucl. Phys.* **B221** (1983) 495.

[127] S. Dimopoulos and H. Georgi, *Nucl. Phys.* **B193** (1981) 150; K. Harada and N. Sakai, *Prog. Theor. Phys.* **67** (1982) 1877; K. Inoue, A. Kakuto, H. Komatsu and S. Takeshita, *Prog. Theor. Phys.* **67** (1982) 1889; L. Girardello and M.T. Grisaru, *Nucl. Phys.* **B194** (1982) 65; L.J. Hall and L. Randall, *Phys. Rev. Lett.* **65** (1990) 2939; I. Jack and D.R.T. Jones, *Phys. Lett.* **B457** (1999) 101.

[128] S. Dimopoulos and D.W. Sutter, *Nucl. Phys.* **B452** (1995) 496; D.W. Sutter, Stanford Ph. D. thesis, hep-ph/9704390; H.E. Haber, *Nucl. Phys. B* (Proc. Suppl.) **62A-C** (1998) 469.

[129] For a review of the two-Higgs-doublet model (both non-supersymmetric and supersymmetric), see Chapter 4 of ref. [2].

[130] H.E. Haber and Y. Nir, *Phys. Lett.* **B306** (1993) 327; J.F. Gunion and H.E. Haber, SCIPP-02/10 and UCD-2002-10 [hep-ph/0207010].

[131] H.A. Weldon, *Phys. Lett.* **B146** (1984) 59; *Phys. Rev.* **D30** (1984) 1547.

[132] J.F. Gunion, H.E. Haber and J. Wudka, *Phys. Rev.* **D43** (1991) 904; J.F. Gunion, B. Grzadkowski, H.E. Haber and J. Kalinowski, *Phys. Rev. Lett.* **79** (1997) 982; B. Grzadkowski, J.F. Gunion and J. Kalinowski, *Phys. Rev.* **D60** (1999) 075011.

[133] L.J. Hall and M.B. Wise, *Nucl. Phys.* **B187** (1981) 397.

[134] Y. Okada, M. Yamaguchi and T. Yanagida, *Prog. Theor. Phys.* **85** (1991) 1; J. Ellis, G. Ridolfi and F. Zwirner, *Phys. Lett.* **B257** (1991) 83.

[135] S.P. Li and M. Sher, *Phys. Lett.* **B140** (1984) 339; R. Barbieri and M. Frigeni, *Phys. Lett.* **B258** (1991) 395; M. Drees and M.M. Nojiri, *Phys. Rev.* **D45** (1992) 2482; J.A. Casas, J.R. Espinosa, M. Quirós and A. Riotto, *Nucl. Phys.* **B436** (1995) 3 [E: **B439** (1995) 466].

[136] J. Ellis, G. Ridolfi and F. Zwirner, *Phys. Lett.* **B262** (1991) 477; A. Brignole, J. Ellis, G. Ridolfi and F. Zwirner, *Phys. Lett.* **B271** (1991) 123 [E: **B273** (1991) 550].

[137] R.-J. Zhang, *Phys. Lett.* **B447** (1999) 89.

[138] J.R. Espinosa and R.-J. Zhang, *JHEP* **0003** (2000) 026.

[139] J.R. Espinosa and R.-J. Zhang, *Nucl. Phys.* **B586** (2000) 3; A. Brignole, G. Degrassi, P. Slavich and F. Zwirner, *Nucl. Phys.* **B631** (2002) 195.

[140] A. Brignole, G. Degrassi, P. Slavich and F. Zwirner, *Nucl. Phys.* **B643** (2002) 79.

[141] H.E. Haber and R. Hempfling, *Phys. Rev. Lett.* **66** (1991) 1815.

[142] J.F. Gunion and A. Turski, *Phys. Rev.* **D39** (1989) 2701; *Phys. Rev.* **D40** (1989) 2333; M.S. Berger, *Phys. Rev.* **D41** (1990) 225; A. Brignole, *Phys. Lett.* **B277** (1992) 313; **B281** (1992) 284; M.A. Díaz and H.E. Haber, *Phys. Rev.* **D45** (1992) 4246.

[143] P.H. Chankowski, S. Pokorski and J. Rosiek, *Phys. Lett.* **B274** (1992) 191; *Nucl. Phys.* **B423** (1994) 437; A. Yamada, *Phys. Lett.* **B263** (1991) 233; *Z. Phys.* **C61** (1994) 247; A. Dabelstein, *Z. Phys.* **C67** (1995) 495.

[144] D.M. Pierce, J.A. Bagger, K. Matchev, and R. Zhang, *Nucl. Phys.* **B491** (1997) 3.

[145] R. Hempfling and A.H. Hoang, *Phys. Lett.* **B331** (1994) 99.

[146] S. Heinemeyer, W. Hollik and G. Weiglein, *Phys. Rev.* **D58** (1998) 091701; *Phys. Rev. Lett.* **440** (1998) 296; *Eur. Phys. J.* **C9** (1999) 343.

[147] R. Barbieri, M. Frigeni and F. Caravaglios, *Phys. Lett.* **B258** (1991) 167; Y. Okada, M. Yamaguchi and T. Yanagida, *Phys. Lett.* **B262** (1991) 54; J.R. Espinosa and M. Quirós, *Phys. Lett.* **B266** (1991) 389; D.M. Pierce, A. Papadopoulos and S. Johnson, *Phys. Rev. Lett.* **68** (1992) 3678; K. Sasaki, M. Carena and C.E.M. Wagner, *Nucl. Phys.* **B381** (1992) 66; R. Hempfling, in *Phenomenological Aspects of Supersymmetry*, edited by W. Hollik, R. Rückl and J. Wess (Springer-Verlag, Berlin, 1992) pp. 260–279; J. Kodaira, Y. Yasui and K. Sasaki, *Phys. Rev.* **D50** (1994) 7035.

[148] H.E. Haber and R. Hempfling, *Phys. Rev.* **D48** (1993) 4280.

[149] M. Carena, J.R. Espinosa, M. Quirós and C.E.M. Wagner, *Phys. Lett.* **B355** (1995) 209; M. Carena, M. Quirós and C.E.M. Wagner, *Nucl. Phys.* **B461** (1996) 407.

[150] H.E. Haber, R. Hempfling and A.H. Hoang, *Z. Phys.* **C75** (1997) 539.

[151] M. Carena, H.E. Haber, S. Heinemeyer, W. Hollik, C.E.M. Wagner and G. Weiglein, *Nucl. Phys.* **B580** (2000) 29.

[152] M. Carena, S. Mrenna and C.E.M. Wagner, *Phys. Rev.* **D60** (1999) 075010.

[153] M. Carena, J. Ellis, A. Pilaftsis and C.E.M. Wagner, *Nucl. Phys.* **B586** (2000) 92.

[154] S. Heinemeyer, W. Hollik and G. Weiglein, *Phys. Lett.* **B455** (1999) 179.

[155] J.R. Espinosa and I. Navarro, *Nucl. Phys.* **B615** (2001) 82; G. Degrassi, P. Slavich and F. Zwirner, *Nucl. Phys.* **B611** (2001) 403.

[156] M. Carena, S. Heinemeyer, C.E.M. Wagner and G. Weiglein, CERN-TH-99-374 [hep-ph/9912223].

[157] S. Heinemeyer, W. Hollik and G. Weiglein, *Comp. Phys. Commun.* **124** (2000) 76; CERN-TH-2000-055 [hep-ph/0002213] describe the programs `FeynHiggs` and `FeynHiggsFast`, respectively. The program `subpole` of M. Carena, M. Quirós and C.E.M. Wagner now includes the leading two-loop non-logarithmic threshold corrections. The program `hmsusytev`, based on ref. [150], now includes the one-loop supersymmetric threshold corrections to the relation between the third generation Higgs Yukawa couplings and quark masses.

[158] D. Comelli and J.R. Espinosa, *Phys. Lett.* **B388** (1996) 793.

[159] J.M. Moreno, D.H. Oaknin and M. Quirós, *Nucl. Phys.* **B483** (1997) 267.

[160] M. Carena, S. Mrenna and C.E.M. Wagner, *Phys. Rev.* **D62** (2000) 055008.

[161] ALEPH, DELPHI, L3 and OPAL Collaborations, The LEP working group for Higgs boson searches, LHWG Note 2001-04 (July 2001) [hep-ex/0107030].

[162] S. Heinemeyer, W. Hollik and G. Weiglein, *JHEP* **0006** (2000) 009.

[163] ALEPH, DELPHI, L3 and OPAL Collaborations, The LEP working group for Higgs boson searches, LHWG Note 2001-05 (July 2001) [hep-ex/0107031].

[164] A. Pilaftsis, *Phys. Rev.* **D58** (1998) 096010; *Phys. Lett.* **B435** (1998) 88; K.S. Babu, C.F. Kolda, J. March-Russell and F. Wilczek, *Phys. Rev.* **D59** (1999) 016004; D.A. Demir, *Phys. Rev.* **D60** (1999) 055006; M. Carena, J. Ellis, A. Pilaftsis and C.E.M. Wagner, *Phys. Lett.* **B495** (2000) 155; M. Carena, J.R. Ellis, A. Pilaftsis, C.E.M. Wagner, *Nucl. Phys.* **B625** (2002) 345.

[165] G.L. Kane and L.-T. Wang, *Phys. Lett.* **B488** (2000) 383; S.Y. Choi, M. Drees and J.S. Lee, *Phys. Lett.* **B481** (2000) 57; S.Y. Choi and J.S. Lee, *Phys. Rev.* **D61** (2000) 015003; S.Y. Choi, K. Hagiwara and J.S. Lee, *Phys. Rev.* **D64** (2001) 032004; *Phys. Lett.* **B529** (2002) 212; T. Ibrahim and P. Nath, *Phys. Rev.* **D63** (2001) 035009; T. Ibrahim, *Phys. Rev.* **D64** (2001) 035009; S. Heinemeyer, *Eur. Phys. J.* **C22** (2001) 521; S.W. Ham, S.K. Oh, E.J. Yoo, C.M. Kim and D. Son, hep-ph/0205244.

[166] A. Pilaftsis and C.E.M. Wagner, *Nucl. Phys.* **B553** (1999) 3.

[167] S. Dimopoulos and S. Thomas, *Nucl. Phys.* **B465** (1996) 23; S. Thomas, *Int. J. Mod. Phys.* **A13** (1998) 2307.

[168] J.F. Gunion, H.E. Haber and J. Kalinowski, in preparation.

[169] W. Loinaz and J.D. Wells, *Phys. Lett.* **B445** (1998) 178; K.S. Babu and C.F. Kolda, *Phys. Lett.* **B451** (1999) 77.

[170] C. Balázs, J.L. Diaz-Cruz, H.-J. He, T. Tait and C.P. Yuan, *Phys. Rev.* **D59** (1999) 055016.

[171] A. Dabelstein, *Nucl. Phys.* **B456** (1995) 25; F. Borzumati, G.R. Farrar, N. Polonsky and S. Thomas, *Nucl. Phys.* **B555** (1999) 53; H. Eberl, K. Hidaka, S. Kraml, W. Majerotto and Y. Yamada, *Phys. Rev.* **D62** (2000) 055006.

[172] J.A. Coarasa, R.A. Jiménez and J. Solà, *Phys. Lett.* **B389** (1996) 312; R.A. Jiménez and J. Solà, *Phys. Lett.* **B389** (1996) 53; A. Bartl, H. Eberl, K. Hikasa, T. Kon, W. Majerotto and Y. Yamada, *Phys. Lett.* **B378** (1996) 167.

[173] S. Heinemeyer, W. Hollik and G. Weiglein, *Eur. Phys. J.* **C16** (2000) 139.

[174] H.E. Haber, M.J. Herrero, H.E. Logan, S. Peñaranda, S. Rigolin and D. Temes, *Phys. Rev.* **D63** (2001) 055004.

[175] L. Hall, R. Rattazzi and U. Sarid, *Phys. Rev.* **D50** (1994) 7048; R. Hempfling, *Phys. Rev.* **D49** (1994) 6168.

[176] M. Carena, M. Olechowski, S. Pokorski and C.E.M. Wagner, *Nucl. Phys.* **B426** (1994) 269.

[177] M. Carena, D. Garcia, U. Nierste and C.E.M. Wagner, *Phys. Lett.* **B499** (2001) 141.

[178] E. Christova, H. Eberl, W. Majerotto and S. Kraml, *Nucl. Phys.* **B639** (2002) 263 [E: **B647** (2002) 359].

[179] E. Boos, A. Djouadi, M. Mühlleitner and A. Vologdin, *Phys. Rev.* **D66** (2002) 055004.

[180] S. Mrenna, private communication.

[181] A. Djouadi, J. Kalinowski and P.M. Zerwas, *Z. Phys.* **C70** (1996) 435; S. Moretti and W.J. Stirling, *Phys. Lett.* **B347** (1995) 291 [E: **B366** (1996) 451].

[182] A. Mendez and A. Pomarol, *Phys. Lett.* **B252** (1990) 461; C.-S. Li, and R.J. Oakes, *Phys. Rev.* **D43** (1991) 855; M. Drees and D.P. Roy, *Phys. Lett.* **B269** (1991) 155; A. Djouadi and P. Gambino, *Phys. Rev.* **D51** (1995) 218.

[183] X.-J. Bi, Y.-B. Dai and X.-Y. Qi, *Phys. Rev.* **D61** (2000) 015002.

[184] A. Djouadi, J. Kalinowski, P.M. Zerwas, *Z. Phys.* **C57** (1993) 569; H. Baer, M. Bisset, D. Dicus, C. Kao and X. Tata, *Phys. Rev.* **D47** (1993) 1062; A. Djouadi, P. Janot, J. Kalinowski and P.M. Zerwas, *Phys. Lett.* **B376** (1996) 220; A. Djouadi, J. Kalinowski, P. Ohmann and P.M. Zerwas, *Z. Phys.* **C74** (1997) 93.

[185] J.F. Gunion, *Phys. Rev. Lett.* **72** (1994) 199; D. Choudhury and D.P. Roy, *Phys. Lett.* **B322** (1994) 368; O.J. Eboli and D. Zeppenfeld, *Phys. Lett.* **B495** (2000) 147; B.P. Kersevan, M. Malawski and E. Richter-Was, hep-ph/0207014.

[186] J.F. Gunion and H.E. Haber, *Nucl. Phys.* **B278** (1986) 449 [E: **B402** (1993) 567].

[187] S. Dawson, A. Djouadi and M. Spira, *Phys. Rev. Lett.* **77** (1996) 16; A. Djouadi, *Phys. Lett.* **B435** (1998) 101.

[188] A. Djouadi and M. Spira, *Phys. Rev.* **D62** (2000) 014004.

[189] A. Djouadi, M. Spira, D. Graudenz and P.M. Zerwas, *Phys. Lett.* **B318** (1993) 347.

[190] R.V. Harlander and W.B. Kilgore, *JHEP* **0210** (2002) 017; C. Anastasiou and K. Melnikov, SLAC-PUB-9373 [hep-ph/0208115].

[191] C. Balázs, H.-J. He and C.P. Yuan, *Phys. Rev.* **D60** (1999) 114001.

[192] R.M. Godbole and D.P. Roy, *Phys. Rev.* **D43** (1991) 3640; M. Guchait and P. Roy, *Phys. Rev.* **D55** (1997) 7263; F.M. Borzumati and N. Polonsky, in e^+e^- *Collisions at TeV Energies: the Physics Potential*, Proceedings edited by P.M. Zerwas, DESY-96-123D, p. 41 [hep-ph/9602433]; F.M. Borzumati and A. Djouadi, hep-ph/9806301. E. Accomando *et al.*, *Phys. Reports* **299** (1998) 1; J.A. Coarasa, J. Guasch, J. Solà and W. Hollik, *Phys. Lett.* **B442** (1998) 326; J. Guasch and J. Solà, *Phys. Lett.* **B416** (1998) 353.

[193] J.A. Coarasa, D. Garcia, J. Guasch, R.A. Jimenez and J. Solà, *Eur. Phys. J.* **C2** (1998) 373.

[194] C.S. Li and T.C. Yuan, *Phys. Rev.* **D42** (1990) 3088 [E: **D47** (1993) 2156]; A. Czarnecki and S. Davidson, *Phys. Rev.* **D47** (1993) 3063; C.S. Li, Y.-S. Wei and J.-M. Yang, *Phys. Lett.* **B285** (1992) 137.

[195] J. Guasch, R.A. Jiménez and J. Solà, *Phys. Lett.* **B360** (1995) 47.

[196] M. Carena, D. Garcia, U. Nierste and C. Wagner, *Nucl. Phys.* **B577** (2000) 88.

[197] R. Bonciani, S. Catani, M.L. Mangano and P. Nason, *Nucl. Phys.* **B529** (1998) 424.

[198] M. Guchait and S. Moretti, *JHEP* **0201** (2002) 001.

[199] K.A. Assamagan *et al.*, in ref. [87], pp. 85–120.

[200] F. Olness and W.-K. Tung, *Nucl. Phys.* **B308** (1988) 813.

[201] F. Borzumati, J.-L. Kneur and N. Polonsky, *Phys. Rev.* **D60** (1999) 115011.

[202] A. Belyaev, D. Garcia, J. Guasch and J. Solà, *JHEP* **0206** (2002) 059.

[203] L.G. Jin, C.S. Li, R.J. Oakes and S.H. Zhu, *Eur. Phys. J.* **C14** (2000) 91; *Phys. Rev.* **D62** (2000) 053008; A. Belyaev, D. Garcia, J. Guasch and J. Solà, *Phys. Rev.* **D65** (2002) 031701; G. Gao, G. Lu, Z. Xiong and J.M. Yang, *Phys. Rev.* **D66** (2002) 015007.

[204] S.-H. Zhu, hep-ph/0112109; T. Plehn, MADPH-02-1275 [hep-ph/0206121].

[205] A.A. Barrientos Bendezú and B.A. Kniehl, *Phys. Rev.* **D59** (1999) 015009; **D61** (2000) 097701; **D63** (2001) 015009.

[206] O. Brein, W. Hollik and S. Kanemura, *Phys. Rev.* **D63** (2001) 095001.

[207] A.A. Barrientos Bendezú and B.A. Kniehl, *Nucl. Phys.* **B568** (2000) 305.

[208] A. Krause, T. Plehn, M. Spira and P.M. Zerwas, *Nucl. Phys.* **B519** (1998) 85.

[209] O. Brein and W. Hollik, *Eur. Phys. J.* **C13** (2000) 175.

[210] A. Belyaev, M. Drees, O.J. Eboli, J.K. Mizukoshi and S.F. Novaes, *Phys. Rev.* **D60** (1999) 075008; A. Belyaev, M. Drees and J. K. Mizukoshi, *Eur. Phys. J.* **C17** (2000) 337.

[211] A.A. Barrientos Bendezú and B.A. Kniehl, *Phys. Rev.* **D64** (2001) 035006; R. Lafaye, D.J. Miller, M. Mühlleitner and S. Moretti, DESY-99-192 [hep-ph/0002238], contributed to Workshop on Physics at TeV Colliders, Les Houches, France, 7–18 Jun 1999.

[212] K.T. Matchev and S. Thomas, *Phys. Rev.* **D62** (2000) 077702.

[213] I. Hinchliffe, F.E. Paige, M.D. Shapiro, J. Soderqvist and W. Yao, *Phys. Rev.* **D55** (1997) 5520; S. Abdullin *et al.* [CMS Collaboration], *J. Phys.* **G28** (2002) 469.

[214] M. Carena, S. Heinemeyer, C.E.M. Wagner and G. Weiglein, hep-ph/0202167.

[215] D. Rainwater, D. Zeppenfeld and K. Hagiwara, *Phys. Rev.* **D59** (1999) 014037; T. Plehn, D. Rainwater and D. Zeppenfeld, *Phys. Rev.* **D61** (2000) 093005.

[216] J. Dai, J.F. Gunion and R. Vega, *Phys. Lett.* **B371** (1996) 71; **B387** (1996) 801; J.L. Diaz-Cruz, H.J. He, T. Tait and C.P. Yuan, *Phys. Rev. Lett.* **80** (1998) 4641.

[217] H. Baer, B. Harris and X. Tata, *Phys. Rev.* **D59** (1999) 015003.

[218] D. Denegri *et al.*, "Summary of the CMS discovery potential for the MSSM SUSY Higgses," CMS NOTE 2001/032 [hep-ph/0112045].

[219] D. Cavalli, R. Kinnunen, G. Negri, A. Nikitenko and J. Thomas, in ref. [75], pp. 67–79.

[220] S. Moretti and D.P. Roy, *Phys. Lett.* **B545** (2002) 329.

[221] K.A. Assamagan, *Acta Phys. Polon.* **B31** (2000) 863; **B31** (2000) 881; K.A. Assamagan and Y. Coadou, *Acta Phys. Polon.* **B33** (2002) 707; K.A. Assamagan, Y. Coadou and A. Deandrea, *EPJdirect* **C9** (2002) 1.

[222] Fig. 27(b) was provided by E. Richter-Was and F. Gianotti on behalf of the ATLAS collaboration.

[223] M. Carena, J. Ellis, S. Mrenna, A. Pilaftsis and C.E.M. Wagner, in preparation.

[224] J.F. Gunion, L. Roszkowski, A. Turski, H.E. Haber, G. Gamberini, B. Kayser, S.F. Novaes, F.I. Olness and J. Wudka, *Phys. Rev.* **D38** (1988) 3444.

[225] A. Djouadi, Montpellier preprint PM-02-13 [hep-ph/0205248].

[226] S.H. Zhu, hep-ph/9901221; S. Kanemura, *Eur. Phys. J.* **C17** (2000) 473; A. Arhrib, M. Capdequi Peyranère, W. Hollik and G. Moultaka, *Nucl. Phys.* **B581** (2000) 34.

[227] H.E. Logan and S. Su, *Phys. Rev.* **D66** (2002) 035001.

[228] A. Gutierrez-Rodriguez and O.A. Sampayo, *Phys. Rev.* **D62** (2000) 055004; A. Gutierrez-Rodriguez, M.A. Hernandez-Ruiz and O.A. Sampayo, *J. Phys. Soc. Jap.* **70** (2001) 2300; S. Moretti, *EPJdirect* **C15** (2002) 1.

[229] S. Kanemura, S. Moretti and K. Odagiri, *JHEP* **0102** (2001) 011.

[230] J. Guasch, W. Hollik and S. Penaranda, *Phys. Lett.* **B515** (2001) 367.

[231] M. Mühlleitner, M. Krämer, M. Spira and P.M. Zerwas, *Phys. Lett.* **B508** (2001) 311.

[232] See, *e.g.*, U. Ellwanger, M. Rausch de Traubenberg, and C.A. Savoy, *Nucl. Phys.* **B492** (1997) 21; U. Ellwanger and C. Hugonie, *Eur. Phys. J.* **C25** (2002) 297, and references therein.

[233] J. Kamoshita, Y. Okada and M. Tanaka, *Phys. Lett.* **B328** (1994) 67; S.F. King and P.L. White, *Phys. Rev.* **D53** (1996) 4049.

[234] J.R. Espinosa and J.F. Gunion, *Phys. Rev. Lett.* **82** (1999) 1084.

[235] U. Ellwanger, J.F. Gunion and C. Hugonie, hep-ph/0111179; J.F. Gunion, H.E. Haber and T. Moroi, in *New Directions for High Energy Physics*, Proceedings of the 1996 DPF/DPB Summer Study on High Energy Physics, Snowmass '96, edited by D.G. Cassel, L.T. Gennari and R.H. Siemann (Stanford Linear Accelerator Center, Stanford, CA, 1997) pp. 598–602.

[236] J. Gunion, T. Han, J. Jiang, S. Mrenna and A. Sopczak, "Determination of $\tan\beta$ at a Future e^+e^- Linear Collider," in *Proceedings of the APS/DPF/DPB Summer Study on the Future of Particle Physics* (Snowmass 2001), edited by R. Davidson and C. Quigg, SNOWMASS-2001-P120 [hep-ph/0112334].

[237] A. Freitas and D. Stöckinger, *Phys. Rev.* **D66** (2002) 095014.

[238] B. Grzadkowski and J.F. Gunion, *Phys. Lett.* **B294** (1992) 361; J.F. Gunion and J.G. Kelly, *Phys. Lett.* **B333** (1994) 110; M. Kramer, J. H. Kuhn, M.L. Stong and P.M. Zerwas, *Z. Phys.* **C64** (1994) 21.

[239] S.Y. Choi and J.S. Lee, *Phys. Rev.* **D62** (2000) 036005; E. Asakawa, S.Y. Choi, K. Hagiwara and J. S. Lee, *Phys. Rev.* **D62** (2000) 115005; S. Bae, B. Chung and P. Ko, KAIST-TH 2002/09 [hep-ph/0205212].

[240] M. Mühlleitner, DESY-THESIS-2000-033 [hep-ph/0008127]; F. Boudjema and A. Semenov, *Phys. Rev.* **D66** (2002) 095007.

[241] P. Osland and P.N. Pandita, *Phys. Rev.* **D59** (1999) 055013.